

AD A 030928

12 FG

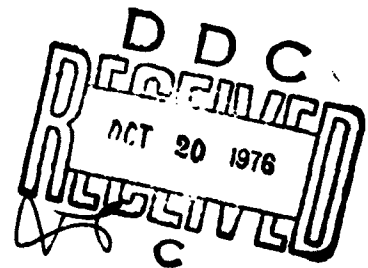
NRL Report 8036

An Unstable Arch Model of a Solar Flare

DANIEL S. SPICER

E. O. Hulburt Center for Space Research

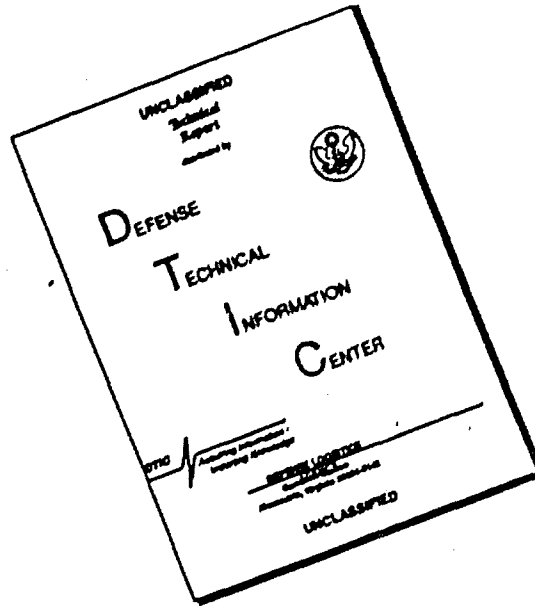
August 10, 1976



NAVAL RESEARCH LABORATORY
Washington, D.C.

Approved for public release; distribution unlimited.

DISCLAIMER NOTICE



THIS DOCUMENT IS BEST QUALITY AVAILABLE. THE COPY FURNISHED TO DTIC CONTAINED A SIGNIFICANT NUMBER OF PAGES WHICH DO NOT REPRODUCE LEGIBLY.

SECURITY CLASSIFICATION OF THIS PAGE (When Data Entered)

REPORT DOCUMENTATION PAGE		READ INSTRUCTIONS BEFORE COMPLETING FORM
1. REPORT NUMBER NRL 8036 8036	2. GOVT ACCESSION NO.	3. RECIPIENT'S CATALOG NUMBER
4. TITLE (and Subtitle) AN UNSTABLE ARCH MODEL OF A SOLAR FLARE.	5. TYPE OF REPORT, PERIOD COVERED Interim report on a continuing NRL Problem	
6. AUTHOR Daniel S. Spicer	7. PERFORMING ORG. REPORT NUMBER	
8. PERFORMING ORGANIZATION NAME AND ADDRESS Naval Research Laboratory Washington, D.C. 20546	9. CONTRACT OR GRANT NUMBER(s) 67448	
10. CONTROLLING OFFICE NAME AND ADDRESS National Aeronautics and Space Administration Washington, D.C. 20546	11. PROGRAM ELEMENT, PROJECT, TASK AREA & WORK UNIT NUMBERS NRL Problem A01-24.601 Project DPR 60404-6	
12. MONITORING AGENCY NAME & ADDRESS (if different from Controlling Office) <i>(12) 143 p.</i>	13. NUMBER OF PAGES 142	
14. DISTRIBUTION STATEMENT (of this Report) Approved for public release; distribution unlimited.	15. SECURITY CLASS. (of this report) Unclassified	
16. DISTRIBUTION STATEMENT (of the abstract entered in Block 20, if different from Report)	17. SECURITY CLASS. (of this report) Unclassified	
18. SUPPLEMENTARY NOTES	19. DECLASSIFICATION/DOWNGRADING SCHEDULE	
19. KEY WORDS (Continue on reverse side if necessary and identify by block number) Solar flares Tearing mode Nonlinear resonant overlap	20. ABSTRACT (Continue on reverse side if necessary and identify by block number) The theoretical consequences of assuming that a current flows along flaring arches consistent with a twist in the field lines of these arches are examined. It is found that a sequence of magneto-hydrodynamic (MHD) and resistive MHD instabilities driven by the assumed current (which we refer to as the toroidal current) can naturally explain most manifestations of a solar flare. <i>is referred</i> The principal flare instability in the proposed model is the resistive kink (or tearing mode in arch geometry) which plays the role of thermalizing some of the field energy in the arch and	

DD FORM 1473 1 JAN 73 EDITION OF 1 NOV 65 IS OBSOLETE S/N 0102- 1-66

SECURITY CLASSIFICATION OF THIS PAGE (When Data Entered)

251 950

LB

20. (Continued)

generating X-configured neutral points needed for particle acceleration. The difference between thermal and nonthermal flares is elucidated and explained, in part, by amplitude-dependent instabilities, generally referred to as overlapping resonances. We show that the criteria for the generation of flare shocks strongly depend on the magnitude and gradient steepness of the toroidal current, which also are found to determine the volume and rate of energy release. The resulting model is in excellent agreement with present observations and has successfully predicted several flare phenomena.



CONTENTS

1.	INTRODUCTION	1
2.	RECENT FLARE OBSERVATIONAL RESULTS	3
3.	MHD STABILITY THEORY OF A DIFFUSE PINCH	7
3.1	Introduction	7
3.2	The Energy Principle and the Diffuse Pinch	9
3.3	Suydam's Condition	14
3.4	Shear Stabilization	17
3.5	The Kink Instability	18
3.6	The Role of Resistivity and Curvature	20
3.7	Nonlinear Studies of Kink Modes	24
4.	RESISTIVE INSTABILITIES IN A DIFFUSE PINCH	24
4.1	Introduction	24
4.2	Resistive Instabilities in Planar Geometry	26
4.3	Resistive Instabilities in Cylindrical Geometry	36
4.4	An Example of MHD and Resistive Instabilities in Cylindrical Geometry	41
4.5	Magnetic Islands	45
4.6	Quasi-Modes	47
4.7	The Rippling Mode and the Superheating Instability ..	48
5.	INSTABILITIES IN MORE COMPLEX MAGNETIC TOPOLOGIES	55
5.1	Introduction	55
5.2	An Example of Three Dimensional Magnetic Configurations	57
5.3	Nonlinear Resonant Phenomena	61
6.	BASIC FLARE MECHANISM	71
6.1	Introduction	71
6.2	Location of Arches that Flare	71
6.3	Mechanisms for Magnetic Energy Conversion	74
6.4	Volume of Energy Release	75
6.5	Anomalous Resistivity and the Energy Release Rate ..	77

7. THE FORMATION OF IMPULSIVE ELECTROMAGNETIC BURSTS AND SHOCKS	81
7.1 Introduction	81
7.2 Thermal or Nonthermal Flares	82
7.3 Mechanisms that can form IEBs and Shocks	83
7.4 Other Modulation Mechanisms	87
8. FLARE MODEL PRECURSORS	90
8.1 Introduction	90
8.2 Mechanisms for Driving Currents	91
8.3 Parametric Excitation of MHD Kink and Resistive Kink Modes	95
8.4 Alteration of the Current Density Profile in the Arch .	96
8.5 Site of Initial Current Buildup	100
8.6 Location of Initial Instability in the Arch	102
9. PHENOMENOLOGICAL ASPECTS OF THE FLARE MODEL	102
9.1 Introduction	102
9.2 Some Speculations on the Role of Instabilities in Other Solar Phenomena	102
9.3 Expected Observational Characteristics of the Model .	103
9.4 Blast Waves and Their Effects	105
9.5 Svestka's Problems	111
10. DISCUSSION AND CONCLUSIONS	115
APPENDIX A — Location of Least Hydromagnetic Stability ...	117
APPENDIX B — Transport Mechanisms	120
APPENDIX C — Resistive Kink Linear Growth Rates	130
REFERENCES	133
ACKNOWLEDGMENTS	138

AN UNSTABLE ARCH MODEL OF A SOLAR FLARE

1. INTRODUCTION

The solar flare, probably the most dramatic event in the solar atmosphere, has long been an enigma to the observer observing it and to the theorist trying to explain it. The principal reason for this lack of progress is simply that the flare theorist has tended to concentrate on mechanisms that can convert stored energy, such as magnetic energy, into the energy of the solar flare, instead of dealing with a specific model with its attendant detailed field geometry. In his quest for such mechanisms the theorist has often shown little regard for the observations, and a specific flare model has never really been elucidated, with the possible exception of Sturrock's (1966, 1968, 1972, 1974). However recently (Vaiana and Gioconni, 1968; Widing and Purcell, 1969; Widing, 1973; Spicer et al., 1974; Widing and Cheng, 1975; Winding, 1974; Widing and Cheng, 1975) the data have shown with little doubt that the principal magnetic topology of a flare is that of an arch and not that of a current sheet as, e.g., is assumed by Sturrock and is currently in the theoretical vogue. Hence it is the purpose of this report to deal with the observed flare geometry and to show that all the theoretical ideas developed in sheet models have not gone to nought but can, in general, be reapplied in an arch geometry or that of a prominence with some rather pleasing results.

For a flare model to be reasonably complete it should be able to describe the basic sequence of events that leads to a flare, its evolution, and finally its secondary effects. Further we should accept the premise that for a model to be useful it must not only explain what is known but should also predict new effects and thus be capable of development. In the model to be presented here we cannot accurately calculate the energy distribution of the accelerated particles, nor can we explain rigorously the origin of the currents necessary to explain the flare within the context of the flare model. However we can explain most of the well-established observations and make some new predictions. Phenomena that require a detailed theoretical prediction are not discussed at this stage, simply because observations of the relevant parameters necessary for accurate calculation do not have sufficient spatial or temporal resolution to make any detailed treatment meaningful. As new detailed observations, e.g., the temperature and density structure of an arch become available, we should then be able to make more accurate predictions; e.g., one could develop an overall computer code for the model which could evolve in sophistication as more detailed input becomes available.

This report is organized as follows: First, in Section 2, we briefly review the recently obtained Skylab data while commenting on how these data affect older flare models. The principal observation is that the magnetic topology of the flare volume is that of an arch, and the principal assumption we will make is that within the arch there exists a current which may have a complicated structure, e.g., currents and return currents. In addition, since we have found it necessary for the arch to contain a current, we are forced to state

DANIEL S. SPICER

criteria for stability of that arch. This comes about because we need to know what precursor effects can trigger the flare mechanism to be discussed, and because we would like to determine the location of the flare in the solar atmosphere, which can be obtained from a combination of stability arguments and flare energy requirements. Further, since we must elucidate the role, e.g., of resistivity, arch curvature, and current perturbations when discussing arch stability, we have included in Sections 3 and 4 a reasonably detailed and self-contained discussion of MHD and resistive MHD modes that can occur in an arch, most of which has not been discussed in the astrophysical literature.

Since the instability found to play the most important role in our model is the "resistive kink instability," i.e., the tearing mode in arch geometry, we discuss in Section 5 the many effects that this instability can lead to in its role as a symmetry-breaking instability. In particular we point out that the nonlinear resonances generated by the tearing mode can result in the phenomenon of overlapping resonances, which results in the magnetic field lines acting stochastically around the separatrices of the magnetic islands generated during the tearing mode. It is pointed out that this stochastic field line behavior can greatly enhance the reconnection rate and thus the rate of energy conversion.

In Sections 6, 7, and 8 we develop the flare model. In Section 7 we discuss the location of the arch in the solar atmosphere which is necessary to explain the observations. We then proceed to discuss the various types of flares which we expect can be accommodated within the model, e.g., impulsive or those with a gradual rise and fall. We then show that the resistivity need not be anomalous to explain the flares observed by Skylab, although if the resistivity were to become anomalous, the required volume of energy release would be very small, $\approx 10^{20}$ cm³. Further, a discussion of mechanisms that can form impulsive electromagnetic bursts and shocks is given in Section 7. Also, mechanisms for particle escape from the arch are pointed out. It is then noted that the model predicts all flares should be impulsive in part, the difference then between thermal and non-thermal flares being only an experimental sensitivity problem. Possible mechanisms that can trigger the resistive kink mode are then discussed under precursors. Here more intense coronal heating by waves and shock waves from other flares are found to act as possible flare precursors.

We conclude, in Sections 9 and 10, with a discussion of the expected flare phenomenology. It is found that many of the classical flare effects can have surprisingly trivial explanations within the context of the model. We also note that if a prominence or filament were carrying a current, it should also be subject to the sequence of instabilities found for the arches. A number of predictions concerning preflare behavior and arch behavior during the flare are made. In addition we note that any arch which carries a current should be subject to the sequences of instabilities discussed and that this point can explain the postflare loop phenomenon, x-ray bright points, and the slow rise and fall events recently reported (Sheeley, et al., 1976). We then conclude by answering a number of questions put forward by Svestka (1975) which a successful flare model should reasonably explain.

Before proceeding, we note that probably the most appealing aspect of this model is its simplicity. That is, the model requires only a current-carrying arch or similar structure, which, as Skylab has aptly proved, is the dominant magnetic structure within an active region. Thus it is hoped that whether the model presented here is correct or incorrect, it will serve to point out that current sheet models, the vogue for nearly 20 years, are not the only answer.

2. RECENT FLARE OBSERVATIONAL RESULTS

Probably the most significant observational result for flares of the last decade has been the determination of the magnetic topology of the flare. With this knowledge one can radically narrow the number of possible mechanisms that can occur in the topology once the topology is determined. Skylab ATM observers have reported (Widing, 1974a, b; Widing and Cheng, 1975; Cheng and Widing, 1975; Spicer et al., 1974; Petrosso et al., 1975; Vorpahl et al., 1975; Gibson, 1976; Kahler et al., 1975; Brueckner, 1975) that the basic magnetic configuration of the solar flare is that of an arch. Figure 1 illustrates the basic conclusions concerning the geometric structure of the flare plasma. One should note:

- The primary flare ingredient appears to be an archlike structure;
- A localized hot plasma cloud ($\geq 20 \times 10^6$ K and $\geq 10^{11}$ particles/cm³) exists near or at the apex of the arch during the early flash phase, which cloud is elongated along the arch;
- The flare kernels have their origins at the ends (feet) of the arch, and these kernels are located in the double ribbons of the flare;
- The arch is oblique to the neutral line (the line along which the measured component of **B** normal to the solar surface vanishes) and each flare ribbon lies on each side of the neutral line;

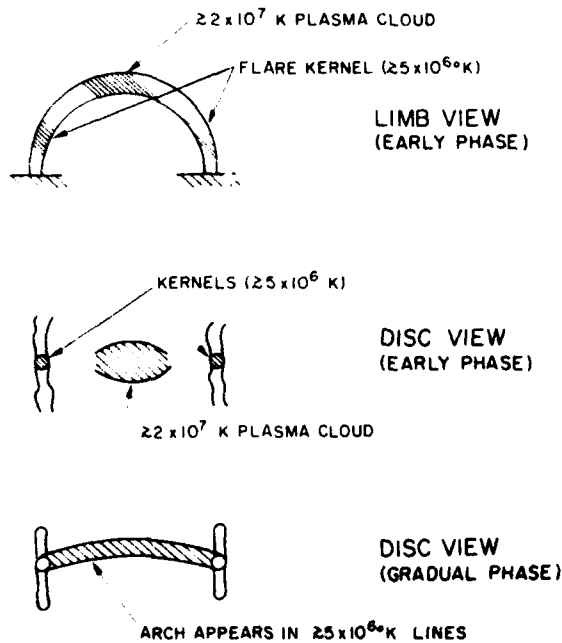


Fig. 1 - Observed flare geometry

DANIEL S. SPICER

- As the plasma cools, the arch becomes very apparent in the cooler lines ($\approx 2 \times 10^6$ K);
- The feet of arch clearly originate in bipolar regions and connect differing polarities;
- The small volume of the hot plasma core is indicative of well-localized heating, and the energy appears to be released in situ in this core;
- The arch exhibits great stability during most of the flare, while at lower altitudes mass motions are observed;
- Many of the observed flares appear to be thermal flares and show little dynamic behavior;
- Evidence has been found that the flare may undergo repeated heatings, occurring at different locations in the arch or in differing arches;
- Evidence shows that neighboring arches may flare due to shock disturbances generated by the initial flare;
- Recent evidence suggests that some arches kink, but it is not clear whether all the kinking arches are the flare arches or higher lying arches;
- The rise time, decay time, and rate of increase of soft-x-ray emission tends to increase with flare volume;
- The volume of in situ intense heating was of about 2 cubic arcseconds, corresponding to volume scales of 1400^3 km³.

Preflare observations (Petrasso et al., 1975; Brueckner, 1975; Gibson, 1976; Patterson et al., 1976) have found:

- The arches are observed to brighten, sometimes gradually (hours) and sometimes quickly (about 10 minutes), prior to flaring;
- Line spectra from the transition zone show that the transition zone is undergoing strong agitation;
- Subflares appear as arches and show strong agitation in transition zone lines;
- The arches are observed to exist prior to flaring.

These observations are in complete contradiction to all existing flare models except possibly the "current interruption model" (Alfvén and Carlquist, 1967). This model however has been criticized theoretically (Smith and Priest, 1972). Although all the criticisms made are not correct (Spicer, 1974), interruption of the bulk current in an arch, by anomalous processes or otherwise, is highly unlikely (a detailed discussion will be published elsewhere). With these results and their obvious inconsistency with present flare theories, there is strong motivation to look elsewhere for an explanation of a flare.

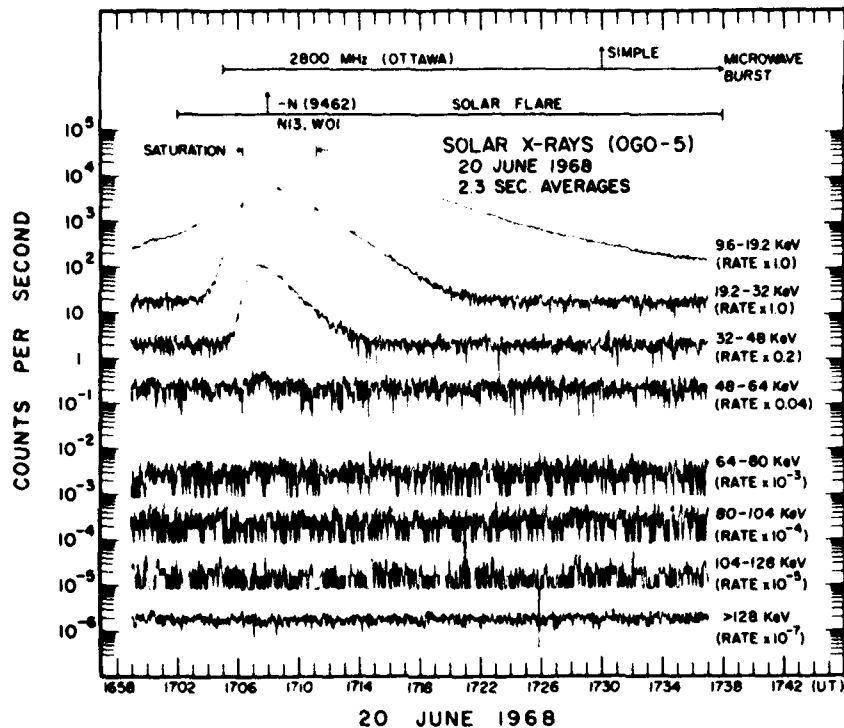


Fig. 2 — "One-component" solar x-ray burst observed by the OGO-5 detector on June 20, 1968. The 2.3-sec averages of the counting rates of the eight x-ray energy channels are plotted against time. The counting rate of the 9.6-19.2-keV channel near the maximum of the burst was close to the saturation level and is therefore not shown.

Recently Svestka (1974) has emphasized the apparent difference between the thermal and nonthermal flare. The principal difference appears to lie in the fact that a thermal flare generates a longer lived electromagnetic burst whereas the nonthermal flare also has impulsive electromagnetic bursts associated with it. This difference is clearly illustrated in Figs. 2 and 3. Svestka further argues that the thermal flare can be explained without recourse to acceleration mechanisms, whereas the nonthermal flare clearly needs impulsively accelerated particles. In general a nonthermal flare acts like a thermal flare but with additional impulsive hard-x-ray, microwave, XUV, and type III radio bursts.

Svestka makes some other interesting points concerning type II, type IV, and type III bursts. He notes that a majority of flares occur without type III bursts whereas x-ray and microwave bursts are always associated with flares. Further one finds that very rarely do type III, x-ray, and microwave bursts occur simultaneously, but when they do, the type III bursts are intense. These observations are interesting, since the principal argument in favor of sheet flare models is that they permit the easy escape of relativistic electrons to form the type III burst during the flare, but here we have a direct contradiction to that argument. Most flares do not produce type III bursts. Svestka further notes

DANIEL S. SPICER

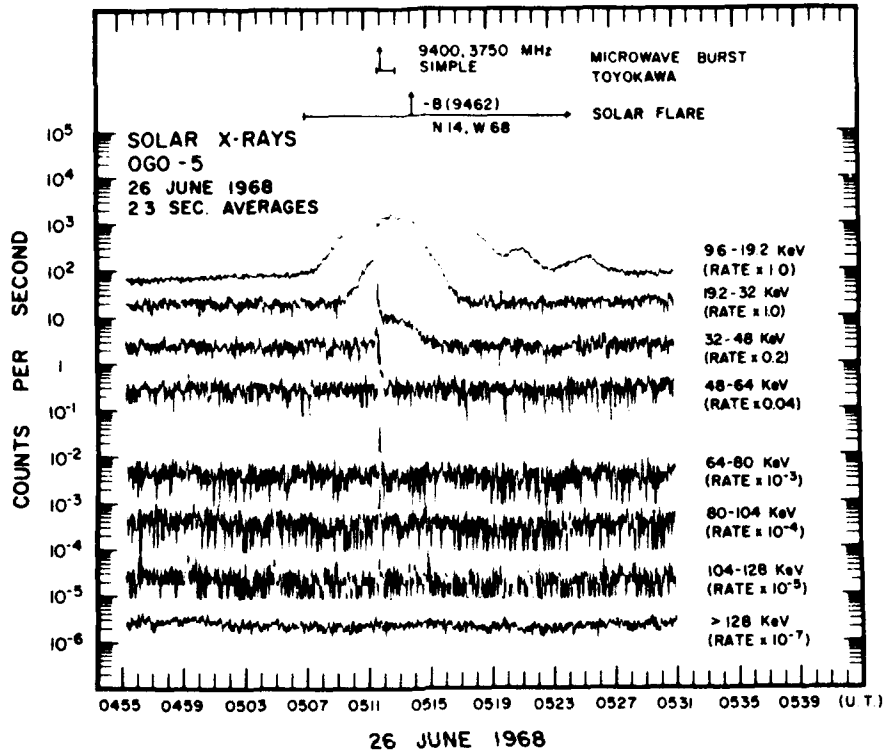


Fig. 3 — "Two-component" solar x-ray burst observed on June 26, 1968. Notice the sharp spike at 0511:44 U.T., nearly coincident with the peak in the microwave radio burst.

that type IV bursts are observed (with the impulsive x-ray and microwave bursts which usually form the subsequent type IV burst) in essentially all events when protons of high energies and relativistic electrons are recorded.

Associated with these effects are the type II bursts, which are a result of shock waves propagating through the corona at speeds of about 1500 km/s. These type II bursts have been shown recently to be closely associated with the high-energy protons and relativistic electrons (Svestka and Fitsova, 1974). Type II bursts are never observed before the microwave bursts, although $\approx 20\%$ are found to occur before the microwave burst maxima. Svestka concludes from this, quite reasonably, that type II bursts are closely associated with the primary acceleration process in flares. In general, type II bursts show a strong preference for occurring when strong proton events occur. Although Svestka argues throughout his discussion that anywhere from two to four acceleration mechanisms are needed to explain the variety of affects caused by a flare, we feel only two are necessary, as will become clear in Section 7. However we do not here treat the second acceleration phase of the flare, since we feel it is clearly a secondary manifestation of the primary energy release associated with stochastic processes, generated either by the pressure pulse of the primary energy release or by the high-energy particles released during the primary release. This subject will be examined elsewhere in more detail.

Our discussion has clearly shown the need for a new, workable, flare model, and such a model should at least be consistent with the results reviewed above as well as those classical manifestations of flares, e.g., double flare ribbons. We will adhere to the concept of a model as outlined in the introduction and attempt to explain the about results as well as some others not discussed.

3. MHD STABILITY THEORY OF A DIFFUSE PINCH

3.1 Introduction

As noted in the introduction, we will find it necessary to review various mechanisms which we will apply rather freely in subsequent sections. Since most of these mechanisms have neither been collected together in a review or text nor been discussed adequately in the astrophysical literature for present purposes, we will briefly review and discuss the applicability of these mechanisms to our flare model. Thus the present section and Sections 4 and 5 will be devoted to this purpose, thereby making the flare model reasonably complete and self-contained (Fig. 4 illustrates the sequence of mechanisms which will lead to a flare in this model).

The principal geometry of the flare model to be proposed is that of a semitoroidal magnetic arch, along which a toroidal current is assumed to flow in some as yet unspecified manner and driven by as yet unknown mechanisms. The assumption that a toroidal current flows along the main toroidal field of the arch implies that we are in reality considering a *diffuse pinch* bent into a half torus. Thus it follows that we will be interested in the stability of such a configuration. As we will soon see, such a diffuse pinch will be subject to MHD kink modes and resistive kink modes; the former differing from the latter in that the former strictly conserves magnetic flux whereas the latter permits reconnection within the arch. However both kink modes are driven by the magnetic field energy stored in the poloidal field generated by the toroidal current, and one can excite the other. Thus we examine the stability of the MHD diffuse pinch in this section and the resistive diffuse pinch in Section 4.

As will become evident during our discussion of the MHD and resistive MHD stability of the diffuse pinch, stability will be determined by the degree of magnetic shear in the pinch and therefore the arch. However the stability criteria obtained depend critically on the quantity $\mathbf{k} \cdot \mathbf{B}$ and where it vanishes, \mathbf{k} being the wave-number vector of the perturbation and \mathbf{B} the magnetic field. Since the stability in both the MHD and resistive cases was analyzed assuming cylindrical symmetry, which an arch clearly does not have, it was necessary to show that the stability criteria obtained using cylindrical symmetry is valid in more complex geometries such as the arch. This is done principally in Section 5.

During our discussion of more complex geometries in Section 5, we note that the increase in complexity of the arch can give rise to complex nonlinear phenomena, which may prove useful in explaining certain behavior of the solar flare in the context of this model. These phenomena arise because of the complex distortion of magnetic surfaces due to the arch curvature and the distortion of magnetic surfaces generated by the flux-conserving MHD kink modes. This follows because, as will be seen, the resistive kink mode can be treated as a symmetry-breaking mechanism, since it does not conserve flux. Indeed, as we will see, the resistive kink mode can result in neighboring surfaces nonlinearly interacting with one another, thereby causing a sudden and dramatic increase in

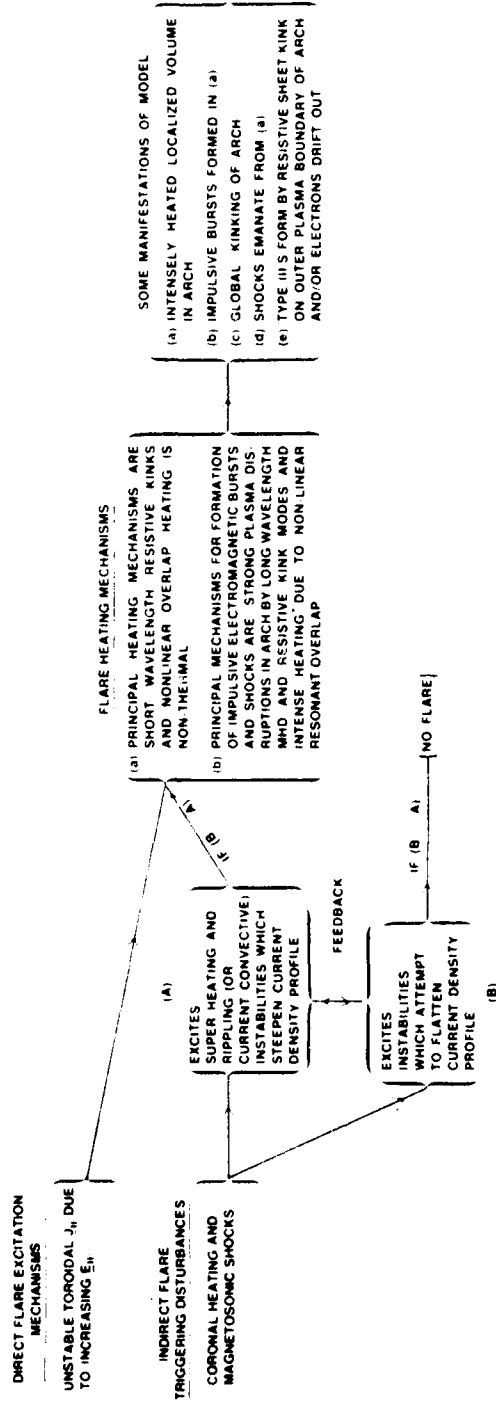


Fig. 4 — Flow chart of the arch flare model being proposed

reconnection, over and above that caused by one surface reconnecting. Since this non-linear phenomenon has a threshold it must cross before occurring, we will argue that it may be one possible explanation for the nonthermal electromagnetic bursts associated with flares. For this reason we review the basic ideas involved.

Because the location where $\mathbf{k} \cdot \mathbf{B}$ vanishes determines in part the stability of the pinch and thus are arch, we examine in Section 4 mechanisms that can steepen the radial profile of the toroidal current. Further, because there are mechanisms that may prevent this current-density steepening, we collect and summarize the applicable mechanisms in Appendix B. This is important, because the arches are observed to exist prior to flaring; i.e., they were not arches emerging from the photosphere. Hence we need to know those mechanisms that can lead to instability and how they manifest themselves.

Although this section and Sections 4 and 5 are principally devoted to reviewing and collecting the instabilities pertinent to this model, there are a number of new discussions not found in the literature, which will play a crucial role in the model to follow.

3.2 The Energy Principle and the Diffuse Pinch

Plasma instabilities are conveniently divided into two broad classes: configuration-space instabilities and phase-space instabilities. Configuration-space instabilities result in displacements of macroscopic portions of the plasma and can usually be treated theoretically by the fluid equations. MHD instabilities are configuration instabilities. It is found theoretically that the infinite-conductivity-limit MHD theory provides a useful means of understanding the gross behavior of plasma stability while providing thresholds and growth rates. As we will show later, the inclusion of resistivity in general reduces the stability of an MHD configuration and in some cases will actually cause an MHD stable configuration to become unstable. A review of the MHD stability of the diffuse pinch will be the primary concern of this section, although a brief discussion of finite resistivity on MHD stability will be included. In addition a discussion of the effects of curvature on stability will be included.

The stability of the diffuse stabilized linear z-pinch is a rather well understood problem in plasma physics, particularly through the work of Newcomb (1960). The theoretical means by which Newcomb studied the stability of a diffuse linear pinch made use of the MHD energy principle of Bernstein et al. (1958). The energy principle originates from the fact that the problem of stability is, mathematically, an investigation of small oscillations about an equilibrium state. One assumes that the amplitudes of the oscillations are small and then proceeds to linearize the equations of magnetohydrodynamics (Kadomtsev, 1966). After the appropriate substitutions and manipulations, one obtains a single second-order differential equation for ξ , the displacement of the plasma away from the equilibrium position, which is given by

$$\rho_0 \frac{\partial^2 \xi}{\partial t^2} = \nabla(\xi \cdot \nabla P_0 + \gamma P_0 \nabla \cdot \xi) + \frac{1}{4\pi} ((\nabla \times \mathbf{B}_0) \times [\nabla \times (\xi \times \mathbf{B}_0)]) + \{\nabla \times [\nabla \times (\xi \times \mathbf{B}_0)]\} \times \mathbf{B}_0, \quad (3.1)$$

DANIEL S. SPICER

where \mathbf{B}_0 and P_0 are the equilibrium magnetic field and scalar pressure respectively. This equation must be supplemented by the appropriate boundary conditions.

We may rewrite Eq. (3.1) as

$$\rho_0 \frac{\partial^2 \xi}{\partial t^2} = - \overleftrightarrow{\mathbf{K}} \cdot \xi = \mathbf{F}(\xi), \quad (3.2)$$

where $\overleftrightarrow{\mathbf{K}}$ is a self-adjoint operator and $\mathbf{F}(\xi)$ is a generalized force function. Since $\overleftrightarrow{\mathbf{K}}$ is self-adjoint, Eq. (3.1) or (3.2) can be derived from an action integral of the form

$$I = \int \int \left(\frac{\rho_0 \xi^2}{2} - \xi \cdot \overleftrightarrow{\mathbf{K}} \cdot \xi \right) d^3 \mathbf{x} dt. \quad (3.3)$$

Since the equations are linear, the time dependence of all quantities can be expressed in the form $\exp(-i\omega t)$. Thus, if the problem is simple enough, Eq. (3.1) can be solved exactly and one has explicitly the characteristic eigenvalues ω^2 , which, as is well known (Landau and Lifschitz, (1960), determine the stability of the system. If $\omega^2 > 0$, the equilibrium state is stable; $\omega^2 = 0$ is the marginal state; and if $\omega^2 < 0$, the equilibrium state is unstable. However, if the geometry is sufficiently complex that one cannot solve Eq. (3.1) exactly, it is then sufficient to determine the sign of ω^2 to determine stability.

Substituting $\xi = \xi(\mathbf{r}) \exp(-i\omega t)$ into Eq. (3.2), multiplying the result by ξ , and integrating over the plasma volume yields

$$\omega^2 = \frac{\int \xi \cdot \overleftrightarrow{\mathbf{K}} \cdot \xi d^3 \mathbf{x}}{\int \rho_0 \xi^2 d^3 \mathbf{x}}. \quad (3.4)$$

The energy principle then states that the problem of stability reduces to determining the sign of the integral in the numerator, which is just the right-hand term in Eq. (3.3), i.e., the potential energy. Hence the energy principle states that an MHD configuration is stable if the potential energy integral is positive for every displacement ξ satisfying the appropriate boundary conditions and is unstable if there exists a ξ for which ω^2 is negative. This energy integral is given by

$$W(\xi) = \frac{1}{2} \int [\mathbf{Q}^2 + \mathbf{j} \cdot (\xi \times \mathbf{B}) + (\nabla \cdot \xi) \xi \cdot \nabla P + \gamma P (\nabla \cdot \xi)^2] d^3 \mathbf{x}, \quad (3.5)$$

where $\mathbf{Q} = \nabla \times (\xi \times \mathbf{B})$, \mathbf{j} is the perturbed current, and γ is the ratio of the specific heats. We are dropping the subscript on the equilibrium quantities when no confusion will result.

Because a coronal arch with a toroidal current has a toroidal magnetic field which is probably a monotonically decreasing function of altitude, a stability treatment of such an arch should take this effect into account. Such a treatment is analytically difficult. However the stability criteria to be derived does not in general depend on the position along

the current path; hence ignoring the z dependence of the problem is a reasonable approximation. It then follows, by virtue of the assumed axial symmetry of the pinch, that we can limit our analysis to displacements of the form

$$\xi(r) = \xi(r) \exp(im\phi + ikz),$$

such that

$$\xi(r) = (\xi, \xi_\phi, \xi_z),$$

without loss of generality. In addition, because the derivation of the energy principle by Bernstein et al. (1958) refers to a class of all possible displacements, it remains valid even if the class of displacements is restricted by fixing m and k . A separate stability criterion is then obtained for each set of values of m and k . This will be important when we limit the wave number k , because of the finite size of the cylinder or arch.

A minimization of the energy integral (3.5) with respect to ξ_z and ξ_ϕ can be carried out algebraically and yields

$$W(\xi) = \frac{\pi}{2} \int_0^b \left[f \left(\frac{d\xi}{dr} \right)^2 + g\xi^2 \right] dr, \quad (3.6)$$

where b is the outside pinch boundary,

$$f = \frac{r}{4\pi} \frac{(krB_z + mB_\phi)^2}{k^2r^2 + m^2}, \quad (3.7)$$

and

$$g = \frac{2k^2r^2}{k^2r^2 + m^2} \frac{dP}{dr} + \frac{1}{4\pi r} (krB_z + mB_\phi)^2 \frac{k^2r^2 + m^2 - 1}{k^2r^2 + m^2} + \frac{2k^2r}{4\pi(k^2r^2 + m^2)^2} (k^2r^2B_z^2 - m^2B_\phi^2). \quad (3.8)$$

A B_r radial component of the magnetic field does not appear in these expressions by virtue of the assumed radial dependence of all the equilibrium variables.

Before extremizing (3.6) with respect to ξ , we can make use of the fact the $W(\xi)$ is unchanged when m and k both change sign to show that the $m = 1$ displacements are the least stable. Excluding the $m = 0$ mode and letting $k = m q$, we find that the second term in g is the only term that depends on m . Since this term is proportional to m^2 and positive definite, the least stable displacements are those for which $m = 1$, the so called kink or helical mode. One can conclude from this result that if the pinch is stable for $|m| = 1$, $-\infty < k < \infty$, it is also stable for all higher values of m . Physically the kink mode can be understood using Fig. 5, which depicts a current, j_z flowing in a plasma

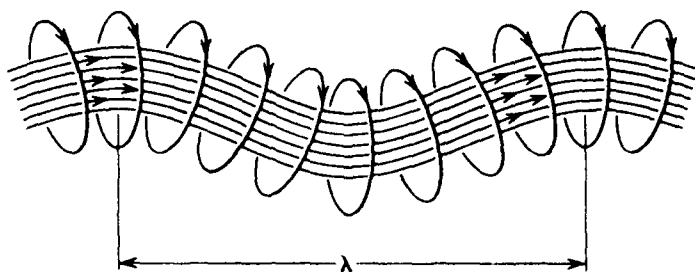


Fig. 5 - Hindering kink instability with tension of trapped axial fields

column along the axial field B_z . The current j_z produces an azimuthal field B_ϕ (in the case of the arch B_ϕ is called a poloidal field B_p). If a kink develops, as illustrated, the lines of force B_ϕ are closer together at the inside of the kink than at the outside. The magnetic pressure, $B_\phi^2/8\pi$ acts to increase the kink, and the bending of B_z results in a restoring force directed oppositely to the B_ϕ force. It should also be pointed out that the kink mode normally appears as one turn of a helix and not a simple displacement as depicted in Fig. 5.

For $m = 0$, Eq. (3.2) reduces to

$$W(\xi) = W_0(\xi) + \frac{\pi k^2}{2} \int_0^b B_z^2 \xi^2 r dr, \quad (3.9)$$

where

$$W_0(\xi) = \frac{\pi}{2} \int_0^b \left[r B_z^2 \left(\frac{d\xi}{dr} \right)^2 + \left(\frac{B_z^2}{r} + 2 \frac{dP}{dr} \right) \xi^2 \right] dr. \quad (3.10)$$

Since the term containing k^2 in Eq. (3.9) is positive definite, the pinch is stable for all k , if it is stable in the limit as $k \rightarrow 0$. The $m = 0$ mode is usually called the sausage mode and appears as an axially symmetric local compression of the plasma column.

At this point it is appropriate to modify the topology used by Newcomb (1960) by demanding periodicity along the axis of the cylinder. This has the effect of simulating the finite length of the cylindrical column or toroidal arch and, as will be seen, enhances the stability of the pinch against both local and nonlocal modes. The wave number k takes on the discrete values

$$k = \frac{2\pi n}{L}, \quad (3.11)$$

where L is the length of the plasma column or arch ($n = 1$ corresponding to the longest wavelength that can be supported by the plasma column). Because k can never equal zero, m and k both cannot vanish. Hence we can modify Theorem 1 of Newcomb as: A

linear diffuse pinch is stable for all values of m and k if and only if it is stable for $m = 1$, $2\pi/L < k < \infty$, and for $m = 0$, $k \rightarrow 2\pi/L$.

Extremizing Eq. (3.6) with respect to ξ leads to the Euler-Lagrange equation

$$\frac{d}{dr} \left(f \frac{d\xi}{dr} \right) - g\xi = 0, \quad (3.12)$$

which must satisfy boundary conditions

$$\xi(r=0) = 0, \text{ if } m \neq \pm 1, \quad (3.13a)$$

and

$$\frac{d\xi(r=0)}{dr} = 0, \text{ if } m = \pm 1. \quad (3.13b)$$

Determining the stability of a diffuse pinch reduces to solving Eq. (3.12) for the given variables $B_z(r)$, $B_\theta(r)$, and $P(r)$ with a given choice of k and m . This is just an example of the Sturm-Liouville problem. Hence the stability conditions for the diffuse pinch can be expressed as follows: a necessary and sufficient condition for stability of a diffuse pinch is that the solution of Eq. (3.12) have fewer than two zeros in the interval $0 < r < b$.

To understand this statement, we proceed following Kadomtsev (1966). To solve the complete eigenvalue problem for the dynamical stability of the diffuse pinch, one must find an extremum of the Lagrangian $L = T - W$ rather than extremize the potential energy W as we have just done. Extremizing L leads us to the expression

$$\frac{d}{dr} \left(f \frac{d\xi}{dr} \right) - (\omega^2 \rho - g)\xi = 0, \quad (3.14)$$

where ω^2 is the square of the frequency and $\rho(r)$ is the mass density. It follows then that Eq. (3.12) represents the marginal state of stability i.e., $\omega^2 = 0$. If $\omega^2 < 0$, the instability case, the contribution to the effective $g(r)$ is positive, and if $\omega^2 > 0$, the stability case, the contribution to the effective $g(r)$ is negative.

If we now assume the solution to (3.12) has two zeros in the interval $(0, b)$, then adding a positive-definite term to (3.12), as (3.14) represents if $\omega^2 < 0$, will shift one zero to the $r = 0$ boundary and the other to the $r = b$ boundary. Since this displacement results in a solution that is still bounded, with both boundary conditions satisfied, the diffuse pinch will be unstable ($\omega^2 < 0$). However, if there are fewer than two zeros in the interval $(0, b)$, we find that a positive contribution, $\omega^2 < 0$, does not give a solution that is bounded, and only a negative contribution gives a solution that both satisfies the boundary conditions and remains bounded. Since a negative contribution corresponds to $\omega^2 > 0$, we conclude that only solutions with fewer than two zeros correspond to a stable solution.

DANIEL S. SPICER

Thus (3.12) has three regular singular points, which occur when

$$r = 0, \quad (3.15a)$$

$$\mathbf{k} \cdot \mathbf{B} = kB_z + \frac{mB_\phi}{r} = 0, \quad (3.15b)$$

and

$$r = \infty. \quad (3.15c)$$

Only the singular point (3.15b) will concern us here, since, as is shown by Newcomb (1960), the solutions to the Euler-Lagrange equation (3.12) never oscillate at the singular points (3.15a) and (3.15c), whereas the solutions near the singular point $\mathbf{k} \cdot \mathbf{B} = 0$ may rapidly oscillate, producing many zeros and thus instability.

Because in general it is not possible to continue an Euler-Lagrange solution which is real past a singular point, we cannot speak of an Euler-Lagrange solution in the entire interval $0 < r < b$ if a singular point exists within the interval. However it is possible to divide the interval $0 < r < b$ into subintervals so that within each subinterval there are no singular points. Hence one modifies the stability criteria to take into account these singular points. It then follows, if zeros succeed each other more rapidly than the end-points of the independent subintervals, that the diffuse pinch is unstable (Newcomb, 1960).

Singular points given by $\mathbf{k} \cdot \mathbf{B} = 0$ may be characterized as those values of r for which $m_\phi + kz$, the phase of the displacement ξ , is constant along a line of force; i.e., the pitch of the lines of force match exactly with the pitch of the perturbation k/m . Since the perturbation is constant along the lines of force, the perturbation is a convective perturbation. Such a perturbation permits the free interchange of lines of force without appreciable distortion of the magnetic field. Such interchanges, as is well known, lead to instability (Kadomtsev, 1966).

3.3 Suydam's Condition

To proceed, we now examine the behavior of the marginal Euler-Lagrange solutions in the neighborhood of the singular point corresponding to $\mathbf{k} \cdot \mathbf{B} = 0$. To do this we first introduce the quantity

$$\mu = \frac{B_\phi}{rB_z}, \quad (3.16)$$

which is related to the pitch of the field lines. Using (3.16), we rewrite (3.7) and (3.8) as

$$f(r) = \frac{r^3 B_z^2}{4\pi} \frac{\left(\mu + \frac{k}{m}\right)^2}{\left(1 + \frac{r^2 k^2}{m^2}\right)} \quad (3.17)$$

and

$$g(r) = \frac{\frac{2r^2 k^2}{m^2}}{\left(1 + \frac{r^2 k^2}{m^2}\right)} \frac{dP}{dr} - \frac{2r^3}{4\pi} \frac{B_z^2 k^2}{m^2} \left(\mu^2 - \frac{k^2}{m^2}\right) \frac{1}{\left(1 + \frac{k^2 r^2}{m^2}\right)^2} + \frac{r B_z^2 \left[m^2 \left(1 + \frac{r^2 k^2}{m^2}\right) - 1 \right]}{4\pi \left(1 + \frac{r^2 k^2}{m^2}\right)} \left(\mu + \frac{k^2}{m^2}\right)^2. \quad (3.18)$$

The singular point (sometimes referred to as the singular surface) occurring at $\mathbf{k} \cdot \mathbf{B} = 0$ then becomes equivalent to

$$\frac{k}{m} = -\mu(r_s), \quad (3.19)$$

where r_s denotes the value of r where $\mathbf{k} \cdot \mathbf{B} = 0$, i.e., where the Euler-Lagrange equation becomes singular. We now expand $f(r)$ and $g(r)$ around the singular point r . Thus

$$\mu + \frac{k}{m} \approx \mu' x, \quad (3.20)$$

where $x = r - r_s$ and $\mu' = d\mu/dr|_{r=r_s}$. Such an expansion necessarily implies that we are examining local perturbations about the singular point which correspond to high m . A Taylor-series expansion of (3.17) and (3.18) yields

$$f(r) \approx \left[r \frac{B_\phi^2 B_z^2}{4\pi B^2} \left(\frac{d \log \mu}{dr} \right)^2 \right]_{r_s} x^2 = \alpha x^2 \quad (3.21)$$

and

$$g(r) \approx \left[\frac{2B_\phi^2}{B^2} \frac{dP}{dr} \right]_{r_s} = \beta, \quad (3.22)$$

where $B^2 = B_\phi^2 + B_z^2$, so that (3.12) reduces to

$$\alpha \frac{d}{dx} \left(x^2 \frac{d\xi}{dx} \right) - \beta \xi = 0. \quad (3.23)$$

DANIEL S. SPICER

The solutions to (3.23) are x^{-n_1} and x^{-n_2} , where n_1 and n_2 are the roots to the indicial equation

$$n^2 - n - \left(\frac{\beta}{\alpha}\right) = 0 \quad (3.24)$$

obtained from the power series solution of (3.23), i.e.,

$$\xi = x^n \sum_{\ell=0}^{\infty} c_{\ell} x^{\ell}. \quad (3.25)$$

The roots of (3.24) are real and unequal if $\alpha + 4\beta > 0$ and are complex conjugates if $\alpha + 4\beta < 0$. The real solutions of the Euler-Lagrange equation corresponding to $\alpha + 4\beta < 0$ are

$$\xi = x^{-n} + x^{-n^*} \text{ and } \xi = i(x^{-n} - x^{-n^*}), \quad (3.26)$$

which are oscillatory in the neighborhood of r_s . Since we require the solutions to be nonoscillatory near r_s , we must take the roots corresponding to $\alpha + 4\beta > 0$, which then gives a necessary condition for stability, first derived by Suydam (1958) and generally called Suydam's condition:

$$\frac{r}{4} \left(\frac{\mu'}{\mu}\right)^2 + \frac{8\pi P'}{B_z^2} > 0. \quad (3.27)$$

Equation (3.27) has a number of physical consequences. Since for small but nonvanishing values of r Suydam's condition reduces to $dP/dr > 0$, we can conclude that a necessary condition for stability is that the plasma pressure should have a minimum at $r = 0$ (Newcomb, 1960). This follows because the dP/dr term is only of order r . It further follows that any pinch with a pressure distribution that decreases in a radially increasing direction is unstable if $\mu = \text{constant}$ and is absolutely unstable if $B_z = \text{constant}$ and the current density is uniform (Kadomtsev, 1966).

Physically it is of interest to ask how the instability manifests itself if the Suydam condition is violated. To answer this question, we follow a heuristic argument due to Suydam (1958). Let us assume a displacement ξ corresponds to an unstable solution to (3.12). This will lead to new values of P , B_{ϕ} , B_z , and ρ in the neighborhood of the singular point $\mathbf{k} \cdot \mathbf{B} = 0$. Since this instability is convective, we expect mixing of the perturbed quantities. We simulate this mixing by replacing P , ρ , B_{ϕ} , and B_z by the values obtained by averaging over the angle ϕ . We then ask whether the new distribution is stable or unstable using Suydam's condition again. We find that the convective mixing results in a distribution which is less unstable on the inside and more unstable on the outside. Thus, if some interior point or surface were unstable, it would convect outward until it became stable, and this in turn will upset the stability of the next surface exterior to it. This perturbation would then convectively propagate toward the outer boundary, greatly increasing the volume of instability. This situation can easily occur in the arch because of its large length and therefore closely spaced modes.

Two things are to be remembered concerning Suydam's condition (3.27). It is only a local stability criteria and thus is valid only for high m modes, $m \gg 1$, near the singular surface $\mathbf{k} \cdot \mathbf{B} = 0$. In addition Suydam's condition breaks down if both $dP/dr = 0$ and $\mu' = 0$ at some value of r . To treat this case requires retention of higher order terms in our Taylor-series expansion of (3.17) and (3.18). Goedbloed (1973) has examined this question and obtains a generalized Suydam's criterion valid even if dP/dr vanishes, e.g., a force-free pinch. Here we only reproduce the result, noting that the analysis follows lines similar to the derivation of the Suydam condition given here. Goedbloed (1973) finds

$$\frac{dP}{dr} + \frac{B_\phi^2 B_z^2}{4\pi B^3} \left| \frac{B_z \mu'}{m\mu} \right| - \frac{B_\phi^2 B_z^4}{2\pi r m^2 B^6} > 0,$$

if

$$1 \ll |m| < \frac{4B_\phi^2}{rB^2} \left| \frac{B_z \mu}{B\mu'} \right|, \quad (3.28)$$

and

$$\frac{dP}{dr} + \frac{rB_z^2}{32\pi} \left(\frac{\mu'}{\mu} \right)^2 > 0,$$

if

$$|m| > \frac{4B_\phi^2}{B^2} \left| \frac{B_z}{B} \frac{\mu}{\mu'} \right|. \quad (3.29)$$

These conditions are necessary conditions for stability and are valid only for low-shear systems.

3.4 Shear Stabilization

Before proceeding, we will discuss the question of shear and its effect on stability. A magnetic-field configuration is said to have shear if

$$\frac{d\mu}{dr} \neq 0, \quad (3.30)$$

μ being defined by (3.16). A magnetic arch with an extreme case of shear is illustrated in Fig. 6. If a magnetic system is shearless, we can easily conclude that the pitch of the lines of force is independent of radius. This permits the free interchange of any two field lines, separated by any radial distance of that magnetic-field configuration. This interchange or convection occurs simply because the field lines are identical, i.e., the system is degenerate. As is well known, such an interchange is highly unstable (Kadomtsev, 1966),

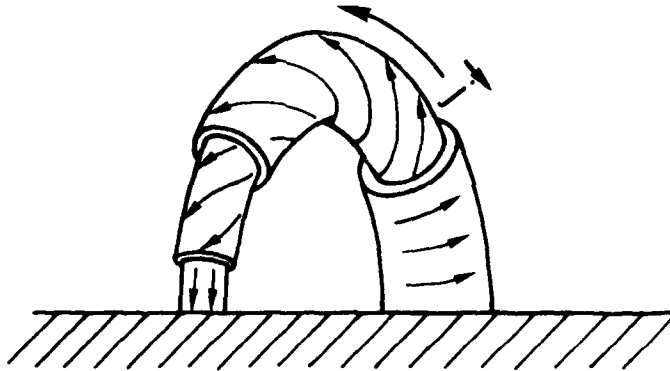


Fig. 6 — An example of a sheared magnetic field in an arch

since it causes a minimal distortion of the magnetic field, thereby minimizing any restoring forces the distortion of the magnetic field might produce which would tend to cause the equilibrium state to be restored. The perturbation would then tend to *grow*. Hence, by inducing shear, the field lines form an angle with respect to one another, which effectively limits the length over which convection of the field lines can occur to a value $L \approx 2\pi B^2 / (B_z^2 r \mu')$.

Imposing the condition that the field lines have a finite length and are embedded in a plasma with high conductivity at each end has an effect similar to shearing the field lines. This occurs for two reasons: it limits the maximum wavelength of a perturbation to the length of the system, as pointed out earlier, and it inhibits the long-wavelength interchange of fields. This can be seen as follows: Suppose two field lines are frozen to conducting endplates. To obtain instability requires the potential energy to be negative. However, the only way to interchange two field lines frozen at different points on an endplate is to twist the field lines. This however requires energy; hence the potential energy of the system will increase, *not* decrease, due to this form of interchange. Thus tying the field lines tends to increase the stability of the system.

3.5 The Kink Instability

As we have found earlier, the most unstable modes correspond to $m = 0$ and $m = 1$, the $m = 1$ mode being the least stable. An examination of Eq. (3.10) shows that the diffuse pinch is unstable to the sausage mode when

$$\beta_z = \frac{8\pi P}{B_z^2} \quad (3.31)$$

is large. Hence demanding a small β_z will stabilize the $m = 0$ mode. However the kink mode (sometimes called the helical or screw mode) is not easily stabilized. As we have already seen from our local analysis of the high m modes, perturbations with a pitch matching the pitch of the field lines are the most dangerous. Although the local analysis

of high- m modes is not valid for nonlocal perturbations $|m| = 1$, it still follows that a perturbation with a pitch equal to that of the field is dangerous.

A condition for stability of the kink mode may be obtained by examining the resonance condition between the pitch of the field and perturbation, namely $\mathbf{k} \cdot \mathbf{B} = mB_\phi / r + kB_z = 0$. Since by Eq. (3.11) $k = 2\pi n/L$, this condition may be written as

$$m + nq = 0, \quad (3.32a)$$

where

$$q(r) = \frac{2\pi r B_z}{L B_\phi} \quad (3.32b)$$

is called the safety factor. When

$$q(r) = \frac{m}{n}, \quad (3.33)$$

the perturbations are resonant and appear helical or like a screw thread. This can be seen by noting that helical lines have a pitch

$$\frac{d\phi}{dz} = \frac{n2\pi}{mL} \quad (3.34)$$

and that the magnetic field lines have a pitch

$$\frac{d\phi}{dz} = \frac{B_\phi}{rB_z}. \quad (3.35)$$

When these pitches are equal, we have the resonance condition $\mathbf{k} \cdot \mathbf{B} = 0$ and the perturbations are thus helical. In particular, when

$$q \leq 1, \quad (3.36)$$

the most dangerous kink mode $m = 1$ and $n = 1$ is unstable, in addition to any other kink mode that satisfies the condition $m/n = 1$. When $q > 1$, we have the so-called Kruskal-Shafranov condition. Hence we can state that if the safety factor q drops to ≤ 1 anywhere inside or outside the plasma, the pinch is unstable. However even if the condition $q > 1$ is satisfied everywhere in the plasma, there can still be unstable kinks (with $m/n > 1$) provided the point $q(r) = m/n$ falls into a plasma region of finite electrical conductivity. In this case the unstable mode is called a resistive kink or a tearing mode (and in the Soviet literature is referred to as the resistive screw instability).

3.6 The Role of Resistivity and Curvature

The effects of resistivity on stability will be discussed in detail in the next section. However it should be obvious that permitting finite resistivity will lower the stability of a pure MHD configuration ($\eta = 0$). The differences between a situation where $\eta = 0$ and $\eta \neq 0$ are principally that with $\eta = 0$ the field and plasma are frozen together: where one moves so must the other. When $\eta \neq 0$, slippage can occur, such that the plasma can lag behind when the magnetic field changes. Hence within a configuration that is MHD stable the presence of finite resistivity will permit previously forbidden deformations of the plasma to take place that are often unstable. In particular we will find that resistivity can destroy stabilization achieved by shear. For example consider the diffuse pinch. If it were to kink without completely carrying the B_z component of the field with it, a j'_ϕ current component will result in addition to the original j_z . This new j'_ϕ will give rise to an additional $j'_\phi \times B_z$ force which causes the perturbation to grow.

It would be appropriate to examine the affect of curvature or toroidal effects of a magnetic arch on MHD stability. Let us first examine Laplace's equation in cylindrical coordinates:

$$\frac{1}{r} \frac{\partial}{\partial r} \left(r \frac{\partial \Phi}{\partial r} \right) + \frac{\partial^2 \Phi}{\partial z^2} + \frac{1}{r^2} \frac{\partial^2 \Phi}{\partial \phi^2} = 0. \quad (3.37)$$

Upon introduction of the new dependent variable

$$\Phi = \sqrt{\frac{R}{r}} \psi \quad (3.38)$$

Eq. (3.37) becomes

$$\frac{\partial^2 \psi}{\partial r^2} + \frac{\partial^2 \psi}{\partial z^2} + \frac{1}{r^2} \left(\frac{\partial^2 \psi}{\partial \phi^2} + \frac{\psi}{4} \right) = 0, \quad (3.39)$$

which in terms of toroidal coordinates

$$r = \rho \cos \theta + R$$

and

$$z = \rho \sin \theta$$

becomes

$$\frac{1}{\rho} \frac{\partial}{\partial \rho} \left(\rho \frac{\partial \psi}{\partial \rho} \right) + \frac{1}{\rho^2} \frac{\partial^2 \psi}{\partial \theta^2} + \frac{\partial^2 \psi}{\partial (R\phi)^2} = 2\rho \frac{\cos \phi}{R} \frac{\partial^2 \psi}{\partial (R\phi)^2}, \quad (3.40)$$

where ρ is the minor radius of the torus and R is the major radius.

The term on the right-hand side of (3.40) represents the correction due to curvature. As $\rho/R \rightarrow 0$, we regain the cylindrical geometry. Hence if the inverse aspect ratio $\epsilon = \rho/R$ is small, then the toroidal effects are small. For magnetic arches $\epsilon \approx 1/5$ to $1/10$, and the approximation of cylindrical geometry is usually sufficient. The only change necessary when considering a magnetic arch is to let $L \approx \pi R$ in Eq. (3.11).

However one must not conclude from the above illustrations that curvature is totally unimportant. Consider first what occurs on bending magnetic field lines: If the lines of force are curved with a constant radius of curvature R_c such that $|\mathbf{B}|$ is constant, then charged particles will feel a force

$$\mathbf{F}_{cf} = \frac{m_e v_{\parallel}^2 \mathbf{R}_c}{R_c^2}, \quad (3.41)$$

which gives rise to a drift

$$\mathbf{v} = \frac{m_e v_{\parallel}^2 \mathbf{R}_c \times \mathbf{B}}{e B^2 R_c^2} \quad (3.42)$$

When we compute the $\nabla|\mathbf{B}|$ drift which would naturally accompany a bent magnetic field, we find a drift

$$\mathbf{v}_{\nabla B} = \frac{1}{2} \frac{m_e}{e} \frac{v_{\parallel}^2 \mathbf{R}_c \times \mathbf{B}}{R_c^2 B^2}. \quad (3.43)$$

The total drift in a curved vacuum field is thus

$$\mathbf{v}_T = \frac{m_e \mathbf{R}_c \times \mathbf{B}}{e R_c^2 B^2} \left(v_{\parallel}^2 + \frac{1}{2} v_{\parallel}^2 \right). \quad (3.44)$$

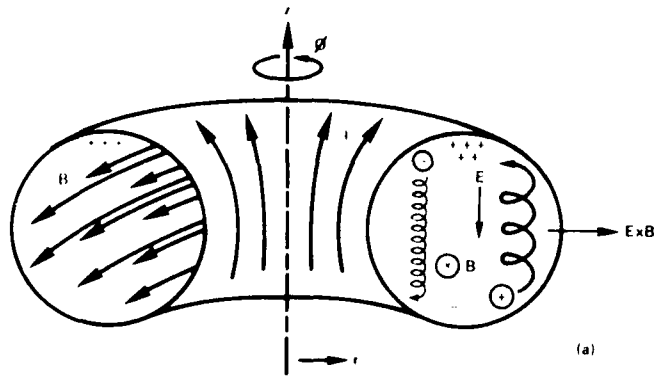
Because the two drifts add, the bent magnetic field or arch cannot confine a plasma within it; the plasma will just drift out, so that an equilibrium cannot be set up. Thus it is appropriate at this point to show why a toroidal current in an arch is needed to contain the high-density plasma observed within arches.

Consider Ampere's law

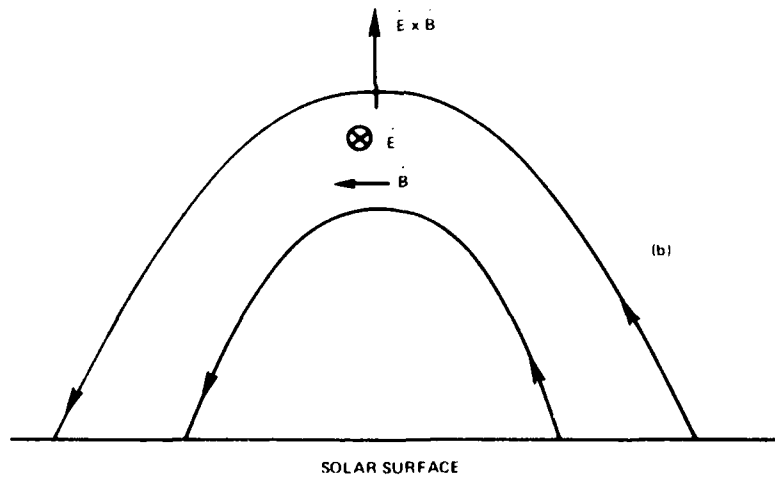
$$\oint \mathbf{B} \cdot d\mathbf{l} = \int_0^{\pi} B_T r d\phi = I, \quad (3.45)$$

where we have assumed that the toroidal field component of the arch B_T varies as $B_T \approx r^{-1}$ for simplicity. Because the gyrating particles have unequal Larmor radii in opposite halves of their orbits (Fig. 7), the ions and electrons drift to the sides of the arch and set up a horizontal electric field. This \mathbf{E} field will cause an $\mathbf{E} \times \mathbf{B}$ drift away from the major axis (upward). To reduce this effect, one permits a current to flow in the toroidal

DANIEL S. SPICER



IN A SIMPLE TORUS IN WHICH THE LINES OF FORCE ARE CLOSED CIRCLES, THE MAGNETIC FIELD VARIES AS $1/r$. THE RESULTING ∇B DRIFTS CAUSE A VERTICAL CHARGE SEPARATION, WHICH IN TURN CAUSES THE PLASMA TO DRIFT OUTWARD.



IN AN ARCH WITHOUT A CURRENT THE ∇B DRIFTS CAUSE A HORIZONTAL CHARGE SEPARATION, WHICH IN TURN CAUSES THE PLASMA TO DRIFT UPWARD.

Fig. 7 -- Plasma drift motions in a curved magnetic field

direction, which causes the field lines to appear twisted to the particles. Thus a particle gyrating along a field line will have an orbit which causes it to move upward and then downward. If one considers this effect from a fluid point of view, a helical line will connect regions of positive and negative polarity and will thereby short-circuit the horizontal electric fields. The helical field line will have a similar effect on any inertially induced electric field, e.g., a Rayleigh-Taylor-type instability.

To determine how good an approximation cylindrical geometry is when considering a curved system, it is sufficient to consider growth rates (Shafranov, 1970). In our discussion we found principally two types of instabilities: localized convective instabilities and nonlocalized kinklike instabilities. A localized convective instability in a pinch will have a growth rate (Rosenbluth et al., 1962)

$$\gamma^2 \approx \frac{g_{eff}}{r_0}, \quad (3.46)$$

where g_{eff} is an effective gravitational acceleration, which for a flute is

$$g_{eff} \approx \frac{B_p^2}{4\pi\rho} \frac{1}{R_s}, \quad (3.47)$$

where $R_s = r_0 B_T^2 / B_p^2$ is the average curvature of the helical field lines (not the arch curvature). The growth rate (3.46) corresponds to a force

$$F = \gamma^2 \rho \xi \approx \left(\frac{B_p^2}{2\pi r_0} \right) \left(\frac{B_p^2}{B_T^2} \right) \frac{\xi}{r_0} \quad (3.48)$$

acting per unit length of plasma.

If we compare this force with the force arising due to the global curvature of an arch,

$$F_R = \left(\frac{B_p^2}{4\pi r_0} \right) \left(\frac{r_0^2}{R^2} \right) \frac{\xi}{r_0}, \quad (3.49)$$

where R is the global curvature of the arch, we find that these forces are comparable when the safety factor q satisfies

$$q \gtrsim 1. \quad (3.50)$$

It then follows that flute instabilities of an arch must be studied by taking into account the global curvature of the arch. However, as we would find if we were to examine growth rates, the kink instability has a growth rate B_T/B_p greater than the convective instability (in cylindrical geometry B_z/B_θ). Since $B_T \gg B_p$ in cases that will interest us, we can conclude that MHD kink instabilities are so strongly growing in comparison to

local convective instabilities that the cylindrical analysis is adequate to treat the nonlocal kink modes (Shafranov, 1970) in arches.

3.7 Nonlinear Studies of the Kink Mode

Most nonlinear studies of the kink mode have been directed toward obtaining stable solutions to the pinch when the kink distorts the pinch sufficiently to cause it to buckle, which is generally referred to as pinch buckling. However to the author's knowledge no steady-state solutions have ever been found. The interested reader should consult Friedrichs (1960) and Yeh (1973) and references therein. Other nonlinear studies have been directed at studying the growth and nonlinear saturation of the kink.

One method employed (Rutherford et al., 1971) was to look at a bifurcation of the equilibrium solutions. Qualitatively the idea was to consider an equilibrium configuration which is marginally stable to a particular mode (m, k) , and seek a neighboring equilibrium with an infinitesimal kink in it. Thus, if the plasma configuration is slightly on the unstable side of marginal stability, then one should look for neighboring equilibria which possess a finite kink. If one can find this new equilibrium, i.e., if it exists, the amplitude of the kink can then be determined.

Kadomtsev and Pogutse (1974) proposed that the kink modes were nonlinearly unstable and, in so being, go to a very distorted final equilibrium which has little relationship to the initial equilibrium. They showed that this final equilibrium would in part have a vacuum or bubble within it, the mode number m determining the number of bubbles. However, numerical stimulation experiments (White et al., 1974) have found that when more realistic current-density profiles are taken into account, the nonlinear kink results in the deformation and compression of the flux surfaces on one side of the pinch.

4. RESISTIVE INSTABILITIES IN A DIFFUSE PINCH

4.1 Introduction

Resistive instabilities are important in the flare model to be developed, because they allow a greater rate of magnetic energy conversion, for a given value of resistivity, than the rate allowed by normal resistive diffusion. Thus resistive instabilities represent a means of rapid transition from a phase of the arch where significant conversion of magnetic energy does not occur to a phase where this conversion occurs at a rapid rate, thereby causing a flare.

Resistive instabilities differ from MHD modes in that finite resistivity is required, so that modes which are topologically inaccessible in the zero-resistivity limit become accessible when resistivity is taken into account. For example, as is well known, the MHD assumption $\eta = 0$ constrains one to conserve magnetic flux, so that

$$\frac{d\Phi}{dt} = 0, \quad (4.1)$$

where

$$\Phi = \frac{1}{c} \oint \mathbf{B} \cdot d\mathbf{S}. \quad (4.2)$$

Thus the potential energy in the MHD limit can be lowered only if the motions obey this constraint. This constraint implies magnetic surfaces remain well defined and the topology of the field cannot be broken up but can only be distorted. However, when finite resistivity is permitted, this constraint is relaxed, so that

$$\frac{d\Phi}{dt} = IR, \quad (4.3)$$

where I is the total current and R the total resistance. Hence magnetic flux need no longer be conserved; i.e., reconnection can occur, e.g., by the tearing mode. The ensuing reconnection manifests itself as thermalization of magnetic energy, i.e., joule heating, and directed plasma flow.

As briefly discussed in the previous section, resistivity can alter the stability of a stable MHD configuration. The high temperatures of the solar atmosphere necessarily imply high electrical conductivities. As is well known (Jackson, 1962), a hydromagnetic state can be characterized by the magnetic Reynolds number

$$S = \frac{\tau_R}{\tau_H}, \quad (4.5)$$

where

$$\tau_R = \frac{4\pi a^2}{\eta c^2} \quad (4.6)$$

and

$$\tau_H = \frac{a(4\pi\rho)^{1/2}}{B}. \quad (4.7)$$

If $S \gg 1$, the plasma is effectively frozen to the magnetic field, and $S \ll 1$ implies the plasma may diffuse relative to the field. Since S is large in the solar atmosphere, S^{-1} may be used as an expansion parameter in the hydromagnetic equations. Assuming there are no discontinuities in the equilibrium configuration of the plasma-magnetic system, one can show that the eigenfrequencies, obtained when using the MHD approximation, are altered at most by terms of order S^{-1} . Unstable MHD modes are therefore affected little, and stable modes cannot become unstable to any degree, since their maximum growth rates are of order τ_R . Hence one must look for new unstable modes, which exist only with the presence of finite resistivity. Specifically one searches for modes which are topologically inaccessible in the MHD analysis; that is, one looks for modes in which magnetic flux surfaces, which are initially separated, can link up during the evolution of the perturbation.

4.2 Resistive Instabilities in Planar Geometry

The treatment of resistive instabilities is in general more complex than MHD instabilities, because the resulting differential equations are fourth order, and the important modes are spatially localized in a small neighborhood centered around the singular surface $\mathbf{k} \cdot \mathbf{B} = 0$, or result from modes which are singular in the absence of dissipation. The significance of the singular surface, as will become clear, derives from the fact that when the resistivity is finite, the plasma is completely detached from the magnetic field in a small region around the singular surface. Such an effect enables the system to go from states of high potential energy to states of neighboring lower potential energy, which are not accessible without dissipation. In particular the energy released when going from the higher potential state to the lower potential state thermalizes the magnetic field and generates directed kinetic energy.

The general development of the theory of resistive instabilities began with the work by Furth, Killeen, and Rosenbluth (1963), whose analysis is based on an extension of the MHD theory by inclusion of the relevant dissipative effects. We will here briefly summarize the analysis involved, using the FKR paper since it provides a useful clarification scheme for the various resistive instabilities to be discussed throughout the remainder of this report. To begin, we assume the MHD approximation is valid and that pressure and inertial terms can be neglected in Ohm's law. Isotropic pressure and resistivity are assumed, and the plasma is considered incompressible. Perturbations in resistivity and the effective gravity (curvature, acceleration of the current layer, etc.) can result only from convection. The equations we will use are

$$\frac{\partial \mathbf{B}}{\partial t} = \nabla \times (\mathbf{v} \times \mathbf{B}) - \frac{c^2}{4\pi} \nabla \times (\eta \nabla \times \mathbf{B}), \quad (4.8)$$

$$\mathbf{E} + \frac{1}{c} \mathbf{v} \times \mathbf{B} = \eta \mathbf{j} \quad (4.9)$$

and

$$\text{curl} \left(\rho \frac{d\mathbf{v}}{dt} \right) = \text{curl} \left(\frac{1}{4\pi} (\text{curl } \mathbf{B}) \times \mathbf{B} + \rho \mathbf{g} \right). \quad (4.10)$$

Since the treatment is principally concerned with resistive instabilities whose growth times are long compared to MHD transit time, we are justified in using the incompressibility approximation $\nabla \cdot \mathbf{v} = 0$.

Since we are examining only changes in resistivity that result from convection, we have

$$\frac{\partial \eta}{\partial t} + \mathbf{v} \cdot \nabla \eta = 0 \quad (4.11)$$

and

$$\frac{\partial}{\partial t} (\rho \mathbf{g}) + \mathbf{v} \cdot (\rho \mathbf{g}) = 0, \quad (4.12)$$

where ρ is the mass density.

First-order quantities are denoted by the subscript 1. Using the equations $\nabla \cdot \mathbf{B}_1 = 0$ and $\nabla \cdot \mathbf{v}_1 = 0$, we obtain the perturbed first-order equations from Eqs. (4.8) through (4.12):

$$\begin{aligned} \frac{\partial \mathbf{B}_1}{\partial t} = & (\mathbf{B}_0 \cdot \nabla) \mathbf{v}_1 - (\mathbf{v}_1 \cdot \nabla) \mathbf{B}_0 + \frac{c^2}{4\pi} (\eta_0 \nabla^2 \mathbf{B}_1 + \eta_1 \nabla^2 \mathbf{B}_0) + c^2 \text{curl } \mathbf{B}_1 \times \nabla \eta_0 \\ & + c^2 \text{curl } \mathbf{B}_0 \times \nabla \eta_1, \end{aligned} \quad (4.13)$$

$$-\rho_0 \frac{\partial}{\partial t} (\nabla^2 \mathbf{v}_1) = \text{curl curl} \left\{ \frac{1}{4\pi} [(\mathbf{B}_0 \cdot \nabla) \mathbf{B}_1 + (\mathbf{B}_1 \cdot \nabla) \mathbf{B}_0] + (\rho \mathbf{g})_1 \right\}, \quad (4.14)$$

$$\frac{\partial \eta_1}{\partial t} + (\mathbf{v}_1 \cdot \nabla) \eta_0 = 0, \quad (4.15)$$

and

$$\frac{\partial}{\partial t} (\rho \mathbf{g}_1) + (\mathbf{v}_1 \cdot \nabla) (\rho \mathbf{g}_0) = 0. \quad (4.16)$$

We will first consider a simple sheet-pinch model. Consider an unperturbed magnetic field which is sheared in the y direction.

$$\mathbf{B}_0 = iB_x(y) + kB_y(y), \quad (4.17)$$

with all perturbed quantities varying as

$$\delta f(\mathbf{x}, t) = f(y) \exp[i(k_x x + k_z z) + \omega t]. \quad (4.18)$$

Following FKR, we find the perturbed equations can be reduced (after some algebra) to two coupled second-order differential equations:

$$\frac{\psi''}{\alpha^2} = \psi \left(1 + \frac{p}{\tilde{\eta} \alpha^2} \right) + \frac{W}{\alpha^2} \left(\frac{F}{\tilde{\eta}} + \frac{\tilde{\eta}' F'}{\tilde{\eta} p} \right) \quad (4.19)$$

and

$$\frac{(\tilde{\rho}W)'}{\alpha^2} = W \left[\tilde{\rho} - \frac{S^2 G}{\rho^2} + \frac{FS^2}{\rho} \left(\frac{F}{\tilde{\eta}} + \frac{\tilde{\eta}' F'}{\tilde{\eta} \rho} \right) + \psi S^2 \left(\frac{F}{\tilde{\eta}} - \frac{F'}{\rho} \right) \right], \quad (4.20)$$

where differentiation is with respect to $\mu = y/a$ and where we define the dimensionless variables

$$\begin{aligned} \psi &= \frac{B_1 y}{B}, & S &= \frac{\tau_R}{\tau_H}, \\ W &= -i v_{1y} k \tau_R, & \rho &= \omega \tau_R, \\ F &= \frac{\mathbf{k} \cdot \mathbf{B}}{kB}, & \tilde{\eta} &= \frac{\eta_0(\mu)}{\langle \eta \rangle}, \\ \alpha &= ka, & B &= (B_x^2 + B_y^2)^{1/2}, \\ k &= (k_x^2 + k_y^2)^{1/2}, & \tilde{\rho} &= \frac{\rho_0(\mu)}{\langle \rho \rangle}, \end{aligned} \quad (4.21)$$

Here a is a length characterizing the width of the current layer, τ_R and τ_H are characteristic resistive diffusive times and MHD transit times, ie,

$$\tau_R = \frac{4\pi a^2}{\langle \eta \rangle c^2} \quad \text{and} \quad \tau_H = \frac{a(4\pi \langle \rho \rangle)^{1/2}}{B},$$

in which $\langle \eta \rangle$ and $\langle \rho \rangle$ are average measures of the resistivity and density and G is a quantity representing the driving force due to the effective gravitational force. For example $G = (\omega_p \tau_H)^{1/2}$, where $\omega_F = (g\rho'_0/\rho_0)^{1/2}$ is the growth rate for a flute. The variable S is the magnetic Reynolds number, which, when large, implies the magnetic field and plasma follow each other's behavior closely, ψ is the perturbed magnetic field, and W is the displacement caused by the perturbation. Since in equilibrium $\mathbf{v}_0 = 0$ and $\nabla \times (\eta_0 \nabla \times \mathbf{B}_0) = 0$, we have the additional constraint

$$\tilde{\eta} F' = \text{constant}. \quad (4.22)$$

The quantity F plays an important role in what is to follow; therefore its interpretation should be made clear. The unperturbed magnetic field always appears in Eqs. (4.19) and (4.20) in the form $\mathbf{k} \cdot \mathbf{B}$. Since \mathbf{B} possesses shear by assumption, we can always choose \mathbf{k} so that there is some $\mu = y/a$ for which $F = \mathbf{k} \cdot \mathbf{B}/kB = 0$. When this occurs, we are at the singular surface as discussed in the previous section. We should expect then that any unstable modes will be sharply peaked about this surface (a plane in the present case and a helical ribbon in the cylindrical case), since at this surface the pitch of the

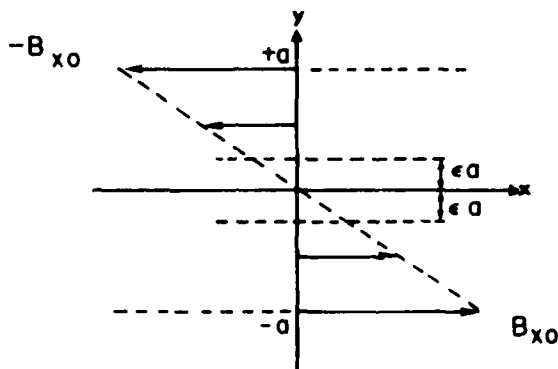


Fig. 8 - Equilibrium sheared magnetic field

perturbation equals the pitch of the unperturbed field. In particular, at this surface the plasma and field are decoupled. To see this, consider Eq. (4.13):

$$\frac{\partial B_{1y}}{\partial t} \approx i(\mathbf{k} \cdot \mathbf{B})v_{1y} + \frac{c^2}{4\pi} \eta_0 \nabla^2 B_{1y}. \quad (4.23)$$

When the plasma temperature is high, η_0 is small, so that the last term on the right-hand side of Eq. (4.23) is small compared to the first term and can be safely neglected. However, when $\mathbf{k} \cdot \mathbf{B} \approx 0$, the last term can no longer be neglected, so that, when $\mathbf{k} \cdot \mathbf{B} = 0$ at the singular surface, the plasma and field are completely decoupled. Also, if reconnection is to occur, i.e., $B_{1y} \neq 0$, η_0 must be finite. This follows because if $\eta_0 = 0$, v_{1y} must be infinite to produce a finite B_{1y} at $\mathbf{k} \cdot \mathbf{B} = 0$.

In the interest of clarity an example is in order. Using Fig. 8, we assume an equilibrium magnetic field exists with the properties $\mathbf{B} = (y, 0, 0)$ such that $B_{x0} = y$ in the interval $-a < y < a$. Thus, it follows from Ampere's law that $\mathbf{j} = (0, 0, c/4\pi)$, and we see that the equilibrium magnetic field reverses direction when crossing the $y = 0$ layer; i.e., the field experiences a 180° shear at the $y = 0$ layer, and a neutral point in \mathbf{B} occurs at $y = 0$ at every x .

The condition $\mathbf{k} \cdot \mathbf{B} = 0$ implies a wave-number vector \mathbf{k} can always be chosen for a given perturbation of that $\mathbf{k} \cdot \mathbf{B}$ will vanish at any desired point. This argument is supported by the fact that the component of \mathbf{B} perpendicular to \mathbf{k} is ignorable in the equations describing the perturbed fluid and field. Thus any field configuration can be reduced to that of a problem in the (k, y) plane by using the plane defined by the vectors \mathbf{k} and \mathbf{B} ; i.e., by choosing \mathbf{k} in the direction of the x axis in Fig. 8, we obtain the configuration previously considered.

Consider a twisted magnetic field that is sheared in cylindrical coordinates (r, ϕ, z) . We know $\mathbf{k} \cdot \mathbf{B} = kB_z + mB_\phi/r$; hence $\mathbf{k} \cdot \mathbf{B} = 0$ represents a helical line drawn about the z axis, with the pitch of the perturbation matching the pitch of the field. Thus on either side of this line the lines of force have a pitch which differs by 180° , which corresponds

to oppositely directed fields on each side of the resonance line $r = r_s$. This line may be rotated about the z axis to form a helical surface, which can be viewed as a helical current sheet.

Using Eqs. (4.19) and (4.20), we can show, following FKR, that the unstable modes grow and do not oscillate. Rearrangement of Eqs. (4.19) and (4.20) yields

$$\frac{p^2}{\alpha^2 S^2 F} \left[(\tilde{\rho} W')' + \alpha^2 W \left(\frac{S^2 G}{p^2} - \tilde{\rho} \right) \right] = (\rho \psi + WF) \left(pF' - \frac{F''}{F} \right) \quad (4.24)$$

and

$$\frac{p^2}{\alpha^2 S^2 F} \left[(\tilde{\rho} W')' + \alpha^2 W \left(\frac{S^2 G}{p^2} - \tilde{\rho} \right) \right] = p\psi'' - p\psi \left(\alpha + \frac{F''}{F} \right) \quad (4.25)$$

Using Eqs. (4.24) and (4.25) with the normalization condition $\tilde{\eta} F' = 1$, we find

$$\int_{\mu_1}^{\mu_2} \left\{ \frac{p^2}{|p|^2 \alpha^2 S^2} \left[\tilde{\rho} |W'|^2 + \alpha^2 |W|^2 \left(\tilde{\rho} - \frac{S^2 G}{p^2} \right) \right] + \frac{\left(pF' - \frac{F''}{F} \right)}{\left| pF' - \frac{F''}{F} \right|^2} \left| \psi' - \psi \left(\alpha^2 - \frac{F''}{F} \right) \right| \right. \\ \left. + |\psi'|^2 + |\psi|^2 \left(\alpha^2 + \frac{F''}{F} \right) \right\} d\mu = 0. \quad (4.26)$$

Taking the imaginary part of Eq. (4.26), we get

$$Im(p) = \int \left\{ \frac{2Re(p)}{|p|^2 \alpha^2 S^2} [\tilde{\rho} |W'|^2 + \alpha \tilde{\rho} |W|^2] + \frac{F' \left| \psi'' - \psi \left(\alpha^2 + \frac{F''}{F} \right) \right|^2}{\left| pF' - \frac{F''}{F} \right|^2} \right\} d\mu = 0. \quad (4.27)$$

By our normalization $\tilde{\eta} F' = 1$ and $F' > 0$. Hence, if $Im(p) \neq 0$, we must have $Re(p) < 0$. For instability ($p > 0$) it is necessary to have negative contributions of sufficient magnitudes from the terms which satisfy Eq. (4.26). Each possibility gives rise to a different type of resistive instability. They are:

- **Gravitational mode.** For large Reynolds number S and $G > 0$, but S not so large that we obtain the MHD mode, the required negative contribution is provided by the term containing G in Eq. (4.26);

- **Rippling mode.** ψ is peaked near the singular surface $F = 0$, and, if $F''/F > 0$, the required negative contribution comes from the second term in Eq. (4.26);

• Tearing mode. If $\alpha^2 = (ka)^2$ is sufficiently small and $F''/F < 0$, the third term in (4.26) can be negative.

The rippling and tearing modes require a nonuniform resistivity and thus a nonuniform shear. This can be seen by differentiating the normalization condition $\tilde{\eta}F' = 1$ with respect to μ :

$$F'' = - \frac{1}{\tilde{\eta}^2} \frac{d\tilde{\eta}}{d\mu} . \quad (4.28)$$

As we have already established, resistivity is important only near the singular surface $\mathbf{k} \cdot \mathbf{B} = 0$. Hence it is reasonable to use the MHD ($\eta \rightarrow 0$) solutions to Eqs. (4.24) and (4.25) for ψ except in the neighborhood of the singular surface. Letting $S \rightarrow \infty$ in Eq. (4.24) yields

$$p\psi = -FW, \quad (4.29)$$

which is valid everywhere except near $F = 0$ ($\mathbf{k} \cdot \mathbf{B} = 0$). Letting $S \rightarrow \infty$ in Eq. (4.25) yields

$$\psi'' - \psi \left(\alpha^2 + \frac{F''}{F} \right) - \frac{WG}{pF} = 0. \quad (4.30)$$

Using Eq. (4.29) in (4.30), we find

$$\psi'' - \psi \left(\alpha^2 + \frac{F''}{F} - \frac{G}{F^2} \right) = 0. \quad (4.31)$$

This equation is called the infinite conductivity equation and must be satisfied everywhere except where $F = 0$. Only Eqs. (4.24) and (4.25) are valid at $F = 0$. A formal means of solving the equations is to use Eqs. (4.29) and (4.31) for asymptotic solutions to Eqs. (4.24) and (4.25), which break down at $F = 0$. Making a power-series expansion of Eqs. (4.24) and (4.25) around the point corresponding to $F = 0$ yields the solutions valid where $F = 0$. Hence matching these two sets of solutions yields a complete solution to the problem. We will not consider these solutions here but rather examine those properties of the modes which lend themselves to simple approximation arguments.

Assume in Ohm's law, Eq. (4.9), that the plasma is moving but the magnetic flux lines are not (i.e., $\mathbf{E} = 0$). Thus $\mathbf{j} = (\mathbf{v} \times \mathbf{B})/\eta c$ and there is a resultant volume force

$$\mathbf{F}_s = \frac{1}{c} (\mathbf{j} \times \mathbf{B}) = \frac{[\mathbf{B}(\mathbf{v} \cdot \mathbf{B}) - \mathbf{v}B^2]}{\eta c^2} , \quad (4.32)$$

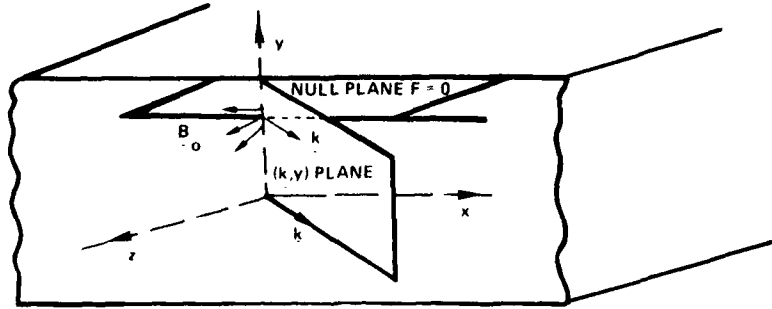


Fig. 9 - Geometry of a resistive sheet pinch

which is a restoring force except where $\mathbf{B} \rightarrow 0$. For our purposes \mathbf{B} refers only to the components in the (k, y) plane (Fig. 9). When instability occurs, there will be a volume driving force \mathbf{F}_0 which opposes \mathbf{F}_s and which is of the same order as \mathbf{F}_s . Thus the rate at which work is done on the plasma at the singular surface ($\mathbf{k} \cdot \mathbf{B} = 0$) is of the order

$$P \approx \mathbf{v} \cdot \mathbf{F}_s \approx \frac{v_y^2 B^2}{\eta c^2} \approx \frac{v_y^2 (B')^2 (\epsilon a)^2}{\eta c^2} \quad (4.33)$$

The component of \mathbf{B} in the (k, y) plane has a value $B = B' \epsilon a$ near the singular surface, in which ϵ is a dimensionless quantity used to measure the width of the region of interest where the mode is localized. Furthermore, since $\nabla \cdot \mathbf{v}_1 = 0$, $v_k \approx v_y / k \epsilon a$. In general $\epsilon k a \ll 1$, so that the plasma kinetic energy in the \mathbf{k} direction is dominant and of order $(k \epsilon)^{-2}$ greater than in the y direction. Equating the driving power and the plasma kinetic energy yields

$$\omega \rho_0 v_k^2 \approx \frac{\omega \rho_0 v_y^2}{(k \epsilon a)^2} = \frac{v_y^2 (B')^2 (\epsilon a)^2}{\eta c^2} \quad (4.34)$$

The perturbation is thus localized to a region of thickness

$$\epsilon a \approx \left(\frac{\omega \rho_0 \eta_0 c^2}{k^2 B'^2} \right)^{1/4} \quad (4.35)$$

Gravitational Mode

Estimation of growth rates requires an examination of specific modes. We consider first the gravitational mode, where the destabilizing force takes the form

$$\mathbf{F}_{D'} = \rho_1 \mathbf{g} = - \frac{v_y \rho_0' \mathbf{g}}{\omega} \quad (4.36)$$

Equating $\mathbf{F}_D \cdot \mathbf{v}$ with Eq. (4.33), we have

$$\frac{(B'_0)^2 (\epsilon a)^2}{\eta c^2} = \frac{\rho'_0 g}{\omega}, \quad (4.37)$$

and making use of Eq. (4.35) gives the growth rate

$$\omega = \left(\frac{\rho'_0 g k c \sqrt{\frac{\eta}{\rho_0}}}{B'_0} \right)^{2/3}. \quad (4.38)$$

In terms of the dimensionless variables previously defined we have

$$p \approx \alpha^{2/3} S^{2/3} G^{2/3}, \quad (4.39)$$

and

$$\epsilon \approx \alpha^{-1/3} S^{-1/3} G^{1/6}. \quad (4.40)$$

It is important to note that since S and α are generally quite large, we will have growth rates which are fast when compared to the classical diffusion time, and, since ϵ is small, the modes will be spatially highly localized. The gravitational mode is of basic interest here, because the term gdP_0/dy can be interpreted approximately as $(dP_0/dy)/R_c$, where P_0 is the plasma pressure and R_c is the radius of curvature of either arch or helical curvature due to the twisting field lines in the arch.

Rippling Mode

We next consider the rippling mode. The rippling mode is of interest because it is an instability which can convect current from a region of high resistivity into a region of low resistivity. In particular the current can form fine filaments of high current density. If certain conditions are satisfied, the current density within these filaments can grow by the resistive superheating instability (Kadomtsev, 1966) leading to other instabilities. This effect will be discussed in detail later.

To consider the rippling mode semiquantitatively, we must consider an additional term in the expansion of Ohm's law, i.e.,

$$\eta_0 \mathbf{j}_1 + \eta_1 j_0 = \frac{\mathbf{v} \times \mathbf{B}}{c}, \quad (4.41)$$

where

$$\eta_1 = - \frac{\mathbf{v} \cdot \nabla \eta_0}{\omega}. \quad (4.42)$$

The additional η_1 term gives rise to a volume force

$$\mathbf{F}'_D = \frac{\mathbf{j}_1 \times \mathbf{B}}{c} = \frac{\mathbf{v} \cdot \nabla \eta_0 \mathbf{j} \times \mathbf{B}}{c \omega \eta_0}, \quad (4.43)$$

which can be stabilizing or destabilizing depending on the sign of $\nabla \eta_0$. Hence both a stabilizing and destabilizing rippling mode exist.

Equating $\mathbf{v} \cdot \mathbf{F}'_D$ with Eq. (4.33), we obtain

$$\frac{v_y^2 \eta_0' (B')^2 (\epsilon a)}{4\pi \omega \eta_0} \approx \frac{v_y^2 (B')^2 (\epsilon a)^2}{\eta_0 c^2} \quad (4.44)$$

or

$$\epsilon a \approx \frac{\eta_0' c^2}{4\pi \omega}. \quad (4.45)$$

Using Eqs. (4.35) and (4.45), we obtain

$$\omega = \left[\frac{\eta_0'^4 c^6 k^2 B'^2}{(4\pi)^4 \rho_0 \eta_0 c^2} \right]^{1/5} \quad (4.46)$$

and

$$\epsilon \approx \frac{\eta_0'^2 c^2}{4\pi \omega a}. \quad (4.47)$$

We see that this mode depends in an essential way on η_0' ($\approx \eta_0/a$); i.e., a resistivity gradient must exist. Since resistivity classically depends only on temperature (with a weak logarithmic dependence on density), we can conclude that classically the rippling mode requires a current distribution in which a temperature gradient exists.

Tearing Mode

The tearing mode differs from the gravitational and rippling modes in that it is a long-wavelength instability in the y direction rather than a short-wavelength mode relative to the dimension of the current layer. Furthermore it is a pinching instability whose driving energy comes from the gross configuration, i.e., the structure of the configuration outside of the singular layer. It does not exist in the limit $\beta \rightarrow 0$. In particular, in the cylindrical diffuse pinch it is just a resistive kink instability. But most important, it is able to lower the energy content of the equilibrium magnetic configuration by joule heating and bulk plasma flow, the flow being directed along the helical sheet formed by the kink.

The perturbed current is

$$\frac{4\pi}{c} j_{11} \approx \frac{\partial B_{k1}}{\partial y} = -B'_k, \quad (4.48)$$

which is perpendicular to the (k, y) plane. Using $\nabla \cdot \mathbf{B}_1 = kB_k + B'_y = 0$, we have

$$j_{11} = \frac{cB''_y}{4\pi k}. \quad (4.49)$$

If $ka \ll 1$, i.e., for wavelengths greater than the current-layer thickness,

$$B''_y \approx \frac{B_y}{(\epsilon ka)a^2}. \quad (4.50)$$

The plasma is still not perfectly decoupled even near the singular surface, and

$$E_{11} \approx \frac{\omega B_y}{kc} \quad (4.51)$$

must be included in Ohm's law,

$$\eta_0 j_1 = \mathbf{E}_1 + \frac{\mathbf{v}_1 \times \mathbf{B}}{c}. \quad (4.52)$$

The quantity ϵa must now be selected so that \mathbf{E}_1 dominates $\mathbf{v}_1 \times \mathbf{B}$ in the region of partially decoupled plasma flow. Hence for instability

$$\frac{\eta_0 c B_y}{4\pi k \epsilon (ka)a^2} \approx \frac{\omega B_y}{kc} \quad (4.53)$$

or

$$\epsilon a \approx \frac{\eta_0 c^2}{4\pi k a^2 \omega}. \quad (4.54)$$

Using Eq. (4.35), we have the growth rate

$$\omega \approx \left[\frac{\eta_0^3 c^6 B'^2}{(4\pi)^4 \rho_0 k^2 a^8} \right]^{1/5} \quad (4.55)$$

DANIEL S. SPICER

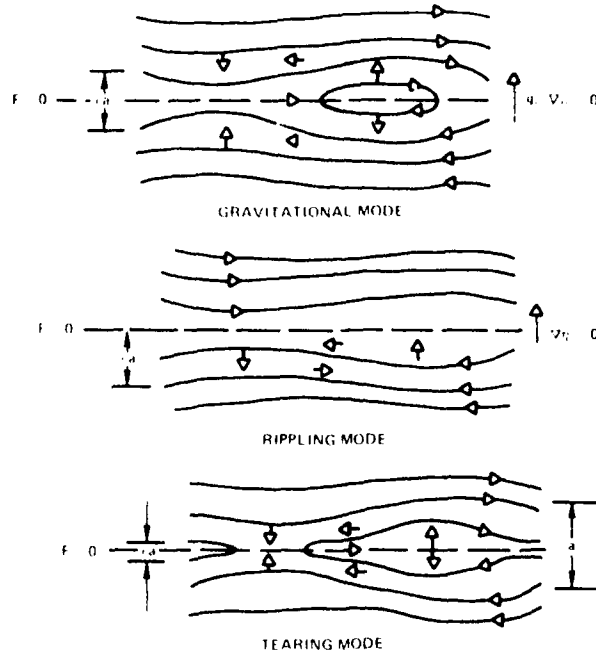


Fig. 10 — Perturbed fields and velocities for resistive instabilities

and

$$\epsilon \approx \frac{\eta_0 c^2}{4\pi k a^3 \omega} \quad (4.56)$$

The perturbed fields and velocities for the three modes discussed are illustrated in Fig. 10, and Table 1 summarizes the growth rates and threshold criteria of all three instabilities.

4.3 Resistive Instabilities in Cylindrical Geometry

At this point we translate the preceding results into the cylindrical geometry appropriate for an arch so that we can visualize the effects in a diffuse pinch with finite resistivity.

In cylindrical geometry Eqs. (4.19) through (4.21) become

$$\frac{1}{\mu m^2} (\mu \psi')' = \psi \left(\frac{1}{\mu^2} + \frac{\tilde{P}}{\tilde{\eta} m^2} \right) + \frac{W}{m^2} \left(\frac{F}{\tilde{\eta}} + \frac{\tilde{\eta}' F_1}{\tilde{\eta} P} \right), \quad (4.57)$$

Table 1 — Growth Rates and Threshold Conditions for Resistive MHD Instabilities

MODE	RANGE OF INSTABILITY	GROWTH RATE ρ	REGION OF DISCUSSION ϵ	VALID RANGE OF EQUATIONS
"RIPPLING"	$\bar{\eta} \neq 0$	$a^{2.5} S^{2.5}$	$a^{-2.5} S^{-2.5}$	$S^{-1.7} < a < S^{2.3}$ $ G < a^{-2.5} S^{2.5}$
"TEARING"	$a < 1$	$a^{-2.5} S^{-2.5}$	$a^{-3.5} S^{-2.5}$	$S^{-1.4} < a$ $ G < a^{-3.5} S^{-2.5}$
GRAVITATIONAL INTERCHANGE	$G > 0$	$a^{2.3} S^{2.3} G^{2.3}$	$a^{-1.3} S^{-1.3} G^{-1.6}$	$S^{-1.4} G^{1.3} < a < S^{1.2} G^{-1.4}$ $G < 1, a^2$ $G > a^{-2.5} S^{-2.5}, a^{-3.5} S^{-2.5}$

$$\frac{1}{\mu m^2} (\mu \tilde{\rho} W')' = W \left[\frac{\tilde{\rho}}{\mu^2} - \frac{S^2 G}{\rho^2} + \frac{FS^2}{P} \left(\frac{F}{\tilde{\eta}} + \frac{\tilde{\eta}'}{\tilde{\eta}} \frac{F_1}{P} \right) \right] + \psi S^2 \left[\frac{F}{\tilde{\eta}} - \frac{1}{\mu P} (\mu F_1)' \right], \quad (4.58)$$

and

$$\tilde{\eta}' \frac{F_1}{\tilde{\eta}} = - \frac{1}{\mu} (\mu F_1)', \quad (4.59)$$

where

$$F = \left(\frac{m B_\phi}{r} + k B_z \right) / k B, \quad (4.60)$$

$$F_1 = \frac{r_s}{m B} \left[\frac{m}{r} \frac{d}{dr} (r B_\phi) - k \frac{d B_z}{dr} \right], \quad (4.61)$$

and $\mu = r/r_s$, where r_s is defined as the singular point $F = 0$, i.e., $\mathbf{k} \cdot \mathbf{B} = 0$. All other quantities have the same definitions. The most important difference between the plane case and cylindrical case is G . Within Eqs. (4.57) through (4.59) the real local curvature is already taken into account. G however can contain the pressure gradient rather than the density gradient; hence

$$G \approx \frac{\left(\frac{dP}{dr} \right)}{R}. \quad (4.62)$$

An examination of Eqs. (4.57) through (4.59) shows that the equilibrium magnetic field appears only in the form $\mathbf{k} \cdot \mathbf{B}$, where $\mathbf{k} \cdot \mathbf{B} = 0$ corresponds to the surface at which a perturbation with the proper pitch matches the pitch of the magnetic field lines. Thus, when this surface does tear via the tearing mode, it will form a helical spiral along the z axis of the diffuse pinch.

We will now discuss the tearing mode in cylindrical geometry. The tearing mode is the most interesting mode in the context of our flare model, as well as in the formation of a number of quiescent features of arches and filaments. As we saw in the sheet pinch case, $\alpha \rightarrow 0$ corresponds to the most unstable case of the tearing mode. Assuming a low- β configuration, we can ignore the $m = 0$ mode, and we find the quantity α can no longer be made arbitrarily small, since α becomes (Furth et al., 1963)

$$\alpha^2 = \frac{m^2 a^2}{r_s^2} \left(1 + \frac{B_\phi^2}{B_z^2} \bigg|_{r=r_s} \right). \quad (4.63)$$

We therefore expect modes with small m and large r_s to be the least stable. In particular the $m = 1$ mode, the kink mode in the MHD approximation, is again the least stable mode although not the fastest growing mode. We might therefore expect some similarity between the MHD and finite resistivity modes, which indeed exists. To appreciate this, we must obtain the infinite conductivity equation in cylindrical coordinates. This is done in a way analogous to that of the sheet pinch. However we will alter the resulting equation so it will have a form similar to Eq. (3.12). By introducing $\xi = \psi/F$, we obtain, after letting $S \rightarrow \infty$, the infinite conductivity equation:

$$\frac{d}{dr} \left(HF^2 \frac{d\xi}{dr} \right) - \xi \left[g + H \left(\frac{dF}{dr} \right)^2 + \frac{Fd}{dr} \left(\frac{HdF}{dr} \right) \right] = 0, \quad (4.64)$$

where

$$HF^2 = \frac{r^3 (\mathbf{k} \cdot \mathbf{B})}{(k^2 r^2 + m^2)} = f, \quad (4.65)$$

$$H = \frac{r^3}{(k^2 r^2 + m^2)}, \quad (4.66)$$

$$F = \mathbf{k} \cdot \mathbf{B} = kB_z + \frac{mB_\phi}{r}, \quad (4.67)$$

and

$$g = \frac{2k^2 r^2}{(k^2 r^2 + m^2)} \frac{dp}{dr} + \frac{1}{r} (krB_z + mB_\phi)^2 \frac{(k^2 r^2 + m^2 - 1)}{(k^2 r^2 + m^2)} + \frac{2k^2 r}{(k^2 r^2 + m^2)} (k^2 r^2 B_z^2 - m^2 B_\phi^2). \quad (4.68)$$

A comparison of Eqs. (3.7) and (3.8) with Eqs. (4.64) through (4.68) shows that Eq. (4.64) is exactly the same Euler-Lagrange equation obtained for the diffuse pinch in the MHD approximation, except for the two additional terms $H(dF/dr)^2$ and $Fd(HdF/dr)/dr$. These two terms represent the magnetic driving energy of the tearing mode (Furth, 1963).

To see this, we write an action integral for Eq. (4.64) corresponding to marginal stability case. This is given by

$$W = \int_0^b \left\{ \left[HF^2 \left(\frac{d\xi}{dr} \right)^2 + \xi^2 g \right] + \xi^2 \left[H \left(\frac{dF}{dr} \right)^2 + \frac{Fd}{dr} \left(\frac{HdF}{dr} \right)^2 \right] \right\} dr \quad (4.69)$$

or

$$W = W_\infty + \int_0^b \xi^2 \left[H \left(\frac{dF}{dr} \right)^2 + F \frac{d}{dr} \left(\frac{HdF}{dr} \right)^2 \right] dr \quad (4.70)$$

or

$$W = W_{\infty} + W_{TM}, \quad (4.71)$$

where W_{∞} represents the MHD driving energy and W_{TM} represents the driving energy of the tearing mode. The difference between the MHD kink and the resistive kink follows from an examination of these two parts of the energy. The driving energy for both modes comes from the gross configuration. The MHD kink releases its magnetic energy principally in the form of oscillatory mechanical motion by the shortening of the lines of magnetic force, which then dissipates the azimuthal component of the magnetic field. The resistive kink (tearing mode) is able to lower its magnetic energy content when the topological restriction of infinite conductivity at the singular surface is removed, which then permits the field lines to reconnect and shorten, thereby lowering the energy of the field. The energy is then transformed to joule heat and directed kinetic energy.

At the singular surface for a given (k, m) , a helical current layer will exist across which there exists a null in $\mathbf{k} \cdot \mathbf{B}$, permitting the current layer to tear (Fig. 11). Many singular layers are possible corresponding to any particular pair (k, m) , and these layers are closely spaced in the arch. As we will find later, the high m and large k have the largest growth rate, but the small m and k are the most dangerous for stability because they involve gross displacements of the magnetic-field-plasma configuration.

As we noted earlier, one solves the infinite-conductivity equation outside of the singular layer and the finite-resistivity equations in the singular layer. One then matches the two sets of solutions across the resistive layer. The change in the solutions across this layer is defined as

$$\Delta' = \frac{d}{dr} (\psi_2 - \psi_1)|_{r=r_s} / \psi(r_s), \quad (4.72)$$

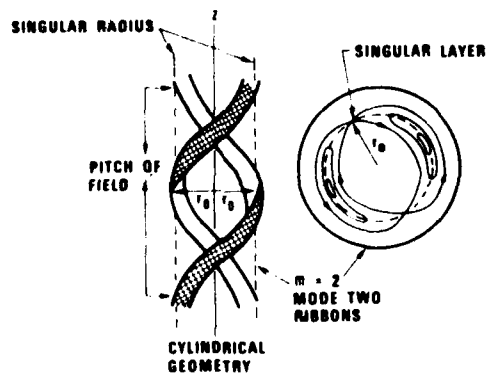


Fig. 11--The $m = 2$ mode in cylindrical geometry

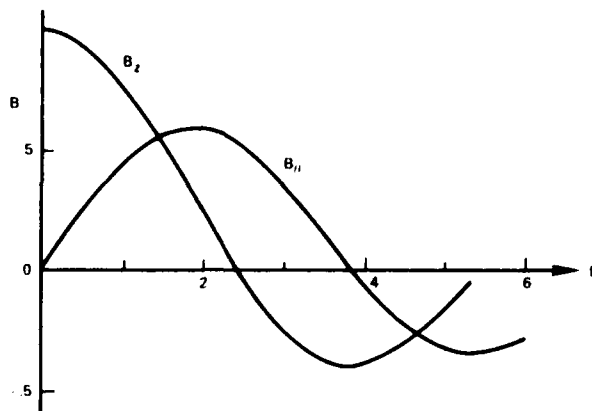


Fig. 12 — Magnetic field profiles for the Bessel-function model (BFM)

where ψ is the perturbed radial magnetic field, $\psi = B_{r1}/|B|$. The finite resistivity analysis in the vicinity of r_s shows that the condition for tearing-mode instability is $\Delta' > 0$, the condition for marginal stability is $\Delta' = 0$, and the condition for stability is $\Delta' < 0$ for the particular combination (k, m) being examined. The growth rate is then given by (Furth et al., 1973)

$$\gamma = 0.5m^{2/5} \Delta'^{4/5} \left(\frac{\eta_0}{4\pi} \right)^{3/5} \frac{\left[d \left(\frac{B_\phi}{r} \right) \right]^{2/5}}{(4\pi\rho_0)^{1/5}} \quad (4.73)$$

4.4 An Example of MHD and Resistive Instabilities in Cylindrical Geometry

To clarify the relationship between MHD instabilities and resistive instabilities in cylindrical geometry, an examination of the cylindrically symmetric Lundquist field is useful (Fig. 12),

$$B_r = 0, \quad B_\phi = B_0 J_1(\alpha r), \quad B_z = B_0 J_0(\alpha r), \quad (4.74)$$

where J_0 and J_1 are Bessel functions and α is constant (here α is taken to be unity). Furthermore we will permit only one reversal of B_z , which implies a conducting wall exists at $r = 5.52$, the second zero of B_z . The position of that wall will be denoted by R_W .

MHD theory shows that the position of the zeros of the solution to

$$\frac{d}{dr} \left(HF^2 \frac{d\xi}{dr} \right) - g\xi = 0 \quad (4.75)$$

determines the stability; i.e., if ξ has a zero before reaching the singular surface, then the particular (m, k) mode corresponding to ξ is MHD unstable. Voslamber and Callebaut (1962) used the MHD theory to study the stability of the Lundquist force-free field. Using the transformation $\xi = \psi/F$, they found for the Bessel-function model (BFM) that the equation for the perturbed magnetic field had no singularity, although ξ remained singular at $\mathbf{k} \cdot \mathbf{B} = 0$. They also show that the equations for ψ has solutions

$$\psi = \frac{kr}{1-kr} (1-k^2)^{1/2} Z_{m-1} [r(1-k^2)^{1/2}] + mZ_m [r(1-k^2)^{1/2}], \quad (4.76)$$

where

$$Z_m(x) = aJ_m(x) + bY_m(x), \quad (4.77)$$

in which a and b are constants and Y_m is a Bessel function of the second kind. Demanding that ξ be well behaved at $r = 0$, Voslamber and Callebaut (1962) obtain

$$\xi = \frac{kr}{1-k} \frac{(1-k^2)^{1/2} J_{m-1}(r\sqrt{1-k^2}) + mJ_m(r\sqrt{1-k^2})}{krJ_0(r) + mJ_1(r)}, \quad (4.78)$$

where the denominator of ξ is just $\mathbf{k} \cdot \mathbf{B}$ (see Eq. (4.74)). Thus for ξ to be stable for any pair of values (m, k) , ξ must not have any zeros before the denominator vanishes. The criteria for MHD stability reduces to examining the relative zeros of ψ and F . Thus, if ψ vanishes at a value of r smaller than the value for which $\mathbf{k} \cdot \mathbf{B} = 0$, that particular (m, k) mode is MHD unstable; if ψ vanishes after $\mathbf{k} \cdot \mathbf{B} = 0$, that particular (m, k) mode is MHD stable. For the BFM Voslamber and Callebaut (1962) show that ξ has no zeros for $k^2 > 1$ except at $r = 0$ and therefore that MHD instability can occur only for $k^2 < 1$.

Let us now examine the two lowest modes $m = 0$ and $m = 1$. For $m = 0$ we have

$$\xi = \frac{\sqrt{1-k^2}}{k-1} \frac{J_1(r\sqrt{1-k^2})}{J_0(r)}. \quad (4.79)$$

Since the first zero of $J_0(r)$ is always less than $J_1(r\sqrt{1-k^2})$, ξ has no singularity before ξ goes to zero. Hence ψ has a zero at a value of r greater than the value for which $\mathbf{k} \cdot \mathbf{B} = 0$. We can then conclude that the $m = 0$ mode for the BFM is stable for all k .

For the $m = 1$ mode the singular surfaces of ξ are obtained from

$$\mathbf{k} \cdot \mathbf{B} = B_0 [krJ_0(r) + J_1(r)] = 0, \quad (4.80)$$

and the $\psi = 0$ equation is

$$J_1(r\sqrt{1-k^2}) + \frac{kr\sqrt{1-k^2}}{1-k} J_0(r\sqrt{1-k^2}) = 0. \quad (4.81)$$

If ψ now has a zero at a radius smaller than that for which $\mathbf{k} \cdot \mathbf{B} = 1$ the ($m = 1, k$) mode is unstable. This occurs for the ($m = 1, k$) mode between the double intersection of the $\Delta' = 0$ curve and $\mathbf{k} \cdot \mathbf{B} = 0$ curves, as shown in Fig. 14) i.e., at $k = 0.272, R_W = 3.176$ and $k = -0.237, R_W = 4.744$, where R_W is the radius of the outer conducting wall. We conclude that the $m = 1$ mode is MHD stable for $R_W < 3.176$ and is MHD unstable for $R_W > 3.176$ for k in the interval $-0.237 < k < 0.272$.

Consider now what finite-resistivity theory predicts. As noted above, it is sufficient to determine Δ' defined by Eq. (4.72) using ψ , as determined by the MHD equations, in order to determine stability. Gibson and Whiteman (1968) have studied the BFM by determining Δ' and found the equation for ψ yields for the marginal case $\Delta' = 0$ and for the $m = 0$ mode

$$J_1(r\sqrt{1-k^2}) = 0, \quad (4.82)$$

i.e.,

$$r = \frac{3.832}{\sqrt{1-k^2}} = \frac{J_{1,1}}{\sqrt{1-k^2}}, \quad (4.83)$$

$J_{1,1}$ being the first zero of J_1 . Figure 13 from Gibson and Whiteman (1968) for the $m = 0$ modes demonstrates the existence of resistive tearing modes where no MHD instabilities exist. Considering $m = 1$, Gibson and Whiteman found the tearing mode alone will occur whenever R_W is larger than the value of r at which $\psi = 0$ and is outside the range of k values for which they are MHD unstable, as can be seen in Fig. 14.

As we have seen, a diffuse pinch that is MHD stable is not necessarily stable when finite resistivity is included in the stability analysis, in addition to the tearing mode not being limited to sheet geometries.

Thus the radial behavior of B_z and B_ϕ are important for determining either MHD or finite resistivity stability. Notice that as $k \rightarrow 0$ the behavior of $F = \mathbf{k} \cdot \mathbf{B}$ is determined primarily by B_ϕ (if $m \neq 0$). Hence it is important that we examine the radial behavior of B_ϕ , especially in the limit $\beta_z \ll 1$ where B_z will remain essentially constant and unperturbed. However the behavior of B_ϕ is determined by j_z , which in turn is determined by the radial temperature profile through the resistivity, assuming that the resistivity behaves classically. Hence, by knowing the temperature profile of the minor radius of an arch, one can predict the basic behavior of B_ϕ . Furth et al. (1973) have examined the

DANIEL S. SPICER

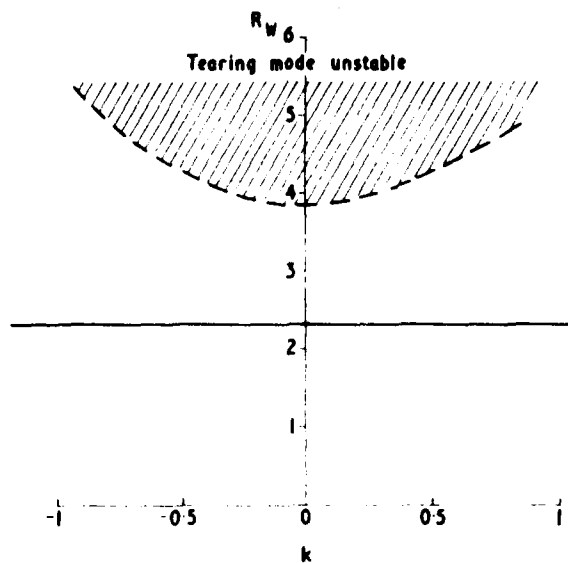


Fig. 13 - Stability diagram for BFM ($m = 0$)
(from Gibson and Whiteman, 1968)

==== MHD unstable.
 //// Tearing mode unstable.

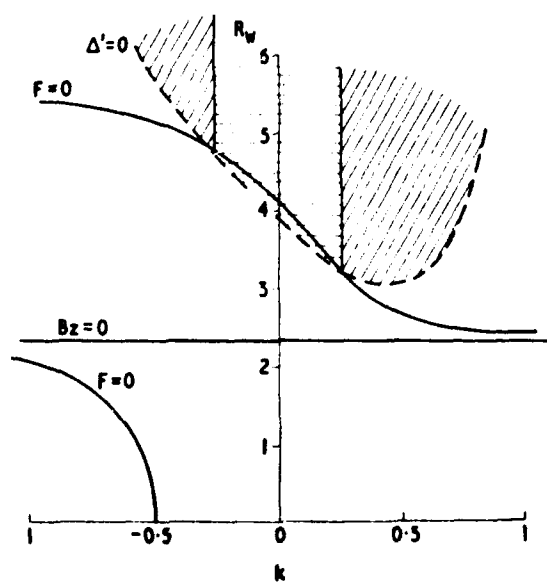


Fig. 14 - Stability diagram for BFM ($m = 1$)
(from Gibson and Whiteman, 1968)

stability of various B_z profiles for the Tokamak. In particular they considered the skin current B_z model and found it to be highly unstable. In Section 8 we will examine such a B_z profile which a solar arch may exhibit.

4.5 Magnetic Islands

Since we are primarily concerned with helical perturbations of the magnetic-field-plasma configuration, it is of interest to examine some quiescent macroscopic effects of the resistive kink instability. These macroscopic effects, although probably not observable during the time scale of a flare, should be observable on a longer time scale. In particular the formation of multiple filaments which may appear as striations of the arches (like a stranded rope) can be predicted and should be considered as strong evidence for currents flowing along magnetic fields.

An analysis by Kadomtsev and Pogutse (1970) shows that as $\mathbf{k} \cdot \mathbf{B}$ approaches zero, there must be a large perturbation in the current parallel to \mathbf{B} . This perturbation in j_{\parallel} is then shown to be directly related to either *electron density* or *electron temperature* and of course to the *electric field* driving the current. This result enables us to limit the types of perturbations that can act as flare precursors in current-carrying arches. In addition such perturbations will lead to the formation of magnetic islands.

Magnetic islands arise when the nonlinearity of the tearing mode is accounted for near the singular layer. This can be seen as follows: consider an equilibrium magnetic field of helical symmetry, which can be specified by the stream functions I_0 and ψ_0 (Johnson et al., 1958). Using the conditions that

and
$$\nabla \cdot \mathbf{B} = 0 \tag{4.84}$$

$$\nabla \cdot \mathbf{j} = 0, \tag{4.85}$$

one finds

$$B_r = \frac{1}{r} \frac{\partial \psi_0}{\partial \xi}, \quad - \frac{\partial \psi}{\partial r} = (-B_{\phi} m + krB_z), \tag{4.86}$$

$$j_r = \frac{1}{r} \frac{\partial I_0}{\partial \xi} \frac{c}{4\pi}, \quad - \frac{c}{4\pi} \frac{\partial I_0}{\partial r} = (-j_{\phi} m + krj_z), \tag{4.87}$$

and

$$I_0 = (mB_z + krB_{\phi}), \tag{4.88}$$

where $\xi = kz - m\phi$. Hence we have

$$B_r = \frac{1}{r} \frac{\partial \psi_0}{\partial \xi}, \quad (4.89)$$

$$B_\phi = \frac{1}{k^2 r^2 + m^2} \left(m \frac{\partial \psi_0}{\partial r} + krI_0 \right), \quad (4.90)$$

and

$$B_z = \frac{1}{k^2 r^2 + m^2} \left(-kr \frac{\partial \psi_0}{\partial r} + mI_0 \right). \quad (4.91)$$

Notice that Eq. (4.86) is just

$$\frac{\partial \psi_0}{\partial r} = r\mathbf{k} \cdot \mathbf{B} = rF, \quad (4.92)$$

where the sign of m was chosen to be negative rather than positive as we had chosen previously. Hence $\partial \psi_0 / \partial r = 0$ will correspond to the singular layer at $r = r_s$, if a perturbation matches the pitch of the unperturbed magnetic field.

As discussed earlier, the nonlinearity of the tearing mode must be taken into account primarily near the singular layer. Since ψ_0 reaches an extremum at $r = r_s$, i.e., $d\psi_0/dr$ vanishes there, ψ_0 must vary slowly in the vicinity of $r = r_s$. Hence even a small perturbation ψ'_0 can lead to a marked alteration of the magnetic surface. In particular the magnetic surfaces $\psi_0 = \text{constant}$ are broken up near $r = r_s$ as shown for the $m = 4$ case in Fig. 15. The breaking of magnetic surfaces is sometimes referred to as the destruction of magnetic surfaces. Thus the tearing mode may be viewed as a form of symmetry breaking; that is, the energy required to maintain the magnetic surfaces is released by the tearing mode when these symmetric surfaces are broken up into lower symmetry surfaces. This can occur only in the presence of finite resistivity. In Fig. 15 the point D corresponds to $\psi_0 = \text{extremum}$, and the point E is a saddle point. The surface passing through the saddle points, called the separatrix, has a width of the order

$$\Delta r = \sqrt{\psi'_0 \left(\frac{d^2 \psi_0}{dr^2} \right)_{r_s}^{-1}} \quad (4.93)$$

or in terms of F defined by Eq. (4.92)

$$\Delta r = \sqrt{\psi'_0 \left[\frac{d(rF)}{dr} \right]^{-1}} \quad (4.94)$$

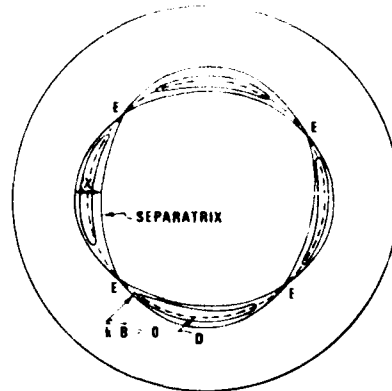


Fig. 15 - Four magnetic islands in the $m = 4$ case

This width is clearly a nonlinear function of ψ' , the linear approximation being meaningful only at large distances from the boundaries of the cell or magnetic islands. The rate of expansion of these islands is of the order

$$t \approx \frac{4\pi\sigma(\Delta r)^2}{c^2} \quad (4.95)$$

Since $d^2\psi_0/dr^2$ is proportional to dj_0/dr , a knowledge of dj_0/dr will yield information about Δr and thus about t . Since island formation is just filamentation, a knowledge of the filament cross section and lifetime will yield information on dj_0/dr and σ . Hence, if arches or filaments are observed with filamentation, such data should be considered as hard evidence for a current parallel to \mathbf{B} and resistive kink modes or tearing modes within the arch or filaments.

4.6 Quasi-Modes

So far we have considered resistive instabilities that are sharply localized about $\mathbf{k} \cdot \mathbf{B} = 0$ (where \mathbf{k} is the component of the wave vector normal to the direction of shear), so that a perturbation can move a magnetic field line uniformly without distortion, producing no restoring force on the plasma. This thin region about $\mathbf{k} \cdot \mathbf{B} = 0$ plays a role similar to that of a boundary layer in hydrodynamics. However the possibility exists of an unstable mode localized about every value of y (in the planar current case) or r (in the cylindrical case); and if these modes are nearly degenerate (almost equal growth rates), the actual displacements obtained by a linear combination of normal modes may not be very localized. Roberts and Taylor (1965) have considered such linear combinations that are not localized and referred to them as quasi-modes. In particular Roberts and Taylor (1965) discard the usual assumption that all perturbed quantities vary as either

$$f_1(y) \exp i(k_x x + k_z z) \quad (4.96)$$

or

$$f_1(r) \exp i(m\phi + kz) \quad (4.97)$$

and replace this assumption with

$$f_1(y, z) \exp(ik_x x) \quad (4.98)$$

or

$$f_1(r, z) \exp(im\phi). \quad (4.99)$$

That is, they do not Fourier-analyze in z , the direction of the main field. With this change, modes are found which are neither localized nor dependent on a boundary layer such as $\mathbf{k} \cdot \mathbf{B} = 0$. Thus localization of instabilities found by Suydam (1959) and Furth et al. (1963) appears as a property not so much of the physical disturbances as of their Fourier transforms.

In their analysis Roberts and Taylor (1965) established that the quasi-modes are limited in the z direction (that of the main field). This enabled them to treat convective plasma motion in an unshered field placed between two conducting endplates, since the plates simply limited the mode. This followed because the quasi-modes twist so as to see an unshered field in the frame corotating with the twisted field. Roberts and Taylor found that because of finite resistivity the G modes (those treated by Roberts and Taylor) could be combined coherently into nonlocal quasi-modes which could greatly enhance the plasma loss by convection with a growth rate

$$\gamma \approx \frac{c^2}{32\pi^2} k_y^2 \frac{\beta\eta}{\beta_{\text{critical}}}, \quad (4.100)$$

where $\beta_{\text{critical}} = aC_s^2/gL$, C_s being the sound velocity and L being the distance between the endplates. When $\beta < \beta_{\text{critical}}$, those G modes are stabilized.

The importance of quasi-modes to a flare model is as follows: First the gravitational resistive instability, the so called G modes, limit the length of the arch, if the arch is to be stable against coherent G modes. Thus conventional G modes can be coherently combined into nonlocal quasi-modes, and the plasma lost will be greatly enhanced. In particular Eq. (4.100) implies a/L must be large for the arch to be stable; i.e., the curvature should be small. Second, since similar arguments can be applied to the tearing mode, one should expect tearing quasi-modes, which would lead to greatly enhanced heating and acceleration over a larger volume than is typically assumed in current-sheet flare models.

4.7 The Rippling Mode and the Superheating Instability

Let us now discuss the rippling mode and its relationship to the superheating instability. As pointed out earlier, the rippling mode can channel current by convection from regions of high resistivity to low resistivity. Such behavior can result in an explosive thermal instability via the superheating instability (Kadomtsev, 1966). The basic chain of events is as follows: First the rippling mode convects current from regions of high

resistivity to regions of low resistivity. The joule heating then rises and exceeds the sink terms in the energy equation. The resistivity then drops due to electron heating, so that the rippling mode can convect more current into the region of lower resistivity, which again results in a higher current density and joule heating. This behavior can run away in an explosive fashion.

Let us first consider the rippling mode. As pointed out earlier, the rippling mode occurs when

$$\frac{F''}{F} > 0 \quad (4.101)$$

in Eq. (4.26). Since by Eq. (4.28)

$$F' = - \frac{1}{\tilde{\eta}^2} \frac{d\tilde{\eta}}{d\mu}, \quad (4.102)$$

we can expect the rippling mode to occur if $F' > 0$ and $d\tilde{\eta}/d\mu < 0$. Such a situation would occur if the temperature profile of an arch had a minimum at $r = 0$, the minor radius of the arch, with temperature increasing radially outward. Normally we would expect most of the current to flow in the higher temperature region. However the existence of a null in $\mathbf{k} \cdot \mathbf{B}$ permits the current to flow preferentially toward the singular layer, permitting the growth of high-current-density filaments if $F' > 0$ and $d\eta/d\mu < 0$ on one side of r . Taking into account the existence of many modes satisfying $\mathbf{k} \cdot \mathbf{B} = 0$ at various radii, one should expect many high-current-density filaments which will grow with a growth rate given by Eq. (4.46).

We shall briefly consider here a number of interesting properties of the rippling mode. The rippling mode is directly related to an instability first studied by Kadomtsev (1962) called the current convective instability. This instability required the existence of a gradient in resistivity perpendicular to the magnetic field, i.e.,

$$\mathbf{B} \cdot \nabla \eta = 0. \quad (4.103)$$

Hoh (1964) compared the rippling mode with current convective instability and found that for low β and strong shear the growth rate given by Eq. (4.46) is applicable. However, if a weak shear exists, Kadomtsev's result

$$\omega = \frac{ck_x j_z \eta'_\parallel}{k_z B_z} \quad (4.104)$$

is applicable, where z is the direction of the main magnetic field, y is normal to the plasma slab of thickness Δ , and $\eta'_\parallel = d\eta_\parallel/dx$. Which growth rate is applicable is determined by the parameter

$$M = \frac{k_x \Delta j_z}{4\pi k_z B_z} \quad (4.105)$$

If $M \gg 1$, Eq. (4.46) is applicable, and if $M \ll 1$, Eq. (4.104) is applicable. In addition Hoh finds that thermal conduction along the field lines does not reduce the growth rate appreciably, as was originally argued by Furth et al. (1963).

Using the constraint that the rippling mode occurs only for

$$S^{-2/3} < \alpha < S^{2/3} \quad (4.106)$$

and that the e -folding time of the rippling mode is

$$\tau_{RM} \sim \frac{\tau_R}{\alpha^{2/5} S^{2/5}}, \quad (4.107)$$

it is easy to show that the e -folding time of the rippling mode is long for long wavelengths. Using the tearing-mode e -folding time

$$\tau_{TM} \approx \frac{\tau_R \alpha^{2/5}}{S^{2/5}}, \quad (4.108)$$

which is small for long wavelengths, and comparing τ_{RM} with τ_{TM} shows

$$\tau_{TM} = \tau_{RM} \alpha^{4/5}; \quad (4.109)$$

i.e., the tearing mode has a shorter e -folding time for long wavelengths if the conditions for instability are satisfied for both instabilities. One should then expect the tearing mode to contribute to the growth of the rippling mode, since the tearing mode forms long-wavelength magnetic islands which aid in convecting the current into filaments of smaller cross section. Such mixing of the rippling and tearing modes has been used as an explanation of the helical current streamers formed in stabilized diffuse pinches (Furth et al., 1963).

The superheating instability is really an effect that occurs when one examines the resistive instabilities of Furth et al. (1963) by using an energy equation rather than Eq. (4.11). The effect of joule heating is then self-consistently included. In fact one can obtain the complete dispersion relation for the current convective instability of Kadomtsev, which ignores the effect of perturbing the current in the energy equation, and the superheating instability (Kadomtsev, 1966), which ignores the effect of the resistivity gradient required by the rippling mode and the current convective instability. The complete dispersion relation is

$$\begin{aligned} & (\omega^2 + i\omega\nu_s - \omega_A^2)(\omega + i\chi_\parallel k_\parallel^2 + i\chi_\perp k_\perp^2 + w_r + w_q) \\ & + 2\omega\nu_s\nu_q \frac{k_\parallel^2}{k^2} + i(\nu_A^2 + i\omega\chi_\parallel) \frac{k_\perp \nu_s \nu_p}{k_\perp} = 0, \end{aligned} \quad (4.110)$$

where

$$\omega_A^2 = v_A^2 k_{\parallel}^2,$$

$$\nu_s = \frac{k^2 c^2}{4\pi\sigma_0},$$

$$\nu_r = \frac{2}{3n_0} \frac{dP_{\text{rad}}}{dT_0},$$

$$\nu_p = \frac{4\pi j_0}{B_0 c} \frac{d(n\sigma_0)}{dx},$$

and

$$\nu_q = \frac{2}{3} \left(\frac{j_0^2}{n_0 T_0 \sigma_0} \right) \frac{d(n\sigma_0)}{d(nT_0)}.$$

However here we will review only the derivation of the dispersion relation for the superheating instability.

Physically we can understand the superheating instability using rather simple arguments. Assume a current j_z flows parallel to the main magnetic field B_z . Suppose further one perturbs the temperature of the current-carrying plasma on a scale for which thermal conductivity can be neglected. One then finds that the current density will grow when the joule heating exceeds the radiative power loss. The basic physical notion of the superheating instability is then as follows: since the electrical conductivity varies with temperature as $T^{3/2}$, and the current density is directly proportional to the conductivity, one can argue that a temperature increase will result in an increased electrical conductivity, an increase in current density, and therefore, joule heating. This effect will cycle in a runaway fashion, so that the current grows at the expense of the external perturbing thermal input.

One may also properly view this mechanism as a form of electron-current runaway, which can occur only if there are no mechanisms to limit the temperature rise which is effectively due to joule heating. For, if these temperature-limiting mechanisms are lacking, or if the joule heating exceeds the limiting mechanism, the electron temperature will continue to increase and the drift velocity will follow the temperature rise during subsequent times. Since the critical electric field for runaway decreases with temperature, the Dreicer regime can eventually be reached, and complete runaway could occur. Coppi and Friedland (1971) have considered a similar instability. For completeness, let us follow some of their arguments before deriving the superheating dispersion relation.

As discussed by Coppi and Friedland (1971), the electron energy transfer equation is

$$\frac{3n}{2} \frac{\partial T_e}{\partial t} = \frac{E_z^2}{\eta} - \frac{3m_e}{m_i} \nu_{ei}(T_e - T_i) - \nu_d n T_e, \quad (4.111)$$

where ν_{ei} is the electron-ion collision frequency, T_e and T_i are the electron ion temperatures, and ν_d is the rate of thermal energy loss by diffusion and radiation. Here we identify E_z with the induced electric field that drives the toroidal currents of the arch. In equilibrium Eq. (4.111) reduces to

$$\frac{E_z^2}{\eta_0 \eta_0} = 3\nu_{ei0} \frac{m_e}{m_i} (T_{e0} - T_{i0}) + \nu_d T_{e0}, \quad (4.112)$$

where the subscript zero denotes the equilibrium values. Coppi and Friedland used Eq. (4.112) in a temperature regime where $\nu_d n T_{e0}$ is small in comparison to the ν_{ei0} term. Hence the electrons heat if

$$E_z > \nu_{ei} m_e e^{-1} \left(\frac{3T_e}{m_i} \right)^{1/2} \quad (4.113)$$

or

$$E_z > \left(\frac{3m_e}{2m_i} \right)^{1/2} E_D, \quad (4.114)$$

where

$$E_D = \frac{\nu_{ei} m_e v_{Te}}{e}, \quad (4.115)$$

E_D being the Dreicer electric field for runaway at the temperature T_e and v_{Te} being the electron thermal velocity. Thus, if the induced electric field driving the current satisfies Eq. (4.113), one should expect runaway.

Let us now follow Kadomtsev (1966) and derive the dispersion relation for the superheating instability. We proceed by using the equations

$$\mathbf{E} = \frac{\mathbf{j}}{\sigma} - \frac{\mathbf{v} \times \mathbf{B}}{c}, \quad (4.116)$$

$$\frac{\partial n}{\partial t} + \nabla \cdot (n\mathbf{v}) = 0, \quad (4.117)$$

$$nm_1 \frac{d\mathbf{v}}{dt} = \frac{\mathbf{j} \times \mathbf{B}}{c}, \quad (4.118)$$

$$\frac{3}{2} \frac{ndT}{dt} = -\nabla \cdot \mathbf{q} + \frac{j^2}{\sigma} - Q, \quad (4.119)$$

and

$$\nabla \times (\nabla \times \mathbf{E}) = -\frac{4\pi}{c} \frac{\partial \mathbf{j}}{\partial t}, \quad (4.120)$$

while assuming a uniform magnetic field $\mathbf{B} = B_0 \mathbf{e}_z$ along which flows a current $\mathbf{j} = j_0 \mathbf{e}_z$, which is weak enough that its own field satisfies $B_\phi \ll B_0$. Furthermore we assume that the β of the plasma is such that $\beta \ll 1$. Assuming that all perturbed quantities vary as $\exp(-i\omega t + i\mathbf{k} \cdot \mathbf{x})$, we have

$$-i\omega \mathbf{v}_1 = \frac{1}{m_1 n c} (\mathbf{j}_1 \times \mathbf{B}), \quad (4.121)$$

$$\mathbf{E}_1 = -\frac{1}{c} (\mathbf{v}_1 \times \mathbf{B}) + \frac{j_1}{\sigma_0} - \frac{j_0}{\sigma_0} \frac{d \ln \sigma_0}{d \ln T_0} \frac{T_1}{T_0}, \quad (4.122)$$

$$-i\omega + \chi_{\parallel} k_{\parallel}^2 + \chi_{\perp} k_{\perp}^2 + \frac{3}{2} n_0 \frac{dQ}{dT_0} + \frac{3}{2} \frac{j_0^2}{n_0} \left(\frac{d \ln \sigma_0}{d \ln T_0} \right) \frac{T_1}{T_0} = \frac{4}{3} \frac{j_0 j_z}{n_0 T_0 \sigma_0}, \quad (4.123)$$

and

$$k^2 \mathbf{E}_1 - (\mathbf{k} \cdot \mathbf{E}_1) \mathbf{k} = i \frac{4\pi\omega}{c} \mathbf{j}_1. \quad (4.124)$$

Using Eq. (4.121) to eliminate \mathbf{v}_1 from Eq. (4.122) and substituting Eq. (4.122) for \mathbf{E} into Eq. (4.124), we obtain

$$(\omega^2 + i\omega c^2 k^2 / 4\pi\sigma_0 - \omega_A^2) j_z = \frac{i\omega c^2}{4\pi\sigma_0} k_{\parallel} j_0 \frac{d \ln \sigma_0}{d \ln T_0} \frac{T_1}{T_0} \quad (4.125)$$

Using Eq. (4.125) in Eq. (4.123) to eliminate j_z then leads to the dispersion relation

$$(\omega^2 + i\omega\nu_s - \omega_A^2)(\omega + i\chi_{\parallel} k_{\parallel}^2 + i\chi_{\perp} k_{\perp}^2 + i\nu_r + i\nu_q) + 2\omega\nu_s\nu_q \frac{k_{\perp}^2}{k^2} = 0, \quad (4.126)$$

where

$$\omega_A^2 = k_{\parallel}^2 v_A^2,$$

$$\nu_r = \frac{2}{3n_0} \frac{dQ}{dT_0},$$

$$\nu_s = \frac{c^2 k^2}{4\pi\sigma_0},$$

and

$$\nu_q = \frac{2}{3n_0} \frac{j_0^2}{T_0 \sigma_0} \frac{d \ell n \sigma_0}{d \ell n T_0}.$$

We would like to examine the effect of short-wavelength perturbations, for which ν_s is much greater than all other frequencies. Hence $\nu_s \rightarrow \infty$ yields

$$\omega = -i\chi_{\parallel} k_{\parallel}^2 - i\chi_{\perp} k_{\perp}^2 - i\nu_r - i\nu_q \frac{(k_{\perp}^2 - k_{\parallel}^2)}{k^2}, \quad (4.128)$$

where χ_{\parallel} is the thermal conductivity parallel to \mathbf{B} and χ_{\perp} is the thermal conductivity perpendicular to \mathbf{B} . Following Kadomtsev (1966), we note that instability can occur when ν_q is either negative or positive. The first case corresponds usually to classical resistivity and results in the formation of current filaments of higher conductivity, greatly elongated along the field lines. The second case corresponds to situations in which the electrical conductivity may be anomalous and decreases with temperature. This case appears as alternating layers of high and low conductivity similar to striations in a glow discharge. The first case is physically the most interesting, because it can occur only if the perturbations are highly elongated along the magnetic field, i.e., $k_{\parallel} \rightarrow 0$. Hence, neglecting conduction perpendicular to \mathbf{B} , we have

$$\omega = -i\nu_r + i\nu_q. \quad (4.129)$$

Thus, if $\nu_q > \nu_r$, instability will occur; i.e.,

$$\frac{j_0^2}{T_0 \sigma_0} \frac{d \ell n \sigma_0}{d \ell n T_0} > \frac{dQ}{dT_0}, \quad (4.130)$$

where

$$Q = P_{\text{rad}} + \frac{3m_e}{m_i} n\nu_{ei}(T_e - T_i).$$

Comparing Eq. (4.130) and Eq. (4.112), we see that they are physically equivalent, as previously argued. However in deriving Eq. (4.130) we have determined under what conditions Eq. (4.112) is valid, i.e., only for long-wavelength perturbations, in addition to obtaining a growth rate for the instability, i.e.,

$$\gamma^{-1} \approx \frac{3}{2} n_0 T_0 \left/ \left(\frac{j_0^2}{\sigma_0} \frac{d \varrho n \sigma_0}{d \varrho n T_0} \right) \right. \quad (4.131)$$

Note that γ is small if the current density is small, but becomes large if j_0 is large.

How $d \varrho n \sigma_0 / d \varrho n T_0$ behaves will depend on whether the resistivity is anomalous or classical. If the resistivity is classical, $d \varrho n \sigma_0 / d \varrho n T_0$ contributes a factor of 3/2 to the denominator of Eq. (4.131). It is important to emphasize that as the temperature grows in the current filaments, the electric-field magnitude necessary for runaway drops. Hence, if a current-carrying arch has a long lifetime compared to the growth time of the superheating instability and of the rippling mode or current convective instability, these modes will undoubtedly occur. This would especially be the case if the source of the current within the photosphere or convection zone resulted in a monotonically increasing current, such as the gradual twisting of the feet of an arch would cause. A number of possible effects may occur as the current within the filaments of the arch grow. The current density may increase until it becomes either MHD unstable or resistively unstable, at which time these filaments will explode in a variety of ways. Or the filaments may remain MHD stable but become unstable to various electrostatic instabilities. However we will defer discussion of these various possibilities until Sections 6, 7, and 8, where we will discuss the flare model in detail.

5. INSTABILITIES IN MORE COMPLEX MAGNETIC TOPOLOGIES

5.1 Introduction

In this section we will examine how the more complex magnetic topology of an arch or filament may alter the application of the results obtained in Sections 3 and 4. The two most obvious differences between a cylindrically symmetric topology and an arch topology is that the arch has global curvature as well as local curvature and that the toroidal component of the magnetic field B_T has maxima at the feet of the arch, with B_T monotonically decreasing with altitude in either leg of the arch. Hence we have a diffuse pinch, which is basically a magnetic mirror, within which a current flows, and which is bent into a half torus. Such a magnetic topology will cause the pitch of the magnetic field to vary, not only with minor radius as in the cylindrically symmetric case but also with altitude. We then must show that the curvature of the arch will not affect our analysis to any great degree and that the behavior of the pitch of the magnetic field is also not of overwhelming importance.

The effect of global curvature on the growth rate of the MHD instabilities was considered in Section 3, and, as argued by Furth et al. (1973), similar arguments apply for resistive instabilities. Hence we may conclude that curvature will not significantly alter

DANIEL S. SPICER

the results obtained in Sections 3 and 4 if the modes we consider have sufficiently large growth rates. However there are effects due to curvature that alter the location of surfaces of constant magnetic flux. In particular the curvature has a tendency to outwardly displace the flux surfaces, in the direction of the convex plasma-magnetic field interface of the arch, by an amount of the order r/R (Moroyov and Solov'ev, 1966). This displacement can cause various m modes to overlap.

To examine the effect of the variation of magnetic pitch with altitude and minor radius, it is best to discuss a trivial example so as to illustrate the physical principles involved. Assume that a magnetic mirror exists between two conducting endplates (Fig. 16a), and suppose a perturbation of the form

$$\mathbf{v}_1 = (0, \epsilon r \omega, 0) \quad (5.1)$$

occurs due to both endplates rotating. This will cause the fluid to rotate about the axis of symmetry with an angular frequency, ω , imparted to the fluid element about the axis (ϵ is a dimensionless parameter which can be made arbitrarily small to insure the condition that \mathbf{v}_1 be a small perturbation). The perturbation on the magnetic field in the presence of this perturbation is just

$$\frac{\partial \mathbf{B}_1}{\partial t} = \nabla \times (\mathbf{v}_1 \times \mathbf{B}_0) - \frac{c^2}{4\pi} \nabla (\eta_0 \nabla \times \mathbf{B}_1 - \eta_1 \nabla \times \mathbf{B}_0). \quad (5.2)$$

As discussed in Sections 3 and 4, an MHD or resistive MHD instability will occur when $\mathbf{k} \cdot \mathbf{B} = 0$, which in general results when one or more components of $\mathbf{v}_1 \times \mathbf{B}$ vanishes. Let us then examine when $(\mathbf{v}_1 \times \mathbf{B})$ vanishes for the perturbation given by Eq. (5.1) and a magnetic mirror configuration given by

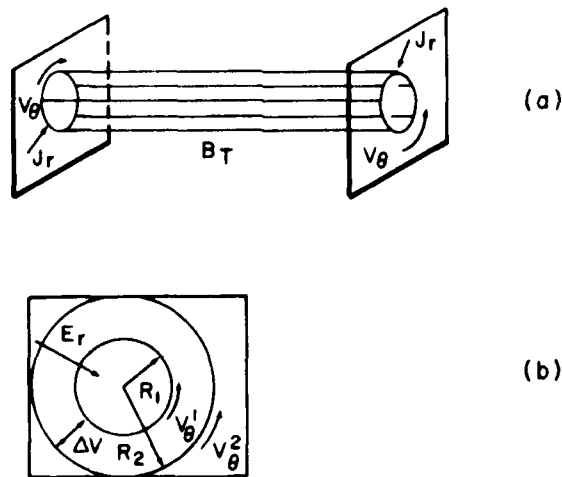


Fig. 16 -- Twisting magnetic mirror between two conducting endplates

$$\mathbf{B}_0 = (B_r, 0, B_z) = \left(\frac{1}{r} \frac{\partial \psi}{\partial z}, 0, -\frac{1}{r} \frac{\partial \psi}{\partial r} \right), \quad (5.3)$$

where ψ is the appropriate stream function. We find that $(\mathbf{v}_1 \times \mathbf{B})$ vanishes only when $\omega = \omega(\psi)$. Hence ω is constant over the surfaces of ψ , and since $\psi = \text{constant}$ represents the surfaces of constant magnetic flux, we find the angular perturbation is constant on these surfaces if $\omega = \omega(\psi)$. If $\omega \neq \omega(\psi)$, then $(\mathbf{v}_1 \times \mathbf{B}_0) \neq 0$ in general and the lines of force will be distorted by the perturbation. Thus, when $(\mathbf{v}_1 \times \mathbf{B}_0) = 0$, the lines of forces are not distorted due to the fluid perturbation; this does not permit the magnetic field to produce a restoring force to counteract the perturbation, and the perturbation can grow. However the important point here is that \mathbf{B}_0 is sheared and is a function of both r and z , not just of r as in the cases discussed in Sections 3 and 4. Indeed, if the perturbation \mathbf{v}_1 were incompressible, i.e., $\nabla \cdot \mathbf{v}_1 = 0$, then \mathbf{v}_1 may be derived from a stream function,

$$\mathbf{v}_1 = \frac{\mathbf{r}}{r^2} \times \nabla \chi, \quad (5.4)$$

χ being the stream function of the perturbation. Writing

$$\mathbf{B}_0 = \frac{\mathbf{r}}{r^2} \times \nabla \psi, \quad (5.5)$$

we see that $\mathbf{v}_1 \times \mathbf{B}_0$ vanishes identically if $\chi = \chi(\psi)$, that is, if the surfaces of the perturbation match the ψ surfaces of the magnetic field. Such a statement is equivalent to the statement that the pitch of the perturbation matches the pitch of the magnetic field, which was our criteria for instability in the cylindrically symmetric cases examined in Sections 3 and 4.

5.2 An Example of Three-Dimensional Magnetic Configurations

Let us now examine a realistic magnetic configuration that may approximate the magnetic field in a filament or an arch with a small inverse aspect ratio. To do this we must first obtain solutions for a magnetic field made up of a mirror field and the field due to a current flowing along the symmetry axis of the mirror. To obtain such solutions, we assume helical symmetry. Using Eqs. (4.89) through (4.91), we have

$$B_r = \frac{1}{r} \frac{\partial \psi}{\partial \xi}, \quad (5.6)$$

$$B_\phi = \frac{1}{k^2 r^2 + m^2} \left(m \frac{\partial \psi}{\partial r} + krI \right), \quad (5.7)$$

DANIEL S. SPICER

and

$$B_z = \frac{1}{k^2 r^2 + m^2} \left(-kr \frac{\partial \psi}{\partial r} + ml \right), \quad (5.8)$$

where

$$- \frac{\partial \psi}{\partial r} = -mB_\phi + krB_z, \quad (5.9)$$

$$l = \frac{c}{4\pi} (mB_z + krB_\phi), \quad (5.10)$$

and

$$\xi = kz - m\phi. \quad (5.11)$$

We now impose the condition that the magnetic field and plasma configuration is force free. Imposing the force-free condition eliminates only pressure-driven instabilities from the analysis, since force-free equilibrium requires that

$$\mathbf{j}_\perp = \frac{c\mathbf{B} \times \nabla P}{B^2} \quad (5.12)$$

vanish; and, as should be clear from Section 3 and 4, only \mathbf{j}_\parallel -driven instabilities are of importance to the instabilities discussed here. Imposing the force-free condition implies

$$\mathbf{j} = \alpha(\mathbf{r})\mathbf{B} \quad (5.13)$$

and

$$\mathbf{B} \cdot \nabla \alpha = 0. \quad (5.14)$$

It follows then that l , the stream function of \mathbf{j} introduced in Section 4, is related to $\alpha(\mathbf{r})$ and ψ through

$$l = \int^\psi \frac{d\psi'}{\alpha(\psi')} \quad (5.15)$$

or

$$l = I(\psi). \quad (5.16)$$

Thus we can satisfy Eqs. (5.6) through (5.8) by an appropriate choice of $I(\psi)$ which satisfies our boundary conditions.

We now need only to find ψ . We can do this by using a solution for a magnetic-mirror field given by

$$B_r(r, z) = -\alpha B_0 J_1(kr) \sin kz \quad (5.17)$$

and

$$B_z(r, z) = B_0(1 - \alpha J_0(kr) \cos kz), \quad (5.18)$$

where α is related to the mirror ratio by

$$R_M = \frac{(1 + \alpha)}{(1 - \alpha)} \quad (5.19)$$

and where $k = 2\pi/L$, L being the full length of the mirror, with the ends of the mirrors located at $z = \pm L/2$. Equations (5.17) and (5.18) satisfy

$$\frac{1}{r} \frac{\partial}{\partial r} (rB_r) + \frac{\partial B_z}{\partial r} = 0, \quad (5.20)$$

with

$$B_r = \frac{1}{r} \frac{\partial \tilde{\psi}}{\partial z} \quad (5.21)$$

and

$$B_z = -\frac{1}{r} \frac{\partial \tilde{\psi}}{\partial r}, \quad (5.22)$$

in which

$$\tilde{\psi} = (\alpha B_0 y J_1(y) \cos x - B_0 y^2/2)/k^2 \quad (5.23)$$

where $y = kr$ and $x = kz$.

Since $\nabla \cdot \mathbf{B} = 0$ for Eqs. (5.20) through (5.23), then

$$\frac{1}{r} \frac{\partial}{\partial r} (rB_r) + \frac{\partial B_z}{\partial \xi} \quad (5.24)$$

should also be satisfied by letting $kz \rightarrow \xi$, defined by Eq. (5.11), and

$$B_\xi = -mB_\phi + krB_z. \quad (5.25)$$

Equation (5.24) is then satisfied by

$$B_r = \frac{1}{r} \frac{\partial \psi}{\partial \xi} \quad (5.26)$$

and

$$B_t = -\frac{1}{r} \frac{\partial \psi}{\partial r} \quad (5.27)$$

Using Eq. (5.23) and letting $kz \rightarrow \xi$ and $\tilde{\psi} \rightarrow \psi k$, we find that

$$\psi = (\alpha B_0 y J_1(y) \cos \xi - B_0 y^2 / 2) / k \quad (5.28)$$

satisfies Eqs. (5.26) and (5.27) and represents the magnetic flux through a helical ribbon. For vacuum fields it follows from $\nabla \cdot \mathbf{j} = 0$ that I is a constant. Taking this constant to be zero and setting $m = 0$, we obtain the mirror solutions (5.17) and (5.18).

Examination of Eq. (5.28) shows that as $y \rightarrow 0$ ($r \rightarrow 0$), $\psi \rightarrow 0$ and that as $y \rightarrow \infty$, $\psi \rightarrow -B_0^2 y^2 / 2k$. If we let $I = I(\psi)$, Eq. (5.7) yields

$$B_\phi = \frac{1}{y^2 + m^2} \{ [\alpha B_0 y J_0(y) \cos \xi - B_0 y] + yI \}. \quad (5.29)$$

We see that as $y \rightarrow 0$, $B_\phi \rightarrow 0$; but as $y \rightarrow \infty$, we have

$$B_\phi \rightarrow \frac{1}{y^2} [-mB_0 y + yI(y \rightarrow \infty)], \quad (5.30)$$

so that to satisfy the boundary condition that B_ϕ vanish at $r = 0$ and $r = \infty$, I can approach a constant at worst. Preferring a faster falloff, a number of choices for I are

$$I = mB_0 + B_0 \exp\left(\frac{k\psi}{B_0}\right), \quad (5.31)$$

$$I = mB_0 \tanh\left(\frac{k\psi}{B_0}\right) \quad (5.32)$$

and

$$I = \frac{B_0}{(A + B\psi^{2n})}, \quad (5.33)$$

where $n = 0, 1, 2$ etc.

Eqs. (5.6) through (5.9) exhibit the following structure. First we note from Eq. (5.9) that

$$-\frac{\partial\psi}{\partial r} = -mB_\phi + krB_z = r\mathbf{k}\cdot\mathbf{B}. \quad (5.32)$$

Since $\mathbf{B}\cdot\nabla\psi = 0$, we know the magnetic field lines lie on surfaces of constant ψ . Further, using $q = krB_z/B_\phi$, we have from Eq. (5.31) that $q = m$ on those surfaces where $\partial\psi/\partial r = 0$; that is, we are on surfaces where $\xi = \text{constant}$ and the magnitude of B_ξ represents the magnetic field parallel to a helix with a pitch

$$\frac{d\phi}{dz} = \frac{1}{r} \frac{B_\phi}{B_z}, \quad (5.33)$$

which is both a function of r and ξ .

The solution given by Eq. (5.28) does not have any surfaces where $q = m$ if $\alpha < 1$, which it must. However a more general solution does exist, i.e.,

$$\psi = \frac{\left(\sum_{\ell=0}^{\infty} a_{\ell,y} J'_\ell(\ell y) \begin{Bmatrix} \cos \ell\xi \\ \sin \ell\xi \end{Bmatrix} - By^2 \right)}{k}, \quad (5.28)$$

where $\ell = 0, 1, 2$, etc. and the prime denotes a derivative with respect to y . This solution definitely has resonant solutions where $q = m$.

Let us summarize our discussion. We have endeavored to show by illustrations that even though in a real arch or filament the pitch of the magnetic field is a general function of r , it is possible to have magnetic surfaces which can still be resonant with perturbations which result in a component or components of $\mathbf{v}_1 \times \mathbf{B}$ vanishing. What we have failed to do is to prove the actual existence of such magnetic surfaces in solar arches, the existence of such surfaces being a crucial assumption of our discussion. Such surfaces are known to exist only in cases with high symmetry, such as cylindrical or helical symmetry. How much the magnetic fields actually depart from these surfaces in more realistic cases is difficult to estimate without more detailed information about the actual arches or filaments. However such departures can lead to the appearance of many new effects.

5.3 Nonlinear Resonant Phenomena

As pointed out in Section 4, the breakup of magnetic surfaces is in general a result of a symmetry-breaking perturbation, such as the tearing mode. There are in principle two kinds of perturbations: magnetic perturbations and those that result from a lack of high symmetry. As shown in Section 4, magnetic perturbations generally result from perturbations in temperature, density, or electric fields through the current density.

Symmetry breaking due to a lack of high symmetry would result, e.g., from the fact that the toroidal component of the magnetic field in an arch is a function of altitude and the strength of the magnetic field may differ at either foot of an arch.

To illustrate more clearly the breaking of symmetry, consider a cylindrically symmetric diffuse pinch in which a helically symmetric perturbation exists. Such a system still possesses magnetic surfaces, since the system possesses helical symmetry defined through the helical variables r and ξ . For a pure (m, k) perturbation we have the stream function

$$\psi(r, \xi) = \psi_0(r) + \epsilon_m \psi'_m(r) \sin \xi_m. \quad (5.34)$$

Since $\nabla \psi_0$ vanishes on the $q = m$ surfaces, we can still expect magnetic islands to form about this surface. Suppose further that more than one perturbation exists in the system, so that Eq. (5.34) becomes

$$\psi(r, \xi) = \psi_0(r) + \epsilon_m \psi_m(r) \sin \xi_m + \epsilon_{m'} \psi_{m'}(r) \sin \xi_{m'}. \quad (5.35)$$

If the pitches of these two perturbations do not match (i.e., $k/m \neq k/m'$), the perturbations have broken the symmetry of the system.

Magnetic islands will still occur within the system at the resonant surfaces $q = m$ and $q = m'$. These surfaces are defined as *primary resonances*. Further, *secondary resonances* occur which cause smaller magnetic islands. These are caused by mode-coupling of the perturbations present. This mode-coupling occurs because linear modes specified by (m, k) generate harmonics which interact with and modify each other. If the perturbations are sufficiently large, then the individual island structures will interact strongly, so that the phenomena referred to as overlapping of resonances occurs (Rosenbluth et al., 1966). The overlapping of such resonances can lead to a rapid destruction of the flux surfaces (Rosenbluth, et al., 1966) and thus the release of magnetically stored energy. It is within these regions of overlapping resonances that the magnetic surfaces are said to be destroyed by reconnection and the magnetic field lines behave in a stochastic manner. Let us consider for example how perturbations due to the tearing mode will evolve.

Suppose a number of helical perturbations resulting from the tearing mode have occurred in a cylindrically symmetric system, all with different pitches. These perturbations will result in primary resonances at the resonant surfaces $q = m$ and secondary resonances due to the interaction between smaller islands. As the perturbation amplitudes are increased, the secondary resonances will begin to interact, because they are more localized. These interactions will cause stochastic wandering of the field lines around the X-configured neutral point formed by the small-island separatrices. If the amplitudes of the perturbations are increased further, the primary resonances will begin to interact with one another, leading to stochastic behavior within a much larger volume near the X-configured neutral point formed by larger islands. Such behavior will lead to greater magnetic energy thermalization over larger volumes by reconnection.

Because these effects could be of great importance in understanding the dynamics of the solar flare, and because onset of these effects strongly depend on the amplitude of the perturbation, which, as we will see later, is highly suggestive in explaining the difference between the thermal and nonthermal flare, we will here attempt to clarify the physics involved.

The first basic point to what will follow is that the effects we will discuss are *amplitude dependent*. Hence the system of equations are necessarily *nonlinear*. The second basic point is that when the amplitude of a perturbation does reach a certain threshold, the system will show a sharp transition from nonlinear oscillatory behavior to *stochastic* behavior, requiring statistical mechanics to describe the motion.

Because a nonlinear oscillator's frequency is amplitude dependent, a nonlinear oscillator's frequency varies when a resonant perturbation acts on it, due to the frequency dependence on the driving-force amplitude. Thus the amplitude and frequency of the oscillator will undergo beating over a finite range $\Delta\omega$ and Δb , where ω is the frequency of the oscillator and b is the amplitude of driving perturbation. Let us suppose a driving perturbation $F(t)$ contains many harmonics, i.e.,

$$F(t) = \sum_n b_n \cos n\Omega_0 t, \quad (5.36)$$

and that the frequency spacing (Ω_0) between each harmonic is such that the beating interval $\Delta\omega$ contains many of these harmonics. Then how will the oscillator behave? The answer is not what one would expect. It is found that the oscillator acts stochastically and that the energy of the oscillator will grow, on the average, proportionally to time. This phenomenon is called the stochastic instability of nonlinear oscillations and is a topic relatively new and little known. Because of this we will review the basics involved without delving deeply into the mathematics nor into the fundamental concepts of ergodic theory with which the phenomenon is closely allied. The reader should consult the literature cited, particularly Zaslavskii and Chirikov (1972), for a more detailed presentation and examples of applications.

In MHD theory magnetic surfaces are conserved, so that there should exist adiabatic invariants. To see this, we convert the field-line equations

$$\frac{dr}{B_r} = \frac{rd\phi}{B_\phi} = \frac{dz}{B_z} \quad (5.37)$$

into canonical form. We have

$$B_z \frac{dr}{dz} = B_r \quad (5.38)$$

and

$$B_z \frac{d\phi}{dz} = \frac{B_\phi}{r} \quad (5.39)$$

Introducing $\xi = kz - m\phi$, we have from Eq. (5.26) and Eq. (5.27)

$$B_r = \frac{1}{r} \frac{\partial\psi}{\partial\xi} \quad (5.40)$$

and

$$B_t = -\frac{1}{r} \frac{\partial \psi}{\partial r},$$

where $\partial \psi / \partial r = mB_\phi - krB_z$. Using r and $\rho = r^2/2$, we find $d\psi/dz = (k - d\xi/dz)/r$. Eqs. (5.40) and (5.41) become

$$B_z \frac{d\rho}{dz} = \frac{\partial \psi}{\partial \xi}$$

and

$$B_z \frac{d\xi}{dz} = -\frac{\partial \psi}{\partial \rho}.$$

Defining $dz/dt = B_z$, we obtain the canonical equations

$$\frac{d\rho}{dt} = \frac{\partial \psi}{\partial \xi}$$

and

$$\frac{d\xi}{dt} = -\frac{\partial \psi}{\partial \rho},$$

where the stream function ψ is the Hamiltonian, ρ is the conjugate coordinate, and ξ is the conjugate momentum.

The adiabatic invariants are just

$$J = \oint r^2 \frac{d\xi}{2}$$

and

$$\frac{d\theta}{dt} = \omega = \frac{\partial H_0}{\partial J},$$

where H_0 is related to ψ by a canonical transformation, J is the flux-tube area, ω is the frequency of rotation of the flux line around the flux tube and is expressed as the number of flux line rotations per rotation about the z axis.

Equations (5.44) and (5.45) can be treated as equations of a nonlinear oscillator with singular points at $d\psi/d\xi = 0$ and $d\psi/d\rho = 0$, i.e., $B_r = 0$ and $\mathbf{k} \cdot \mathbf{B} = 0$.

To determine ω , we note that normally

$$\omega' = \frac{\delta\phi}{\delta z} = \frac{B_\phi}{rB_z},$$

where $\delta\phi$ is the change in the azimuthal coordinate when the angle ξ changes by 2π . Hence, since we have $d\theta/dt = \omega$,

$$\omega = \frac{d\theta}{dt} = \frac{\delta\theta}{\delta\xi} \frac{\delta\xi}{\delta z} \frac{dz}{dt},$$

which gives, using $\xi = kz - m\phi$ and $\delta\theta = 2\pi$ when $\delta\xi = 2\pi$,

$$\omega = \frac{B_z}{m} \left(\frac{k}{m} - \omega' \right).$$

At resonant surfaces $\omega' = k/m$, from $mB_\phi/r - kB_z = 0$, so that $\omega = 0$ there. Th $q = 2\pi r B_z / L B_\phi$ and $k = 2\pi n / L$, we have

$$\omega = \frac{nB_\phi}{r} \left(q - \frac{m}{n} \right) = n\omega_0.$$

Proceeding, we assume a perturbation exists which destroys the adiabatic in of the field, e.g., the tearing mode, so that the equations of motion in terms of angle variables becomes (Zaslavskii and Chirikov, 1972)

$$\dot{J} = -\epsilon \frac{\partial V}{\partial \theta} (J, \theta, \phi),$$

$$\dot{\theta} = \omega(J) + \epsilon \frac{\partial V}{\partial J} (J, \theta, \phi),$$

and

$$\dot{\phi} = \omega_0(J) + \epsilon V(J, \theta, \phi),$$

where $\epsilon \ll 1$, ϕ characterizes the perturbation which has a frequency $\phi = \Omega t$, a the perturbation. The perturbation is assumed to be periodic in θ and n , n being harmonic number of θ . In general the perturbation ϵV can be expanded into a

$$V(J, \theta, \phi) = \frac{1}{2} \sum_{\ell, n} [V_{\ell, n}(J) e^{i(\ell\phi + n\theta)} + V_{-\ell, -n}(J) e^{-i(\ell\phi + n\theta)}],$$

where $V_{-\ell, -n} = V_{\ell, n}^*$, $\theta = \omega t$, and $\phi = \Omega t$.

A resonance (ν, n) , n being the harmonic of the oscillations of the osc being the harmonic of the external perturbation, is determined by

$$(\nu\Omega + n\omega) = 0.$$

The accuracy to which this equality must be satisfied is determined by the $\Delta\omega$ of the resonance.

The simplest case one can examine is that of single resonance, i.e., ω these circumstances, only two real terms remain in V , corresponding to $\phi - \theta$. The $\phi - \theta$ term corresponds to the resonance, and $\phi + \theta$ corresponds to a frequency perturbation. If the width of the resonance is small enough, then resonance can occur for a given set of initial conditions. If we include only resonance term in V , we can introduce the resonance phase $\Phi_{\nu n} = \nu\phi + n\theta$ into Eqs. (5.52) and (5.53) into

$$\dot{J} = cnV_{\nu n} \sin \Phi_{\nu n}$$

and

$$\dot{\Phi}_{\nu n} = (\nu\Omega + n\omega(J) + cn \frac{\partial V_{\nu n}}{\partial J}) \cos \Phi_{\nu n}.$$

At resonance $J = J_r$ and $(\nu_0\Omega + n_0\omega(J_r)) = 0$. Hence, expanding $\omega(J)$ about

$$\dot{\Phi}_{\nu_0 n_0} = n_0 \left. \frac{d\omega}{dJ} \right|_{J_r} (\Delta J) + cn_0 \left. \frac{dV_{\nu_0 n_0}}{dJ} \right|_{J_r} \cos \Phi_{\nu_0 n_0},$$

where $\Delta J = J - J_r$.

We can derive Eqs. (5.56) and (5.58) at resonance from a so-called ut tonian which is nonlinear and conservative,

$$\tilde{H}_{\mu} = n_0 \left. \frac{d\omega}{dJ} \right|_{J_r} \frac{(\Delta J)^2}{2} + cn_0 V_{\nu_0 n_0}(J_r) \cos \Phi_{\nu_0 n_0},$$

using

$$\Phi_{\nu_0 n_0} = \frac{\partial \tilde{H}_{\mu}}{\partial (\Delta J)}$$

and

$$(\Delta J) = - \frac{\partial \tilde{H}_{\mu}}{\partial (\Phi_{\nu_0 n_0})}.$$

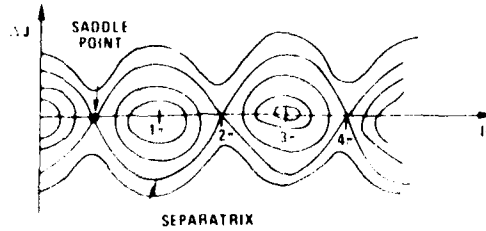


Fig. 17 -- Phase space diagram for a nonlinear oscillator

In Fig. 17 we plot the phase space for this Hamiltonian. From the Hamiltonian it is trivial to determine the maximum width of the nonlinear resonance in $\Delta\Phi_{\ell_0 n_0}$ and ΔJ

$$\Delta\Phi_{\ell_0 n_0} = 2\pi \tag{5.62}$$

and

$$\Delta J = 4 \sqrt{\frac{\epsilon V_{\ell_0 n_0}}{\left. \frac{d\omega}{dJ} \right|_{J_r}}}, \tag{5.63}$$

which corresponds to the length and width of a separatrix envelope. The resonance width $\Delta\omega$ is obtained using Eq. (5.63) and $\Delta\omega = \omega' \Delta J$:

$$\Delta\omega = 4 \sqrt{\epsilon \left. \frac{d\omega}{dJ} \right|_{J_r} V_{\ell_0 n_0}}. \tag{5.64}$$

We can use these results immediately to obtain the width of a resonance at $\mathbf{k} \cdot \mathbf{B} = 0$, due to a perturbation resulting from the tearing mode. Using Eq. (5.46) we obtain

$$\left. \frac{d\omega}{dJ} \right|_{J_r} = \frac{1}{r} \left. \frac{d\omega}{dr} \right|_{r_s}, \tag{5.65}$$

where r_s is the radius of the singular layer. We find from Eq. (5.51)

$$\left. \frac{d\omega}{dr} \right|_{r_s} = \frac{B_\phi}{r} \left. \frac{dq}{dr} \right|_{r=r_s}. \tag{5.66}$$

Equating $\epsilon V_{\ell_0 n_0}$ and ψ' and noting that from Section 4

$$\left. \frac{d^2\psi}{dr^2} \right|_{r_s} = B_\phi \frac{dq}{dr}, \tag{5.67}$$

we obtain from Eq. (4.93)

$$\Delta r = \left(\frac{\psi'}{B_{\psi}} \frac{dq}{dr} \right)^{1/2} \quad (5.68)$$

Since $\Delta J \approx r \Delta r$ and

$$\left. \frac{d\omega}{dJ} \right|_{J_r} = \left. \frac{B_{\psi}}{r^2} \frac{dq}{dr} \right|_{r_s},$$

it follows from Eq. (5.64) that

$$\Delta r = 4 \left(\psi' / \left(B_{\psi} \frac{dq}{dr} \right) \right)^{1/2} \quad (5.69)$$

A comparison of Eq. (5.68) and Eq. (5.69) shows that they are identical except for a factor of 4 for the island width, one being obtained using straightforward perturbation theory and the other being obtained from nonlinear resonance arguments. We have also found that there is a substantially large width $\Delta\omega$ over which resonance can occur which is related to the island width. All of this has a rather straightforward interpretation. First, because of the nonlinearity any change in the amplitude of the oscillations during resonance will lead to a shift in frequency, which then departs from the resonance value. This departure in frequency then stops the change in amplitude. However this frequency departure leads to a departure from resonance, which in turn will cause the amplitude of the oscillations to begin to vary in the opposite direction, so that the frequency of oscillation again returns to the resonance value, etc. This behavior is just what one would expect from a nonlinear system, since nonlinear systems will generally evolve into a state of *marginal stability*; in this case marginal stability about the resonance frequency.

The most interesting effects occur when two resonances are near one another. It is this interaction of nonlinear resonances that is of fundamental importance. Geometrically one can imagine two resonances separated by a frequency shift $\Delta = \omega_2 - \omega_1$, where ω_1 and ω_2 correspond to the frequencies of the two resonances. Hence when $(\Delta\omega)_{J_r}$ is of the order Δ , we can expect overlap of these resonances. Thus we can define the parameter

$$s = \frac{(\Delta\omega)_{J_r}}{\Delta} \quad (5.70)$$

which is a measure of overlap. When $s \ll 1$, the nonlinear resonances are well isolated; but if $s \geq 1$, overlap of nonlinear resonances will occur. It is during overlap that the pattern of motion will change abruptly and substantially.

Figure 18 depicts what would occur if one nonlinear resonance, due to a tearing mode, overlapped with another. The most important point for flare theory is that many more reconnections can occur because of the abrupt and substantial increase in

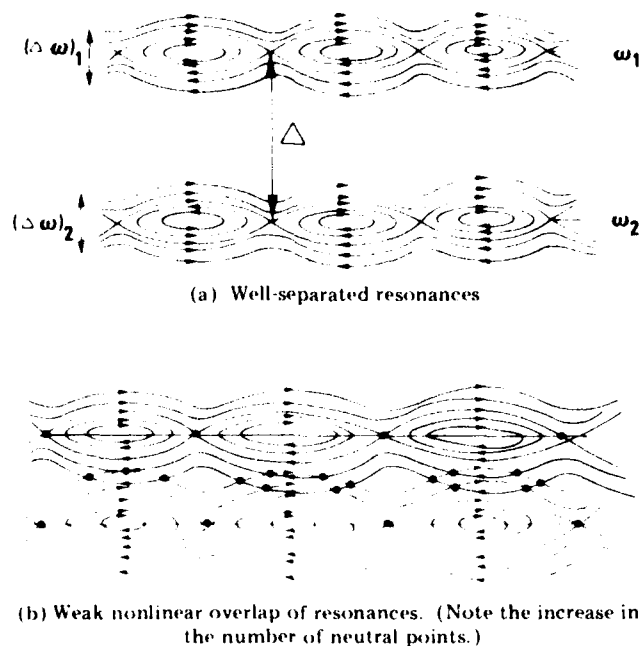


Fig. 18 Effect of resonances overlapping

X-configured neutral points. Hence, during overlap, reconnection is extremely rapid and sudden, much more so than what would occur from two isolated resonances. In addition the diffusion step sizes are increased across the magnetic field, making plasma transport unusually rapid. We see however that for islands to overlap, the strength of the perturbation must exceed some threshold. Hence nonlinear resonance overlap is an amplitude-dependent instability.

An interesting result that follows from overlap is that increasing the magnetic shear is a destabilizing factor (Finn, 1975). To see this, one first converts Δr , the width of the resonance islands, to the form $\Delta r \approx [\epsilon/(d\mu/dr)]^{1/2}$, where $\mu = B_\phi/rB_z$ and $d\mu/dr$ is the shear. The distance between resonant surfaces d is inversely proportional to the shear; thus the condition for overlap $\delta \approx 1$ corresponds to $\Delta r = d$ or $\epsilon \approx (d\mu/dr)^{-1}$. This implies that the larger the shear of the magnetic field, the smaller the perturbation amplitude required for overlap.

Let us now back up and address ourselves to the question of stochastic behavior. As we have seen, the periodic nature of a perturbation leads to the possibility of resonances at very high harmonics between the perturbed motion and unperturbed motion. If $\omega(J)$ is sufficiently nonlinear, it is possible that the normal isolated nonlinear resonance instability (e.g., the tearing mode at one singular layer and its associated destruction of magnetic surfaces) will not develop, due to a rapid departure of ω from resonance. However in this situation an even more dangerous instability sets in: the overlap of resonances. This overlap manifests itself in the virtually random behavior of

the phase point, in our case the magnetic field line, in the $J\theta$ plane, and it is found that the behavior of the distribution function for the field lines is described by a Fokker-Planck type of equation (Rosenbluth et al., 1966; Filonenko et al., 1967; Zaslavskii and Chirikov, 1972). To see this, we introduce the Liouville equation

$$\frac{\partial f}{\partial t} + \frac{\partial}{\partial \theta} (\omega f) + \frac{\partial}{\partial J} \left(\frac{dJ}{dt} f \right) = 0, \quad (5.71)$$

where $f = f(\omega, J, t)$ is constant along a field line. By use of Eqs. (5.46) and (5.47) this becomes

$$\frac{\partial f}{\partial t} + \omega(J) \frac{\partial f}{\partial \theta} = c \frac{\partial (Vf)}{\partial J}, \quad (5.72)$$

where cV is the perturbation. This equation can be transformed by standard techniques involving Fourier and Laplace transforms (Rosenbluth et al., 1966; Filonenko et al., 1967) into an equation that has the form

$$\begin{aligned} \frac{\partial F}{\partial t} = & 2\epsilon \frac{\partial}{\partial J} \operatorname{Re} \sum_{n_1 n_2 \ell} \left[V_{n_2, \ell} g_{-n_1} (0) e^{-(\omega - \ell\Omega)t} \right] \delta_{n_2 - n_1, 1} \\ & + 8\pi\epsilon^2 \frac{\partial}{\partial J} \sum_{n, \ell} |V_{n, \ell}| \delta(\omega - \ell\Omega) \frac{\partial}{\partial J} (|V_{n, \ell}| F), \end{aligned} \quad (5.73)$$

where F is related to f through the above-mentioned transforms. However the important thing to notice is that if the term proportional to ϵ is zero, i.e., the term that preserves phase memory, the equation takes the form of a Fokker-Planck equation:

$$\frac{\partial F}{\partial t} = 8\pi\epsilon^2 \frac{\partial}{\partial J} \sum_{n, \ell} |V_{n, \ell}| \delta(\omega - \ell\Omega) \frac{\partial}{\partial J} (|V_{n, \ell}| F). \quad (5.74)$$

As has been discussed, because of the nonlinear behavior of ω when passing through resonance, the amplitude changes and causes ω to change so that it will depart from the resonance value of $\omega = \omega_r$. Hence two possibilities occur: we find either

$$\Delta r \ll d \quad (5.75)$$

or

$$\Delta r \gg d. \quad (5.76)$$

The motion of the field lines is then described as follows: The neighboring resonances are well separated from one another. The field lines are trapped in an effective potential well near the resonance value, with an accuracy of order ϵ . Hence the magnetic surfaces are well behaved within the separatrix. However, when $\Delta r \gg d$, the system changes

radically. Here there is no capture of field lines, a field line may fall within any resonance, and the representative point of the field line may move about in a stochastic manner, so that the system loses all phase memory and the first term in Eq. (5.73) vanishes. Hence the behavior of the field lines obeys a Fokker-Planck equation and appears stochastic. The reader should consult the references cited for a more complete and rigorous analysis.

In summary:

- The concept of nonlinear resonance is of fundamental importance during field line reconnection.
- Overlap of resonances (separatrices) is the condition for the appearance of stochastic instability.

- Overlap causes an amplitude-dependent instability.

- Strong magnetic shear can reduce stability, contrary to what MHD theory predicts.

We will make use of these results throughout the flare model to be discussed.

6. BASIC FLARE MECHANISM

6.1 Introduction

The purpose of this section is to establish whether a current-carrying arch in the solar atmosphere, subject to the MHD kink and resistive kink modes discussed in Sections 3 and 4, can release the explosive energy (typically of the order 10^{28} ergs/s for a small flare) associated with a flare. We establish this by determining the location of the current-carrying arches that we expect will cause the classically defined flare, i.e., those flares that result in intense chromospheric heating. This allows us to assume reasonable magnitudes for various parameters, such as poloidal field strengths in the arches. With the location of these arches determined, we then show that the occurrence of MHD kink and resistive kink instabilities in arches can explain the energy release of a flare.

6.2 Location of Arches That Cause Flares

To determine precisely the location of arches that flare is difficult without a substantial improvement in our empirical knowledge of the physical conditions within these arches. However we can heuristically determine where we expect the arches that do flare to exist. Hence what follows should be considered in part as predictions of the model.

We begin by recognizing that the location of a particular kind of flare (e.g., impulsive rise versus gradual rise) is undoubtedly related to the rate of energy released, which in turn is determined by the magnitudes and gradients of quantities like the magnetic field and density, which are in turn determined by the arches' size and location. Keeping this in mind, one can represent the rate at which magnetic energy is thermalized by the tearing mode by

$$\frac{dc}{dt} \approx \frac{\gamma B_p^2 \Delta V}{4\pi}, \quad (6.1)$$

where ΔV is the incremental volume along the arch in which the tearing mode occurs. The poloidal component of B_p occurs in Eq. (6.1) because it is the principal component of field dissipated. Since γ and B_p are in general functions of position in the arch, dc/dt will differ at different locations along the arch. Further, since γ and B_p are strongly influenced by both the magnitudes and gradients of various parameters, we should expect $\gamma B_p^2/4\pi$ to be greatest where the magnitudes and gradients of these parameters maximize it. Hence we should expect the location of instability to appear well localized within the arch; i.e., the incremental volume ΔV should be such that $\Delta V/V \ll 1$, where V is the total arch volume. This is what is observed (Widing and Cheng, 1975; Cheng and Widing, 1975). Indeed, since observationally ΔV is small, $\gamma B_p^2/4\pi$ must necessarily be large, which implies steep gradients and large B_p , which in turn clearly implies the arches must exist low in the solar atmosphere if they are to explain solar flares.

If we were to require the bulk current to be electrostatically unstable at flare onset, we again would be forced to require the arches to be low lying, since the field gradients would then have to be of the order of a skin depth, if the current is to be electrostatically unstable.

An alternate means of determining which arches will flare is to ask about the global stability of the arch. As discussed in Section 2, arches are observed to exist prior to their flaring and appear stable. If they are to be MHD stable, they must be stable against the global kink mode prior to flaring. This requires the safety factor q , defined in Section 3, to satisfy $q \gg 1$ at every point in the arch. To see this, we note that by flux conservation $B_T r_0^2 = \text{constant}$ and $B_p \approx 2I/cr_0$, where I is the total toroidal current and assumed here to be constant. Hence, since $q = 2\pi r_0 B_T / B_p L$, we find q approximately independent of position along the current path (In Appendix A we examine this point more critically.) Two things are clearly represented in $q \gg 1$: the larger is $2\pi r/L$, the greater is q , and the larger is the ratio B_T/B_p , the greater is q . These requirements however can be satisfied in small or large arches for suitable parameter regions. Thus, to continue our argument, we must turn again to flare energy requirements.

Since B_p must be relatively large to explain the energy release from an arch, we must also have B_T large for a fixed $2\pi r/L$ if q is to remain above 1. However, to obtain a large B_T requires that we descend in altitude, since B_T increases with decreasing altitude. But in so doing L will usually decrease, causing $2\pi r/L$ to increase. These arguments imply that for an arch to be kink stable prior to flaring and then to release enough energy to explain a flare, it must have a relatively low altitude.

These arguments can be supplemented by noting the stabilizing effect of the conducting ends on the arch and demanding the arch be stable against G modes. As shown by Solovév (1971), a sufficient condition for stability for a cylindrical diffuse pinch attached to conducting ends is

$$\frac{j_T L}{\pi c B_T} < 1, \quad (6.2)$$

and the necessary condition is

$$\frac{j_T^2 r L}{8\pi B_T^2 c^2} < 1. \quad (6.3)$$

Both conditions require B_T to be large and L to be small. Further, according to Eq. (4.100) the arch will be stable against resistive G quasi-modes if the β of the arch satisfies $\beta > \beta_{\text{critical}}$, where

$$\beta_{\text{critical}} = \frac{rc_s^2}{g\pi L^2}. \quad (6.4)$$

This can be cast in the form

$$\frac{L^2 \pi g \beta}{rc_s^2} < 1, \quad (6.5)$$

which again implies L must be small and B_T must be large. We can then predict that for an unstable arch to act as a flare and to release the appropriate amount of energy in the required amount of time, it must be low lying with a small length.

So far we have demanded the arch be MHD stable. Alternately we can demand that the bulk toroidal current density j_T be electrostatically stable prior to flare onset. A sufficient condition for the bulk current to be electrostatically stable is that the drift velocity v_d be less than some critical thermal velocity. Since the Buneman instability is the least likely current-driven instability, we impose the condition that the bulk current be stable against the electrostatic ion cyclotron and ion sound modes. Using Amperes' law, $j_T = nev_\alpha$, and $v_d \ll c_s$ (Appendix B), we require

$$n \gg 2.29 \times 10^5 \frac{j_T}{\sqrt{T_e}} \quad (6.6)$$

within the arch, if the current is to remain electrostatically stable. Since, the larger is n , the greater is the conductive and radiative cooling, we should expect T_e to be low in the stable low-lying arch. Further, since observationally $n \approx 10^{11}$ to 10^{12} cm^{-3} in the flaring arches, and the smallest observed temperature in the solar atmosphere is 6000 K, we should expect j_T to satisfy $j_T \ll 10^8$ statamperes/ cm^2 in the arch prior to its flaring. As we shall see, $j_T > 10^7$ statamperes/ cm^2 is of the order required to explain the energy release of the flare. We can then foresee requiring a preflare buildup of current within the arch.

To summarize, we have predicted that the arches prior to flaring are low lying, with a small length, a high density, and probably a low temperature, at least in the arch core, i.e., $r \approx 0$. Later, after we discuss flare energy requirements, we will estimate the length and height of an arch for the parameters to be adopted.

From the preceding discussion one should expect various classes of flares to occur, from an extremely impulsive rise to an extremely slow rise, all on the basis of gradient steepness and field magnitudes. The fast-rise flares should occur in regions of steep gradients, and slow-rise flares should occur in regions of weaker gradients. Since in general gradients can be expected to weaken with altitude, one should expect the most impulsive flares to occur in small compact arches, and gradual-rise-and-fall (GRF) flares should occur in larger arches, i.e., arches with larger L . On the other hand, great flares, in the sense of quantity of energy released, should occur in arches with very large currents but not necessarily large gradients, and small flares should occur in arches with smaller currents but not necessarily with weak gradients. Hence on the basis of these relatively trivial arguments we should expect four basic classes of flares originating in arches:

- GRF with small energy release,
- GRF with large energy release,
- Impulsive rise with little energy release,
- Impulsive rise with large release.

6.3 Mechanisms for Magnetic Energy Conversion

The most crucial question of any flare model is how the stored energy is converted into the kinetic processes associated with a flare. As we have seen, there are basically three means by which current in a diffuse pinch, and therefore an arch, can be converted into kinetic energy: pure MHD modes, resistive MHD modes, and electrostatic instabilities.

Electrostatic instabilities will play a role in our flare model only as mechanisms to alter the transport coefficients. This follows because, if the bulk current were to become electrostatically unstable, the rate of anomalous heating by microturbulence is of the order $\eta_{an} j_T^2 \Delta V$, where η_{an} is the anomalous resistivity resulting from the electrostatic instability. Since ΔV is small observationally, $\lesssim 10^{25}$ cm³, j_T must be large to explain the energy release, and η is of the order 10^{-13} s. Hence, if $j_T \approx 10^7$ statamperes/cm², $dc/dt \lesssim 10^{26}$ ergs/s, which is insufficient to explain a flare unless ΔV or j_T are increased. In addition, it is easy to show that most MHD modes will be excited prior to the bulk current becoming electrostatically unstable. Hence one expects the MHD modes to come into play long before the arch current ever becomes electrostatically unstable. Therefore the pure MHD and resistive MHD modes will be of primary concern.

As should be clear, the MHD modes and the resistive modes differ only in that the MHD modes assume an infinite-conductivity model, whereas the resistive modes relax this constraint and in so doing permit instabilities *not* because they are *energetically favorable* but because the infinite conductivity constraint excluded them from the outset. Thus we found that once finite conductivity is introduced, a much wider class of instabilities was permitted. We should therefore be careful not to make the mistake of assuming that if a pure MHD mode were to occur, a resistive mode cannot also occur or

vice versa. Indeed we should expect both classes of instabilities to occur during the duration of the flare, if conditions are satisfied. Thus, although we emphasize the tearing mode in our discussion of energy conversion, we should still expect MHD kink modes to occur.

6.4 Volume Of Energy Release

When we consider the volume within which instability can occur, we have to ask: what is the thickness in minor radius Δr where instability occurs, and over what portion of the arch ΔL should it occur? However, to determine ΔL or Δr requires precise knowledge of the current density and B_T over the whole of the arch. This of course is not known. We can however argue that although Δr and ΔL have certain minimal values initially, they will enlarge as the instability convects out of the region of initial instability. For example we noted in Section 3 that Suydam's condition implied convective mixing outward toward the outside boundary until stable and that this convection should easily occur because of the small separation of modes due to the scale of the arch. Further, because $\mathbf{k} \cdot \mathbf{B} = 0$ requires specifying two mode numbers (k, m), there are potentially an infinite number of singular layers possible to excite. In addition singular layers within a distance δr of one another will have nearly the same mode numbers (k, m) and therefore similar growth rates, if unstable. Hence this region of thickness δr will be subjected to the nonlocal quasi-modes, which can greatly increase the volume in which instability occurs. Or, if the amplitudes of the current perturbations which result from the tearing mode are large enough, resonances can overlap, substantially increasing the effective volume of reconnection. We can then conclude that Δr should be much greater than a thickness of a singular layer. Thus we assume $\Delta r \gg \epsilon a$ and we take $\Delta r \approx r_{\max}/10$, where r_{\max} is the minor radius of the outside boundary of the arch.

An examination of Eq. (6.2) shows that the critical current density for kink instability is a function of the location along the arch as well as of r . We should therefore expect there is some length ΔL in which instability will occur. We will let observations of small flares guide us here and assume $\Delta L \approx 1400$ km. Since r_{\max} observationally appears to be of the order 700 km, we have that $\Delta r \approx 70$ km. Hence we will adopt in all the estimates to follow an incremental volume $\Delta V \approx 2\pi r_{\max} \Delta r \Delta L \approx 4.3 \times 10^{23}$ cm³ for a small flare. This necessarily implies $\gamma B_p^2/4\pi$ must be $\gtrsim 10^5$ ergs/cm³ s if we are to explain the small-flare energy release, which is typically of the order 10^{30} ergs over 100 s. In addition we will adopt the values $B_p = 500$ gauss, $n = 10^{12}$ cm⁻³, and $T = 5 \times 10^5$ K as the initial temperature at instability onset. It must be recognized that the adopted values all correspond to the values obtained from small flares as observed by the ATM. We will assume for the present that one can explain large flares by an appropriate scaling of these parameters.

In what follows we will assume that conditions existing within the arch are such that the tearing mode can be excited, i.e., $\Delta' > 0$ (Eq. (4.72)). Further, we will use the growth rate corresponding to the fastest growing tearing modes in sheet geometry, i.e., $\alpha = 0.2 = ka$ (FKR, 1963) these being the modes we expect to grow first. This implies a growth rate

$$\gamma \approx \frac{1}{\sqrt{\tau_R \tau_H}} \quad (6.7)$$

We are using sheet geometry only for ease in calculation, since the numerically calculated growth rates for various cylindrical magnetic-field models in Appendix C are difficult to apply in parameterized form. However the growth rates obtained for cylindrical models are generally greater for the same Reynolds number and α . In particular the numerical growth rates appear to be very model dependent; e.g., the force-free BFM with $S \approx 10^6$ and $\alpha = 0.2$ gives $\gamma \approx 10^2$, whereas the sheet pinch gives $\gamma \approx 10$.

Using

$$\tau_R = \frac{4\pi a^2}{\langle \eta \rangle c^2} \quad (6.8)$$

and

$$\tau_H = \frac{a(4\pi\rho)^{1/2}}{B} \quad (6.9)$$

where $a \approx (\cdot B_p/B_p)^{-1}$ across the singular layer or layers, we obtain from Eq. (6.1)

$$\frac{d\epsilon}{dt} \approx 1.6 \times 10^{14} \left(\frac{\langle \eta \rangle}{\sqrt{n}} \right)^{1/2} \Delta V \left(\frac{B_p}{a} \right)^{3/2} B_p \quad (6.10)$$

Consider first the behavior of the energy release when the resistivity is classical. Since $\eta \sim T^{-3/2}$, $dc/dt \sim T^{-3/4}$, which suggests the energy release by the tearing mode evolves into a state of marginal stability. That is, since $dc/dt \sim T^{-3/4}$, the rate of energy release drops off and continues to do so until the mechanisms that cool result in a temperature drop, which then drives dc/dt back up above the cooling rate, so the instability evolves to a marginal state.

The marginal state will occur at some temperature T_F , at which time

$$\frac{1}{\Delta V} \frac{d\epsilon}{dt} \approx nm_e v_{Te}^3 \frac{(T_F)}{\Delta L} \quad (6.11)$$

where we have used the fact that thermal conduction appears to be the dominant cooling mechanism during flares. Hence near marginal stability the growth rate is given by

$$\gamma(T_F) \approx nm_e v_{Te}^3 \frac{(T_F)4\pi}{B_p^2 \Delta L} \quad (6.12)$$

which is much less than $\gamma(T_m)$. We identify this marginal state with the so-called gradual phase of the flare and identify the initial growth phase with the impulsive phase or flash phase. Such identifications necessarily imply that the energy release is continuous but decreasing during the gradual phase.

Inserting the adopted values for T_m , n , B_p , and ΔV into Eq. (6.10), we obtain

$$\frac{dc}{dt} \approx \frac{6.8 \times 10^{33}}{a^{3/2}} \quad (6.13)$$

A typical small flare releases $\approx 10^{30}$ ergs in a time $\Delta t \approx 100$ s. Thus we require $dc/dt \approx 10^{28}$, which implies $a \approx 7.7 \times 10^3$ cm. An $a \approx 7.7 \times 10^3$ cm corresponds to a perturbation with a wavelength $\lambda \approx 10\pi a = 2.4 \times 10^5$ cm if $\alpha = 0.2$. Such a wavelength perturbation will not cause the arch to be globally kink unstable; hence we do not expect these perturbations to cause global kinks in a *flaring arch*, although longer wavelength kinks can develop.

A gradient of the order 7.7×10^3 cm and a $B_p \approx 500$ gauss corresponds to a toroidal current density $j \approx 1 \times 10^8$ statamperes/cm² in, or $B_p/a \approx 0.06$ gauss/cm across the singular layer: a value $\approx 10^2$ times greater than has been observed in active regions (Title and Andelin, 1971). This value of the field gradient should not however be considered excessive, since the observations typically have a spatial resolution $\gg 700$ km and thus average over the whole of the arch cross section, whereas this value of B_p/a should exist only in a localized region, which, as we will see, can occur because of a rapidly growing current density in the region of the stability.

6.5 Anomalous Resistivity and the Energy Release Rate

Using Eq. (6.6) and inserting T_m and $j \approx 1 \times 10^8$ statamperes/cm², we find that $n \leq 2.26 \times 10^{10}$ cm⁻³ is required for stability against the electrostatic ion sound or ion cyclotron mode. Since we have chosen $n = 10^{12}$, we still satisfy this requirement and the bulk current is electrostatically stable. Similarly the value a obtained earlier also is above the gradient scale for the ion sound instability (Table B1), which yields for the adopted values $a \approx 10^2$ cm. However both of these equivalent results imply that it may be possible to drive the current electrostatically unstable in the regions around the singular layer. Hence it is important that we consider how anomalous resistivity will affect the rate of energy release.

As discussed in Appendix B, we can expect two types of instabilities that can lead to anomalous resistivity: current driven, either parallel or perpendicular to the magnetic field, and beam driven. We will consider only the parallel current-driven and beam-driven instabilities, while noting that the cross-field-driven instabilities have thresholds similar to the parallel-field-driven instabilities and as such will yield similar results. However a more correct treatment of current-driven anomalous resistivity would examine \mathbf{j}_\perp -driven instabilities, since the current is flowing perpendicular to \mathbf{B} near the singular layer. But because the magnetic field changes sign at $\mathbf{k} \cdot \mathbf{B} = 0$, it is small there, and we will neglect it to first order.

Let us assume that the parallel-field current-driven ion sound instability is excited and that $T_e/T_i = 10$. As given in Table B2, the a required for instability is

$$a \lesssim \frac{c}{\omega_{pi}} \left(\frac{1}{\beta_p} \right)^{1/2} \frac{1}{1 + \left(\frac{T_e}{T_i} \frac{m_i}{m_e} \right)^{1/2} \exp\left(-\frac{T_e}{2T_i}\right)}$$

which for the adopted values yields $a \approx 1.4 \times 10^2$. Such a gradient corresponds to $j_T \approx 8.52 \times 10^9$ statamperes/cm² or $B/a \approx 3.57$ gauss/cm in or across the singular layer. Such a field gradient is not likely to be found along the whole length of arch but rather in a well localized region and will act as a localized current interruption or discharge, generating localized voltage drops along the singular layer.

These regions will expand somewhat, since the unstable waves of the excited instability will propagate out of the region of instability, at their group velocity, into a region where they are stable. Within these small regions the resistivity will be anomalous, the instability exciting the anomalous resistivity, here assumed to be the ion sound instability, will saturate in a few ion plasma times to a state of marginal stability. Within these regions one should expect extreme localized heating much greater than in the regions where the resistivity is classical. However it is unlikely that the bulk of the energy across the total cross section of the arch will become electrostatically unstable, because of the steep gradients required.

Since the effective collision frequency, due to the current-driven turbulence, is typically as $\nu_{eff} \sim A\omega_{pe}$, the growth rate of the tearing mode in the presence of this bulk current-driven anomalous resistivity will be dominated by the density, so that $\gamma \sim n^{-1/2}$ rather than $\gamma \sim T^{-3/4}$. Equation (6.1) becomes

$$\frac{1}{\Delta V} \frac{d\epsilon}{dt} \approx 10^{10} \left[\frac{A}{n} \right]^{1/2} \left(\frac{B_p}{a} \right)^{3/2} B_p,$$

where A for the ion sound instability is of the order 1/100. Using the adopted values for n and B_p and $a \approx 10^2$ cm, we find

$$\frac{1}{\Delta V} \frac{d\epsilon}{dt} \approx 4.26 \times 10^7 \text{ ergs/cm}^3 \text{ s},$$

which is approximately 10^2 greater than if the resistivity were classical.

If the flare were due only to these small regions within the arch, then the volume of instability would be $\approx 10^{20}$ cm³, or if a given flare resulted from a combination of tearing modes dominated by classical and anomalous resistivity, that particular flare would show evidence of extremely intense emission within regions 5×10^7 cm² in cross-section and length $\gtrsim 10^5$ cm.

However the heating at the onset of anomalous resistivity is dominated not by the tearing mode but by the current-driven microinstability, since the growth rates for microinstabilities are so much greater than the growth rates for any macroinstability. Thus the temperature within an electrostatically unstable singular layer will grow rapidly at a rate

$$\frac{\partial T_e}{\partial t} \approx \gamma_{\text{micro}} T_e$$

After saturation of the microinstability, which occurs in a few ω_{pi} , the heating rate the microinstability is given by

$$nk \frac{\partial T_e}{\partial t} \approx \eta_{AN} J_T^2,$$

which is of the order $7 \cdot 10^5$ ergs/cm³ s within the electrostatically unstable singular layer. This heating however is dominated by the tearing-mode energy release, which turn is dominated within these singular layers by anomalous resistivity, as given by (6.15).

Let us summarize what we have found as far as energy release is concerned. We have considered two cases: an electrostatically stable bulk current which leads to a by the tearing mode dominated by classical resistivity, and an electrostatically unstable current occurring only in some singular layers while the remaining singular layers are electrostatically stable. This second case results in what should be construed as normal thermal heating within the electrostatically unstable singular layers. Further, the total volume occupied by all the singular layers dominated by anomalous resistivity is \approx cm³, which is $\approx 10^{-5}$ less than the resolution-limited volume of $\lesssim 10^{25}$ cm³ reported by the Skylab observers, whereas the volume required to explain the flare with a classical resistivity dominated energy release was 10^{23} cm³, which is $\approx 10^2$ less than the observed volume. However present observations do not require that we invoke bulk current-anomalous resistivity to explain the flare energy, nor do present observations support assumptions of such gradients. Hence we will not comment on this further.

Let us now consider a source of anomalous resistivity that is generated by a non-thermal beam trapped in a current-carrying arch, as developed by Papadopoulos and Coffey (1974a, 1974b) and briefly discussed in Appendix B. If this beam is inhibited from relaxing quasilinearly by nonlinear processes, the beam will represent a nonlinear driving mechanism, capable of producing ion density fluctuations. The particular nonlinear process considered by Papadopoulos and Coffey is the parametric oscillating stream instability (OTS). The requirement that OTS stabilizes the beam before the linear relaxation of the beam occurs is given by

$$\frac{\Delta v_b}{v_b} > \left[10^2 \left(\frac{n_b}{n} \right)^{2/3} \left(\frac{v_{Te}}{v_b} \right)^{2/3} \left(\frac{m_i}{m_e} \right)^{1/3} (k_{r1} \lambda_d)^{-2/3} \right]^{3/7},$$

where v_b is the beam velocity, Δv_b is the beam thermal spread, n_b is the beam density and $k_m \lambda_d \approx 0.15$, k_m being the wave number with the maximum growth rate.

The assumption that a beam exists in an arch (the origins of such a beam will be discussed in Section 8) with $v_b \approx 10^{10}$ cm/s and $T_e \approx 10^6$ K yields

DANIEL S. SPICER

$$\frac{\Delta v_b}{v_b} \geq 10 \left(\frac{n_b}{n} \right)^{2/7}.$$

If $\Delta v_b/v_b \approx 1/3$ and $n \approx 10^{12} \text{ cm}^{-3}$, Eq. (6.20) implies $n_b \lesssim 7 \times 10^6 \text{ cm}^{-3}$ is to be stable against quasi-linear relaxation. If such a beam exists within the arch will lead to purely growing ion-density fluctuations with an effective collision

$$\nu_{eff} \approx 2 \left(\frac{\pi}{2} \right)^{1/2} \omega_{pe}(k_m \lambda_d) \left(\frac{n_b}{n} \right) \left(\frac{v_b}{v_{Te}} \right)^2 \frac{\Delta v_b}{v_b}$$

(Papadopoulos and Coffey, 1974b). Using the values previously obtained, we

$$\nu_{eff} \approx 86.7 \omega_{pe} \left(\frac{n_b}{n} \right).$$

As noted by Papadopoulos and Coffey, Eqs. (6.21) and (6.22) show the anomalous resistivity is proportional to the beam energy, and for fixed beam resistivity scales as $n^{-1/2}$. Thus the anomalous resistivity will be a decreasing altitude in the arch.

Since the Coulomb collision frequency $\nu_{ei} \approx 80nT_e^{-3/2}$, we find for $T_e \approx 10^6 \text{ K}$, $n \approx 10^{12} \text{ cm}^{-3}$, and $n_b/n \approx 10^{-6}$ that

$$\frac{\nu_{eff}}{\nu_{ei}} \approx 3 \times 10^2.$$

Hence we expect the *bulk* resistivity η to increase by $\approx 3 \times 10^2$ over its classical value. Using Eq. (6.10), we find that the energy release will increase by a factor of those values obtained when the resistivity was assumed classical.

Since the time scales for beam stabilization by OTS are so short, a quasisteady state should be established so together the beam plasma and parametric instabilities exist to a marginally stable state. Thus the bulk anomalous resistivity generated by the beam will exist with a ν_{eff} given by Eq. (6.22) over the duration of the beam. However, the effectiveness of this mechanism is clearly related to lifetime of the beam, or the time in which beam replenishment occurs, as well as the cross-sectional area of the beam exists. Since these questions are clearly related to the origins of the arch, we will postpone its discussion until we take up the question of flare precursors.

We are now in a position to estimate the size of the arch. Taking the value of B_p and taking the total energy released during a small flare to be $\approx 10^{30} \text{ erg}$, the total storage volume required is of the order $5 \times 10^{25} \text{ cm}^3$, which is relatively

If the volume of the observed arches is greater than this, with $B_p \sim 500 \text{ G}$, the arch will have sufficient volume to store the energy necessary to explain the

release. If the volume is less than this, a current reservoir must exist beneath the photosphere which maintains the current throughout the flare duration.

If we take $2\pi r/L \approx \pi/5$, with $B_p \approx 500$ gauss we require $B_T \gg 795$ gauss, if the arch is to be MHD stable prior to flaring. A ratio of $r/L \approx 1/10$, using $V \approx \pi R$, we find $R \approx 3 \times 10^8$ cm. Hence, the arch will have an altitude of the order 3000 km for the small flare considered.

We will conclude this section by discussing briefly the validity of Eq. (6.1). First, it should be obvious that the use of

$$\frac{d\epsilon}{dt} \approx \frac{\gamma B_p^2 \Delta V}{4\pi}$$

sweeps many problems under the rug. It ignores the fact that one should expect things like nonlinear mode coupling between primary resonances, secondary resonances, etc. which occur by generating higher harmonics and subharmonics of the original modes. Everything else being equal, these higher harmonics necessarily have higher growth rates, by Eq. (4.23). Similarly, the stochastic behavior of the field lines around the separatrices may enhance the resistivity, thereby generating an MHD turbulence spectrum. Indeed Ichimaru (1975) has recently shown that an explanation of the reconnection rate empirically derived by Parker (1973) can be derived theoretically by invoking MHD turbulence in the neutral sheet. Hence it is not unreasonable to conjecture that the MHD turbulence required by Ichimaru is generated by the stochastic field-line behavior during resonance overlap, as discussed in Section 5, but this is clearly not built into Eq. (6.1). In addition Eq. (6.1) ignores the fact that different singular layers are tearing at different places at different times within the flare volume. Or, to put it otherwise, Eq. (6.1) averages over a multitude of sins which the complexities of the physics and mathematics forces on the physicist.

7. THE FORMATION OF IMPULSIVE ELECTROMAGNETIC BURSTS AND SHOCKS

7.1 Introduction

As is clear from Section 6, the mechanisms we have proposed for the thermalization of the magnetic field in an arch are more than adequate to explain the total energy release of a flare. If these thermalization mechanisms were to lead to a thermal plasma only, our model could explain only the thermal flare, i.e., those flares that do not lead to impulsive electromagnetic bursts (IEBs) and to shocks. Hence the purpose of this section is to examine the means by which MHD and resistive MHD instabilities can lead to IEBs and to shocks.

As a way of introduction to what we feel is a more realistic explanation of IEBs, we briefly illustrate a well-known laboratory phenomenon that has many features similar to those that occur during a nonthermal flare.

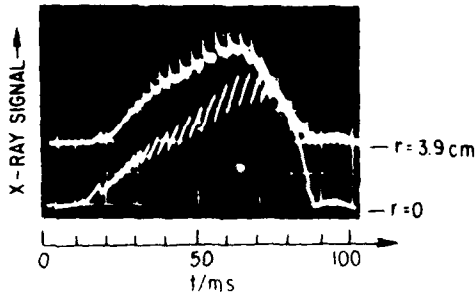


Fig. 19 X-ray trace due to disruptive instability

Figure 19 illustrates the x-ray trace, obtained from the ST Tokamak (von Goeler et al., 1974), generated by an instability referred to as the disruptive instability. This figure illustrates two things: an extended x-ray burst and, superimposed on it, impulsive x-ray bursts. The similarity between this laboratory phenomenon and the impulsive flare should be obvious and appears to be quite significant. First, the explanation of this impulsive behavior, as we will discuss in more detail, is believed to result from a combination of MHD and resistive MHD modes, and, second, the bremsstrahlung bursts are not due to just accelerated particles but rather from both intense thermalization of the magnetic fields and electron acceleration in the induced electric fields generated during instability. Hence soft and hard components of these IEBs exist, both emanating from the same volume.

7.2 Thermal or Nonthermal Flares

To make clear what we mean by thermal and nonthermal flares, we examine under what circumstances the tearing mode is a thermal or nonthermal process. The definition we will adopt is: a thermal plasma is a plasma in which relaxation between like species has occurred or in which the approach to relaxation has reached some semblance of a steady state. Hence a *necessary* condition for the heating to be nonthermal is: the heating per particle per second must exceed the rate at which relaxation occurs between like species. In our case the species of interest is the electron.

The above definition implies that the tearing mode will act as a nonthermal heating mechanism for electrons if

$$\frac{\gamma B_p^2}{4\pi n_s} > \nu_{ee} kT_e \quad (7.1)$$

where n_s is the number density of those electrons in "resonance" with the tearing mode and ν_{ee}^{-1} is the relaxation time between electrons, defined (Spitzer, 1967) as

$$\nu_{ee}^{-1} \approx 0.266 \frac{T_e^{3/2}(\text{K})}{n_e \ln \Lambda} \text{ sec.} \quad (7.2)$$

Equation (7.1) states that those electrons in resonance with the tearing mode will be heated at a faster rate than electron-electron collisions can relax the electron distribution. Generally only the fast-growing short-wavelength tearing modes will satisfy this condition.

Equation (7.1) has a number of consequences which can better define the origins of the thermal and nonthermal flares. Clearly the larger the ambient density, the harder (7.1) is to satisfy, and the larger the B_p and γ , the easier (7.1) is to satisfy. Since we expect B_p and γ to increase as we descend in altitude and n to decrease as we ascend in altitude, there should exist an annulus, with a thickness Δh in altitude and mean altitude h , within which nonthermal flares generally occur.

Using the adopted values from Section 6, we find the energy transmitted to an electron per second, by the tearing mode, is of the order 86 keV/s, if $n_s = n$. This rate of nonthermal heating is more than sufficient to explain the observations.

The tearing mode will also accelerate a selected few electrons by the *induced* toroidal fields, generated during reconnection. The magnitude of this electric field, and the subsequent energy gain $\Delta\epsilon$ can be crudely obtained from Faraday's equation. We obtain $\Delta\epsilon \approx e\gamma B_p a^2 2\pi/c\alpha$, and using the values adopted for B_p , γ , a , and α , we find a maximum energy gain of the order 2MeV.

7.3 Mechanisms That Can Form IEBs and Shocks

As noted, nonthermal flares are invariably associated with shocks. This is highly suggestive, because the formation of a shock requires a sudden increase in pressure, and to form such a pressure pulse requires either that the flare heating mechanism rapidly thermalize part of the stored energy or a that rapid motion of the bulk plasma takes place. We consider both these possibilities.

If we require the impulsively heated and/or accelerated electrons and shocks to emanate from the same thermalization volume within the arch, we must also require the conversion of potential energy to kinetic energy be extremely rapid during their formation. This suggests the difference between the thermal and nonthermal flare lies in the rate of energy conversion per unit volume. Since the greater the conversion rate for this model, the greater the rate of current dissipation, it follows that during such rapid dissipation the magnitudes of the expected current perturbations by the tearing mode are also greater. Hence the likelihood of nonlinear resonant overlap is greatest in this situation.

Nonlinear resonant overlap, we have noted earlier, will result in abrupt and dramatic increases in the rate of reconnection. During overlap we can therefore expect impulsive heating and acceleration at rates which are much greater than linear analysis would predict. Overlap should also increase in likelihood of (7.1) being satisfied.

Finn (1975) has calculated the magnitude of the required current perturbation for overlap of the $m = 2$ islands and $m = 3$ islands for a peaked current model (Furth et al., 1973). He found that the perturbations necessary were typically $\approx 1.5\%$. For a less peaked current profile (less shear) Finn found somewhat larger current perturbations necessary (4%). These studies illustrate that relatively weak perturbations can lead to resonant overlap and may play a very important role in flares.

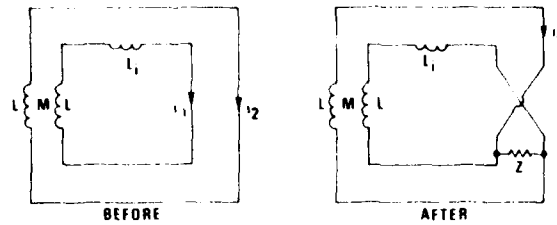


Fig. 20 -- Circuit analogy showing reconnection of current paths following resonant overlap of the magnetic fields in a plasma (STIX, 1975)

To estimate the magnitude of energy dissipated during overlap of two separatrices, we follow a simple circuit analog (Stix, 1975) illustrated in Fig. 20. We assume the presence of two primary chains of islands at resonant surfaces $q = m$ and $q = m'$, both growing due to the tearing mode. Next we assume a sheet geometry for simplicity. Initially a current i_1 flows on the inner of the two adjacent magnetic surfaces and a current i_2 , $i_2 \neq i_1$, flows on the outer surface. We can represent the poloidal magnetic energy stored between these resonant surfaces by $L_i i^2/2$, where L_i is the leakage inductance. Similarly the magnetic energy stored outside of the outer surface is given by $(Li_1^2 + 2Mi_1 i_2 + Li_2^2)/2$, where M is the mutual inductance arising between the adjacent surfaces. Overlapping intermixes the field lines, effectively generating a series connection, illustrated in Fig. 20.

Initially the current through the inductive elements is i_1 and i_2 . Because $\nabla \cdot \mathbf{j} \approx 0$, the difference in current $i_2 - i_1$ must flow radially between the former adjacent surfaces. The transient flow will then generate a polarization current

$$\mathbf{j}_p = \frac{\rho c^2}{B^2} \frac{\partial \mathbf{E}}{\partial t} \quad (7.3)$$

This polarization current will then lead to a net gain in plasma energy

$$\Delta \epsilon = \Delta \frac{m_{e,i} c^2 E^2}{2B^2} \quad (7.4)$$

or, since

$$\mathbf{v}_d = \frac{c \mathbf{E} \times \mathbf{B}}{B^2}, \quad (7.5)$$

$$\Delta \epsilon = \Delta \left(\frac{m_{e,i}}{2} v_d^2 \right); \quad (7.6)$$

which, as Eq. (7.6) shows, appears principally as ion energy.

The radial current path is represented by some high-impedance Z bridging the inductive elements. Stix (1975) shows that with perfect coupling, $L = M$, the total loop current has a net change $\Delta i \sim (L_i/2L)(i_1 - i_2)$ and a magnetic energy $L_i(i_1 - i_2)^2/8$ is dissipated in the bridging impedance. The magnitude of this dissipated magnetic energy can be considerably greater than what one would find from one resonant surface.

An alternate as well as complementary means by which this model can generate IEBs and shocks is by global kink modes. That is, the whole arch or a substantial portion of it may undergo kinking, leading to a strong disruption of the bound plasma. Since a kinking arch will produce effects similar to the disruptive instability previously mentioned, this would be an appropriate place to include it in our discussion.

The disruptive instability (DI) develops when the toroidal current in a tokamak causes the safety factor q at the plasma boundary to be small, i.e., $q \approx 3$ or 4. The DI manifests itself either as singular or quasi-periodic abrupt changes in the plasma parameters. These changes are a result of a slow $m = 1$, $n = 1$ internal kink mode which has a growth rate $\gamma \approx v_A/R$. During the growth x rays are formed which are suddenly reduced in magnitude because of a rapid cooling in the central region of the Tokamak. This cooling disruption appears as a symmetric $m = 0$, $n = 0$ mode (in an arch the $n = 0$ mode is forbidden, although the $m = 0$, $n = 1$ mode can occur). After the cooling disruption a slow process of relaxation sets in with $q < 1$ at the magnetic axis, i.e., $r = 0$, and the whole sequence may repeat itself.

Kadomtsev (1976) has recently proposed a new explanation for this phenomenon. Qualitatively Kadomtsev argues that as the internal kink grows, it will compress neighboring magnetic surfaces to one side, which then undergo resistive kink modes and thus reconnection. As the kink attempts to stabilize itself, it will nonlinearly swing back and forth between stability and instability. During this period the reconnection process will repeat itself quasi-periodically, so the magnetic field dissipated will appear as impulsive joule heating and subsequently as x rays. If the distortion of the magnetic surfaces by the kink modes is great enough, the kink can cause resonant overlap with an accompanying increase in field dissipation and subsequent heating. This should be especially true in an arch, because of the close spacing of the modes.

If we apply these ideas to an arch, we find similar effects. Since a kink oscillates with a frequency of the order $f \approx 2\pi/kv_A$, we find for the $m = 1$, $n = 1$ mode $f = L/v_A$. This corresponds to a frequency range of about 1 to 30 s, the exact magnitude being determined by the local conditions within the arch.

If the kink were an external kink rather than an internal kink, the kink could thrash about, causing shock waves in the ambient atmosphere. If these shocks have a large enough Mach number, the shocks can excite various two-stream instabilities (Tidman and Krall, 1971), thereby causing a rapid "thermalization" of the shock's ordered energy. Hence, in this case, one should expect bursts of bremsstrahlung with a period similar to those obtained earlier.

If the kink were instead a resistive kink which formed on the plasma boundary of the arch, as depicted for a diffuse pinch in Fig. 21 and for an arch in Fig. 22, it could explain why impulsive x-ray bursts and type III bursts sometimes appear in groups, five

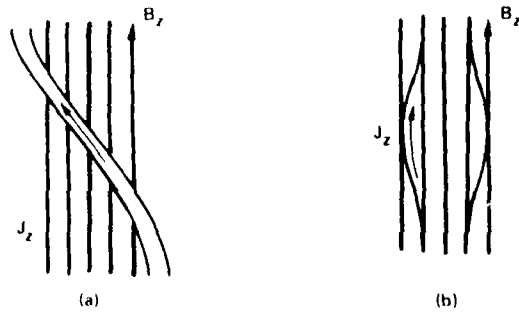


Fig. 21 - Resistive instabilities for a diffuse pinch (a) stabilized pinch with kink in $J_z(m = 1)$ (b) stabilized pinch with sausage in $j_z(m = 0)$

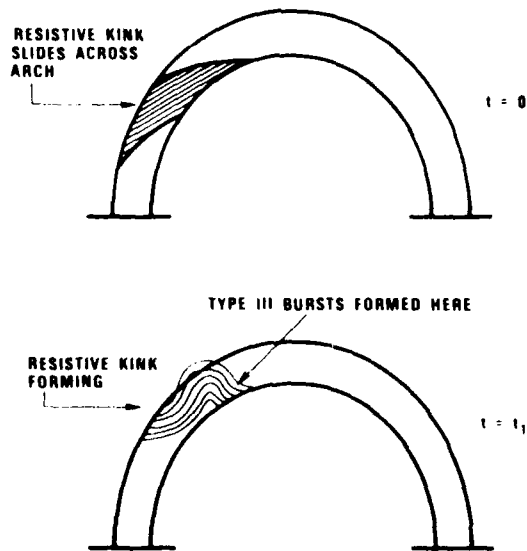


Fig. 22 - Type III bursts and resistive sheet kink

type III bursts and five x-ray bursts with similar structure. This follows because an MHD kink results in a strong distortion of the plasma column and in so doing results in an appreciable induced electric field, which can accelerate particles (Glasstone and Lovberg, 1960).

A similar situation can occur when resistivity is taken into account. Here a kinking current sheet will be formed at the boundary of the plasma column and will slide across the column as it kinks (Fig. 21). Hence the electrons can escape from the sheet as the sheet undergoes resistive kinking. However, for this mechanism to explain the repetitive behavior typical of many type III chains, the wavelength of the kinking portion of the arch must be much less than the arch length, so as the kink thrashes back and forth, it will accelerate electrons in bursts with the proper frequency $f \approx 2\pi/kv_A$. If such behavior should be observed and is correlated with type III bursts, it will be strong evidence in support of this resistive-kink flare model.

The formation of IEBs by the above mechanisms has a number of advantages over the standard explanation that IEBs form by electron deposition into the denser atmosphere beneath the acceleration site. These advantages are:

- There is no need to find an exotic acceleration mechanism that accelerates only electrons with a 90 to 100% efficiency;
- We need not accelerate $\approx 10^{39}$ electrons to form the IEBs, as required by the deposition hypothesis, since the same electrons can be repeatedly heated and/or accelerated within the same volume (the accelerated electrons being stopped quickly by the high arch densities);
- We need not develop separate mechanisms to form IEBs and shocks, since they appear together as a natural consequence;
- We can show that similar behavior manifests itself in laboratory experiments, serving as a guide to our understanding.

In summary we have argued that IEBs and shocks can result from impulsive heating and/or acceleration. This explanation we believe is more natural than previous explanations.

7.4 Other Modulation Mechanisms

One odd thing about nonthermal flares is that occasionally chains of type III bursts are formed, the bursts sometimes being separated by intervals of $\lesssim 1$ s. Since the type III burst results from an electron stream, these chains may be simply a result of pinching instabilities to which electron streams are inherently subject. However, although this explanation may be correct, there are two other means by which one could explain these chains within the context of this model.

Consider first the MHD $m = 0$ mode. As discussed by Glasstone and Lovberg (1960), this mode in the presence of a stabilizing axial field B_z is known to oscillate with a frequency

DANIEL S. SPICER

$$\omega^2 \approx \frac{B^2}{4\pi r_l \rho_s}, \quad (7.7)$$

where r_l is the equilibrium pinch radius, B is the magnitude of \mathbf{B} , and ρ_s is the surface density of the current sheath which is assumed to exist at the equilibrium radius. These oscillations, unlike the $m = 0$ oscillation in the unstabilized pinch ($B_z = 0$), are usually small but discernible. However they generally do not generate the radial shocks characteristic of the unstabilized pinch.

Since the period of oscillation that is characteristic of the observed quasi-periodic bursts is typically about 1 to 10 s, and we have adopted a value for $B \approx 500$ gauss, we find that $r_l \rho_s \approx 10^{28}$. This implies both the equilibrium radius of the arch and its length must be large. Using a value of $r_l \approx 10^8$ cm, and demanding the period be of the order 10 s, we find the $m = 0$ mode will induce an electric field

$$E_T \approx \frac{r_l B_p}{c}, \quad (7.8)$$

which gives $E_T \approx 10^{-2}$ statvolts/cm. The energy accumulated by these particles per oscillation is $\Delta \epsilon \approx 5\Delta L$ (eV), where ΔL is the length in centimeters of the region where B_p is changing within the sausage. Thus, if an arch were sausage-mode unstable, it can generate modulated-heated and accelerated electrons of reasonably high energy, with a period given by (7.7).

An alternate cause of quasi-periodic bursts may be the fusing of one or more island chains formed at the resonant surfaces $q = m$. The associated rapid change of magnetic flux as the islands are fused will produce voltage spikes due to flux changes, i.e., $V = d\Phi/dt$, where $\Phi = 1/c \int \mathbf{B} \cdot d\mathbf{S}$.

The evolution of an island chain is as follows: Short wavelength island chains are formed first during the evolution of the tearing mode, because the shorter wavelength islands have a much greater growth rate than the longer wavelength islands. These short-wavelength islands then represent parallel filaments, which then fuse to form lower energy and slower growing islands (Fig. 23). This process repeats itself until the lowest energy longest wavelength is reached. Investigations by Finn and Kaw (1976) have shown that fusing of islands will occur at the fast MHD rate, when the forces of fusion overwhelm the stabilizing forces, due to the compression of the magnetic field between islands. We can treat this phenomena in a semiquantitative form by developing a circuit analog to the problem. To do this we can introduce lump circuit parameters to describe the physical mechanisms at work in a plasma. Following Tidman and Stamper (1973), we convert the electron momentum equation to the form

$$V = IR + \frac{d(IL)}{dt} + \frac{Idt}{C}, \quad (7.9)$$

where I is the total current, R is the total resistance, L is the inductance, and C is the plasma capacitance.

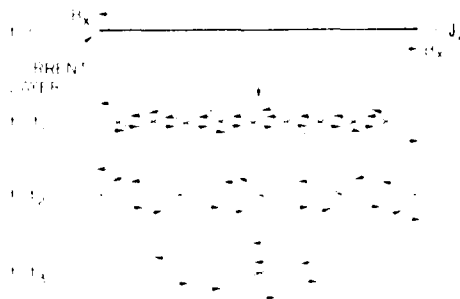


Fig. 23 - Evolution of the tearing mode

Recognizing that a magnetic island represents a circuit filament, we can treat each island as a conducting wire with a self-inductance and a mutual inductance between differing islands. First we assume each island is part of one island chain on a resonant surface $q = m$, so that each island is in parallel. The inductance of multiple conductors may be found from circuit theory, using formulas for the self-inductance of a straight conductor and for the mutual inductance of parallel conductors. In our simple case, that of m equal wires corresponding to m islands spaced uniformly on a circle whose radius is determined by $q = m$ and connected in parallel, the inductance is given (Grover, 1946) by

$$L = 0.002 \Delta L \left[n \left(\frac{2\Delta L}{R} \right) - 1 \right] \text{ microhenries,} \quad (7.10)$$

where

$$R = (nmr_s^{m-1})^{1/m}, \quad (7.11)$$

in which $r = (n\rho - 1/4)$, ρ being the mean island radius, and in which r_s corresponds to the radius of the resonant surface. When the islands fuse, we expect a voltage drop

$$V(t) = \frac{I dL(t)}{dt}, \quad (7.12)$$

assuming I is constant.

Typically in conventional electric circuits inductances are constant, so that the dL/dt term is zero. However in plasma configurations this is not the general situation, and one finds rather novel electrical behavior. Indeed, as noted by Glasstone and Lovberg (1960), the $I dL/dt$ term is commonly much larger than the voltage driving the circuit. It is from this term we expect the chains of voltage spikes to have their origins. To see this, assume that Δm islands fuse in a time Δt . Differentiating Eq. (7.10) with respect to time gives

DANIEL S. SPICER

$$\frac{dL}{dt} \approx 0.002 \frac{\Delta L}{R} \frac{dR}{dm} \frac{\Delta m}{\Delta t}, \quad (7.13)$$

which leads to Δm voltage spikes every Δt seconds. Assuming $\Delta t \approx \gamma^{-1}$, where γ is the rate of island fusion, we expect Δm voltage spikes per second. These voltage spikes will lead to Δm bursts of heated and accelerated electrons per second, which will appear as a chain of bursts when an island chain fuses to form the lowest energy island. Since other island chains can fuse, more than one chain of bursts can occur.

Estimating the magnitude of Eq. (7.12) is difficult, since the total current is distributed throughout the cross section of the arch; and each island when it forms will have a portion of the total current, which differs from that of its neighbor on a different resonant surface. However it is not difficult to convince oneself that the maximum energy gained by a charged particle during these voltage changes is of the order 2MeV found earlier, and the time between bursts is like an MHD growth time, which is of the order 1 to 0 s, depending on the wavelength of the mode.

8. FLARE MODEL PRECURSORS

8.1 Introduction

The role of precursors is of particular importance in this model, because the precursor mechanisms must set up conditions for onset of the MHD and resistive MHD instabilities used to explain the energy release of the flare. Since these instabilities are driven by j_r , we shall be interested in mechanisms that can modify the radial-current-density profile. As noted in Section 4.5, a perturbation in j_r is directly related to perturbations in either electron density or electron temperature and to the driving electric field.

An examination of the possible mechanisms for altering the current density requires a knowledge of the sources of the current. One can conveniently but somewhat articially split the possible sources of current into those that occur in or above the photosphere and those that occur below in the convection zone or deeper. Examples of mechanisms that can cause currents by motion of the photospheric fluid are: shearing of one foot of an arch with respect to the other, the differential rotation of one foot of the arch with respect to the other, and the rotation of the individual feet of the arch (Fig. 24).

Mechanisms that may cause currents to flow in the convection zone are poorly understood and can only be assumed to exist. This assumption however is reasonable, since the fluid in this zone is a partially ionized plasma with anisotropic transport coefficients, much like the ionosphere. Hence, due to collisions with neutral particles, electrons and ions can move across field lines in the convection zone, with different velocities and directions, thereby generating currents. Under these circumstances the current will have large components perpendicular to \mathbf{B} , and the force-free behavior usually assumed in the solar atmosphere has absolutely no validity in the convection zone or in most of the photosphere.

Further, if one believes the typical models of solar magnetism, a safe assumption is that the magnetic topology is multiply connected in the subphotospheric zones and

represents an enormous reservoir of stored energy in the form of currents, so that the source of flare energy which is released in situ above the photosphere need not be totally stored there. Consequently we will assume that a current does exist in the convection zone and that this current can be carried up with the magnetic tubes of force into the solar atmosphere.

8.2 Mechanisms For Driving Currents

We will here examine heuristically two examples of current sources, the first due to the twisting of the feet of an arch and the second due to an evolving arch expanding from beneath the photosphere. Consider an arch that is straightened into a cylinder with its feet anchored on two endplates, and assume these plates rotate with an equal and opposite velocity v_ϕ (see Fig. 16a).

Using Fig. 16b we see that the plasma flow, tangential to the longitudinal field, generates a voltage difference between the two radii R_1 and R_2 given by

$$\Delta V = v_\phi B_T \frac{(R_2 - R_1)}{c} \quad (8.1)$$

This voltage corresponds to a radial electric field

$$E_r = - \frac{\Delta V}{\Delta R} = - \frac{v_\phi B_T}{c} \quad (8.2)$$

Taking $B_T \approx 2500$ gauss and $v_\phi \approx 10^4$ cm/s yields $E_r = 8.3 \times 10^{-4}$ statvolts/cm. This magnitude of E_r is large but not surprising. To see this we make use of the boundary conditions for a plasma-plasma interface (Krall and Trivelpiece, 1973)

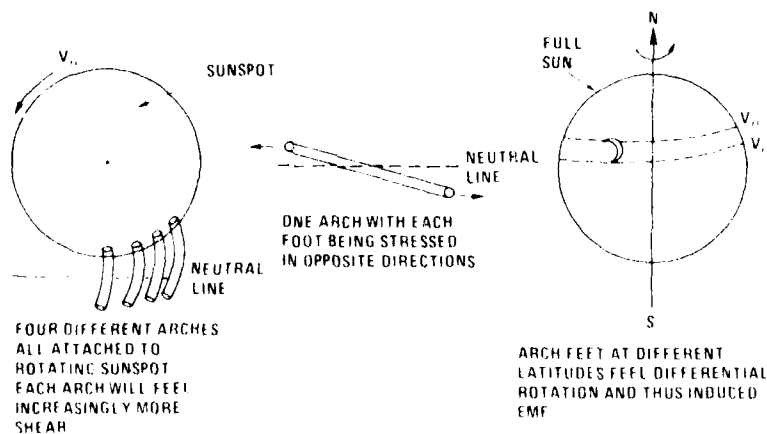


Fig. 24 Examples of photospheric fluid motion that can cause currents

DANIEL S. SPICER

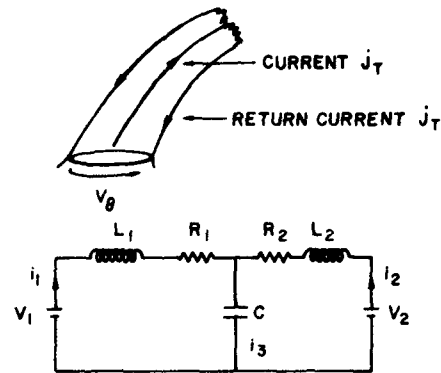


Fig. 25 — Reverse current circuit analog of a current system due to the twisting of the feet on an arch

$$\mathbf{n} \times \mathbf{[E]} = \frac{\mathbf{n} \times \mathbf{v} \times \mathbf{[B]}}{c}, \quad (8.3)$$

$$\mathbf{n} \cdot \mathbf{[B]} = 0, \quad (8.4)$$

$$\mathbf{n} \times \mathbf{[B]} = \frac{4\pi \mathbf{j}_s}{c}, \quad (8.5)$$

and

$$\mathbf{n} \cdot \mathbf{[v]} = 0, \quad (8.6)$$

where \mathbf{n} is the interface normal and \mathbf{j}_s the surface current. Equations (8.4) and (8.6) simply state that the normal component of \mathbf{B} and \mathbf{v} are continuous across the interface, which here corresponds to B_T and $v_T = 0$. Equations (8.3) and (8.5) require the tangential components of \mathbf{E} and \mathbf{j}_s to be continuous across the interface. For a poloidal component of \mathbf{B} to arise at this boundary due to twisting in ϕ , requires one to drive a current across the B_T field and then upward along the arch and down to the other leg to form a complete current system, as is illustrated in Fig. 25. However this flow cannot occur if the conductivity is a scalar. To see this we write Ohm's law in its standard form

$$\mathbf{j} = \sigma \left(\mathbf{E} + \frac{\mathbf{v} \times \mathbf{B}}{c} \right). \quad (8.7)$$

Projecting out the components of \mathbf{j} parallel to \mathbf{B} gives $j_{\parallel} = \sigma E_{\parallel}$. However our current-driving mechanism is due to the $\mathbf{v} \times \mathbf{B}$ term. Hence a $\mathbf{v} \times \mathbf{B}$ force cannot drive the current that flows along the arch unless the conductivity is a tensor. Ohm's law then becomes

$$\mathbf{j} = \vec{\sigma} \cdot \left(\mathbf{E} + \frac{\mathbf{v} \times \mathbf{B}}{c} \right), \quad (8.8)$$

and the $\mathbf{v} \times \mathbf{B}$ force can give rise to a current component in another direction.

For the conductivity to be anisotropic the ion neutral and electron neutral collision frequencies ν_{in} and ν_{en} must be large. In particular they must satisfy the conditions

$$\frac{\Omega_{ci}}{\nu_{en}} < 1 \quad (8.9)$$

and

$$\frac{\Omega_{ce}}{\nu_{en}} < 1, \quad (8.10)$$

where Ω_{ce} and Ω_{ci} are the electron and ion gyro frequencies, so that the ions and electrons are effectively unmagnetized in the presence of the neutrals. Under such circumstances the twisting of the arch's feet must occur in regions deep in the photosphere where conditions (8.9) and (8.10) are satisfied. It is for these reasons that E_{\parallel} is so large, since $\vec{\sigma}$ will not approach the magnitude one would find if σ were simply a scalar, and determined completely by the electron-ion collision frequency.

The electric fields generated by this twisting will generally damp in magnitude as one moves higher into the arch, so that when $\vec{\sigma}$ becomes a scalar, the currents perpendicular to \mathbf{B} become extremely small. The arch will then be approximately force free.

Observations by Severny (1965) have found vertical current densities of the order 2×10^3 statamperes/cm², and Moreton and Severny (1968) have found that prior to flares this value is even greater. Their angular resolution however was poor, ≈ 7 seconds, and therefore averaged over a substantial fraction of the observed region. Title and Andelin (1970) have found somewhat larger values $j \approx 4 \times 10^5$ statamperes/cm² averaged over an angle of ≈ 1 second. Since the observable photosphere has a temperature of $\approx 6 \times 10^3$ K, the plasma has a scalar resistivity of $\approx 2.36 \times 10^{-13}$ s. Thus the plasma can support a vertical current $j \approx 4 \times 10^5$ statamperes/cm², driven by a vertical electric field $E_{\parallel} \approx 9 \times 10^{-8}$, which is $\approx 10^{-4}$ smaller than the radial electric field calculated earlier. This suggests an anisotropic conductivity of $\approx 4 \times 10^9$ s⁻¹ beneath the photosphere.

There are two important points concerning this example. First, the source of current must exist deep in the photosphere. Such circumstances permit strong convective behavior on the part of the field lines there and thus permit perturbations caused by this convection to propagate upward into the arch. Hence line tying will not be that effective in stabilizing the arch against long-wavelength convective instabilities. Second, the

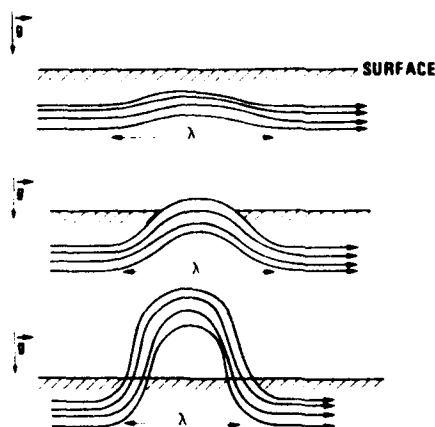


Fig. 26 — Kink forming and propagating up through the photosphere into the solar atmosphere

requirement on the part of the boundary conditions that return currents exist, if both feet rotate in the same direction but at different rates, implies that the B_p component of B will reverse its sign many times and therefore that the field is strongly sheared. Such fields are strongly susceptible to resistive instabilities.

The second example we will consider is simply a magnetic tube in the convection zone of length L , along which a current flows. The source of current is considered unknown. Initially the tube is assumed to be in equilibrium, so that

$$P_{int} + \frac{(B_p^2 + B_T^2)}{8\pi} = P_{ext}, \quad (8.11)$$

where P_{int} is the internal gas pressure, P_{ext} is the external pressure, and we assume, along with Parker (1955), that there is no magnetic field outside the flux tube. Since $B_p^2 + B_T^2$ is positive, $P_{int} < P_{ext}$. Thus, if the tube has a small thickness in comparison to the scale height, the temperature on the inside will equal that of the outside, which implies $\rho_{ext} > \rho_{int}$. Under such circumstances the tube will have magnetic buoyancy and will rise if perturbed.

In equilibrium the magnetic tension must balance the buoyant force. Suppose then that the tube kinks, as depicted in Fig. 26, and $B_p > 2\pi a B_T / \lambda$, where λ is the wavelength of the kink. The kinking force and buoyant force will cause the kink to rise if

$$\lambda g(\rho_{ext} - \rho_{int}) + \frac{B_p^2}{4\pi} > \frac{B_T^2}{4\pi}, \quad (8.12)$$

or, using $B_p > 2\pi a B_T / \lambda$,

$$\frac{4\pi g \lambda \Delta \rho}{\left(1 - \frac{\pi a^2}{\lambda^2}\right)} > B_T^2, \quad (8.13)$$

where $\Delta \rho = \rho_{ext} - \rho_{int} > 0$. When $\lambda \approx \sqrt{\pi a}$, this condition is most easily satisfied and the kinked tube will float to the surface at a velocity somewhat less than the Alfvén velocity. This occurs because the kink generates a surface wave of depth λ , which causes more magnetized mass to be dragged along by the kinking motion. The increase in accelerating mass is of the order $(\lambda/a)^2 (\rho_{ext}/\rho_{int})$ (Manheimer et al., 1973). As the tube accelerates upward, the strength of the toroidal component of \mathbf{B} will be reduced; thus the cross sectional area of the tube will increase. The current density will then try to redistribute itself within the cross section to minimize the system's energy. During this period the tube will be susceptible to MHD and resistive MHD instabilities. However the global instabilities will have reduced growth rates, because of the surrounding high-density gas (Manheimer et al., 1973), until they reach the lower densities of the upper solar atmosphere. The tube, now an arch, will continue to expand until in equilibrium or will cause a flare in an attempt to minimize its energy and thus come into equilibrium with its surrounding atmosphere. If the tube carries a total current of the order 10^{21} statamperes, it will be more than sufficient for the energy release.

It is difficult to be more precise in these matters because of the enormous physical complications implied by anisotropic transport coefficients and the clear lack of knowledge concerning the environment below the photosphere. However, if these arches do carry current when they break through the solar surface, they can flare by the mechanisms discussed.

8.3 Parametric Excitation Of MHD Kink Or Resistive Kink Modes

It is interesting to consider how one might parametrically excite the MHD kink and resistive kink modes. To excite these modes, there must be a coupling to an imposed oscillation, i.e., a pump wave. This parametric coupling is provided by nonlinear effects, and to make these modes grow, one must feed energy to them at a rate which exceeds the rate at which energy is dissipated for the mode in question. Thus, to excite these modes parametrically, the amplitude of the pump has to exceed a certain threshold.

Recent work in dynamic stabilization of kink modes in CTR (controlled-thermonuclear-research) devices has shown that dynamic stabilization, as well as destabilization, can occur by parametric resonances (e.g., Keller et al., 1976). For example the excitation and suppression of kink modes by coupling to ion sound waves has been shown to be possible (Guzdar et al., 1975). This is accomplished by generating a torsional Alfvén wave, whose azimuthal field B_ϕ has an associated velocity v_ϕ , leading to a relative shear between concentric layers. The Alfvén wave leads to a coupling between the kink modes and ion-sound modes. If the ion sound modes are growing, they can pass their energy to kink modes, thereby driving them unstable. Thus it appears possible that waves from the photosphere can lead to eventual instability in the arch. Undoubtedly other means exist to parametrically excite kink modes.

DANIEL S. SPICER

Parametric excitation of kink modes is of particular interest in the arch, because the spacing between normal modes of the system will generally be very small because of the large size of the arch. Thus it will be much easier to find modes which are close enough together so as to satisfy the resonance conditions and thus become parametrically excited.

A twisting of the arch can produce torsional Alfvén waves. However the existence of growing ion sound waves in an arch is in doubt unless $T_e \gg T_i$, although growing acoustic waves are a possibility, since they satisfy a dispersion relation similar to the ion sound waves. Hence it may be possible for acoustic waves to couple with the torsional Alfvén wave and excite the kink modes.

8.4 Alteration Of The Current Profile In The Arch

Let us examine mechanisms and perturbations that will alter the current-density profile of an existing arch, assuming it is still evolving. The simplest types of perturbations that immediately come to mind are those perturbations that satisfy $\mathbf{k} \cdot \mathbf{B} = 0$, i.e., perturbations which are slowly varying in the toroidal directions. One such mechanism is a magnetosonic wave generated by perturbations external to the arch. For example, if a Moreton wave generated by another flare were to strike the arch, it could very easily give rise to magnetosonic waves propagating perpendicular to \mathbf{B} which could compress the magnetic surfaces, exciting the tearing mode, or which could cause the arch to kink.

An alternate mechanism, using magnetosonic waves, is the conversion of Alfvén waves into magnetosonic waves, as the Alfvén waves propagate along the twisted field lines of the arch. This requires the wavelength of the original Alfvén wave to be less than the local or global curvature. Such a mechanism has been proposed by Wentzel (1974) as a source of heating in arches. The wavelength of the Alfvén waves required are such that $\lambda < R$ and/or $\lambda < r B_T^2 / B_p^2$. We will comment more on this later. However we are interested in all perturbations that have long wavelengths parallel to \mathbf{B} along the arch so that thermal conduction will not play an important role, thereby permitting resistive instabilities such as the superheating instability to occur, which we consider next.

As shown in Section 4, the superheating instability is a resistive instability that grows only when $k_{\parallel} \rightarrow 0$, i.e., $\mathbf{k} \cdot \mathbf{B} = 0$. Thus, when this instability does occur, the current density within the singular layer will grow. Assuming the resistivity is classical, the condition for growth is

$$\frac{3j_0^2}{2\sigma_0 T} > \frac{dQ}{dT_0}, \quad (8.14)$$

where $Q \approx P_{\text{rad}}$ and we have neglected the $k_{\perp}^2 \chi_{\perp}^2$ term due to thermal conduction perpendicular to the field lines. Rewriting Eq. (8.14) as

$$\frac{j_0^2}{\sigma_0} > \frac{2P_{\text{rad}}}{3}, \quad (8.15)$$

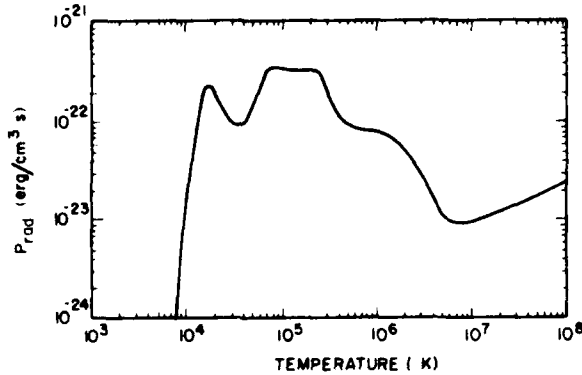


Fig. 27 — The radiated power function of the solar corona (McWhirter et al., 1974) The power radiated per unit volume is $n_e n(H) P_{\text{rad}}$ ergs/cm³ s.

where $P_{\text{rad}} = n_0^2 f(T)$, we can obtain $f(T)$ from Fig. 27. Since $j_0 = en_0 v_d$ we can rewrite Eq. (8.15) as

$$v_d^2 > \frac{f(T)}{e^2 \eta} = 2T_e^{2/3} (eV) f(T) \frac{3.77 \times 10^{32}}{3Z \ell_n \Omega} \quad (8.16)$$

Note that the condition for growth expressed by Eq. (8.16) is independent of density.

An examination of the radiation power function for the solar corona (Fig. 27), shows that thermal instability is most likely to occur when $T \gtrsim 10^5$ K, which corresponds to $f(T) \approx 3 \times 10^{-22}$ erg/cm³ s. Inserting these values for T and $f(T)$ into Eq. (8.16) shows that $v_d > 4.98 \times 10^5$ cm/s, if the superheating instability is to occur. Requiring a number density of 10^{12} cm⁻³, yields a current density around $k \cdot B = 0$ of $j_T \approx 2.4 \times 10^8$ statamperes/cm², which is very nearly the value found to be necessary to explain the energy release of the flare by the tearing mode. This corresponds to a growth rate for the superheating instability of $\gamma \approx 2.07 \times 10^{-1}$ s⁻¹ or one e-folding time of 4.8 s. If the arch had a lower number density, for example at its outer boundary, it would have a correspondingly lower critical current density and growth rate. For example, if $n \approx 10^9$ cm⁻³, we must have $j_T \approx 2.39 \times 10^5$ statamperes/cm², which is close to the value reported by Title and Andelin (1970). The superheating growth rate would be $\gamma \approx 2 \times 10^{-4}$ s⁻¹, or one e-fold time of 1.34 hr. Since superheating will cause the temperature to increase, it will produce a temperature gradient across $k \cdot B = 0$ such that the resistivity gradient will have a minimum there, which is one of the criteria for the rippling-mode or current-convective instabilities. Assuming the rippling mode is excited, we find that for the adopted values of B , a , n , and T the limits on the growth rate for the rippling mode lie within the range ($9 \lesssim \gamma \lesssim 7.43 \times 10^2$) s⁻¹. Hence, this mode can greatly enhance the growth of the current within the singular layer before it saturates.

To excite these modes again requires perturbations that satisfy the condition $k \cdot B = 0$. As already noted, magnetosonic waves can accomplish this by bringing the temperature around $k \cdot B = 0$ above $\approx 10^5$ K. Thus in this model the mechanism that Wentzel (1974)

has suggested to heat the arch may trigger the flare. An alternative to this possibility is the long-wavelength ($\approx 10^5$ km) photospheric horizontal waves observed by Tanaka (1972) prior to flares. Mullen (1973) has calculated the energy flux associated with these oscillations and finds an energy flux $\mathcal{E}_{flux} \approx 2 \times 10^{10}$ ergs/cm² s. Using the observed flaring-arch length of $\approx 5 \times 10^8$ cm, the possible maximum total power that can be transmitted to an arch is ≈ 40 ergs/cm³ s, which is of the same order as the radiation losses if $n \approx 10^{12}$ cm⁻³. A density less than 10^{12} cm⁻³ would lead to a heating of the arch, especially at the outer boundary.

This wave energy input could occur in the following way. Assume that these photospheric waves modulate the tension of the magnetic field in the arch. If the modulating period of the photospheric waves is T , and the natural frequency of the arch is Ω , and they together satisfy the condition

$$\Omega T = n\pi (n = 1, 2, 3, \dots), \quad (8.17)$$

then the photospheric oscillations can result in an amplification of the natural modes of the arch by parametric excitation (Minorovsky, 1962). In general one natural mode of the arch will be the Alfvén mode, whose amplitude can be increased through energy input by the photospheric pump. Since $T = 2\pi/\omega$ and $\Omega = k_{\parallel} v_A$, we have from Eq. (8.17) $\omega = 2k_{\parallel} v_A/n$. Assuming higher frequency harmonics of the photospheric waves exist, we can write $\omega = \omega_0^m$, $m = 1$ corresponding to the fundamental harmonic. Then $\omega = 2k_{\parallel} v_A/mn$.

In general, v_A is large for an arch and is about 10^7 or 10^8 cm/s. Since the waves reported by Tanka (1972) had a period of ≈ 300 s, we find $\omega_0 \approx 2 \times 10^{-2}$, and it follows that the excited Alfvén waves correspond to very long wavelengths parallel to \mathbf{B} , or the pump waves correspond to very high harmonics, and/or a combination of these possibilities. With the excitation of these Alfvén waves, we can then invoke the mechanisms discussed by Wentzel (1974) for decay of Alfvén waves into magnetosonic waves.

In the derivation of the superheating instability, no allowance was made for the coronal heating mechanism. This was neglected simply because the coronal heating mechanism is poorly understood and its inclusion during the derivation would only complicate matters. However the coronal heating will act as a driving term if (defining the coronal heating by the function $C(T)$) $dC/dT > 0$; i.e., the coronal heating can actually excite the superheating instability, particularly if the electrons are preferentially heated over the ions.

Unlike laboratory pinches, arches in the solar atmosphere have a cold core and a hot sheath (Foukal, 1975). We should therefore expect the superheating and rippling modes to be most easily excited within or near this sheath. This should occur for two reasons: first, the density will be lower there and more susceptible to thermal instability; second, the resistivity gradient will be negative as one moves toward the hot sheath, which means the current density will have a maximum in the sheath. Such a circumstance is highly unstable to the double tearing mode (Furth et al., 1973), as we will soon discuss.

The formation of this peaked current profile will compete with the mechanisms for current penetration discussed in Appendix B. The first competing mechanism to be considered is that of normal thermal conduction, perpendicular to the field lines. Earlier we ignored conduction perpendicular to \mathbf{B} . We were justified then because, as noted above,

arches are typically observed to have hot sheaths; hence, the thermal conductivity would be inward and will only enhance the superheating instability initially. However, as the temperature gradient builds due to the increased joule heating, the increased temperature gradient could stop the growth of current due to increased conduction out of the region of instability and into the cooler core. During the rise of j_1 the electrons and ions are not very well coupled by collisions, particularly in the low-density sheath, where the collision frequency is further reduced. Hence the only means by which heat can be conducted inward is by electron conduction, the ions being no longer well coupled to the electrons. We therefore need to compare the joule heating terms with the electron thermal conduction perpendicular to \mathbf{B} .

Using the results of McBride et al. (1975) for a similar situation, we find $\beta_p^2 > (R/a)^2$, where $\beta_p = (B_p^2/8\pi nkT_e)^{-1}$. If this condition is satisfied, thermal conduction will stop the current runaway. Since normally $\beta_p < 1$ in the solar atmosphere, and since $R/a > 1$ for an arch, thermal conduction is not expected to inhibit the growth of the current sheath by the resistive instabilities discussed.

The other current penetration mechanism of importance is the low frequency electron-temperature-gradient drift wave instability, which is important when the temperature profile is the inverse of the density profile (Kadomtsev, 1965; Lui et al., 1972). This mode requires the magnetic shear to be sufficiently weak so as to not damp the mode. The condition for instability is expressed as

$$\left(1 + \frac{T_i}{T_e}\right) \left(\frac{L_n}{L_s}\right)^{3/2} < \left[-\frac{L_n}{2L_T} + \left(1 + \frac{T_e}{T_i}\right) \frac{k_y^2 \rho_i^2}{\sqrt{2}} \left(\frac{m_e}{m_i}\right)^{1/2} \ln \left[\frac{m_i}{m_e} \left(\frac{L_n}{L_s}\right)^{1/2}\right]\right], \quad (8.18)$$

where $L_s \approx 2.39 \times 10^9 B_p/j_T$, $L_n \approx (n^{-1}dn/dr)^{-1}$, and $L_T \approx (T_e^{-1}dT_e/dr)^{-1}$.

To see if the condition for this mode can be satisfied, we assume the pressure profile is force free, i.e., $|L_T| \approx |L_n| \approx r_0$. Equation (8.18) shows that when $|L_s| \gtrsim |L_n|$, the condition is most easily satisfied. Taking $L_s \approx L_n \approx r_0$, we find

$$5.23 \left(1 + \frac{T_i}{T_e}\right) < \left[\frac{1}{2} + \left(1 + \frac{T_e}{T_i}\right) \frac{k_y^2 \rho_i^2}{\sqrt{2}}\right]. \quad (8.19)$$

Since $\rho \approx 0.81$ cm and $k_y \approx m/r_0$, we find $\rho_i^2 k_y^2 \ll 1$, and Eq. (8.19) reduces to $5.23(1 + T_i/T_e) < 1/2$. However, since $T_e/T_i \gg 1$ by assumption, this relation can never be satisfied, and it appears that unless the shear length is such that $L_s \gg L_n$ in an arch, this condition is almost impossible to satisfy.

Apparently once the current runaway begins, there is nothing to stop the buildup of current in the hot sheath of an arch except MHD kink and resistive kink instabilities or current-driven electrostatic instabilities. Using the condition $j_T R/cB_T < 1$ and the threshold conditions for current-driven electrostatic modes given in Appendix B, it is easy to show that MHD kink and resistive kink instabilities have a much lower instability threshold than current-driven electrostatic instabilities. Thus we expect the MHD kink and resistive kink instabilities to occur in the arch long before the bulk current could ever

become electrostatically unstable. These macromodes will then flatten the current profile by releasing the energy in the form of a flare.

The peaked current profile, caused by the mechanisms discussed above, is particularly unstable to macromodes, because $\mathbf{k} \cdot \mathbf{B} = 0$ can vanish on either side of the peak. This is because $q\alpha r/B_p$ is a double-valued function of r . This can be seen using the skin-current-layer model (Furth et al., 1973) $b = x^3/(1+x^2)^2$, where $b = B_p(r)/|B|$, $x = r/r_0$, and r_0 corresponds to where $x = 1$ and measures the current shell width.

A more dramatic form of the tearing mode, in which multiple tearing should occur, follows from the force-free Bessel-function model considered in Section 4 and the helically symmetric three-dimensional solutions obtained in Section 5. To see this, we first note $\mathbf{j}(r) = \alpha(r)\mathbf{B}(r)$. In equilibrium j_T is proportional to $B_T = B_0 J_0(\alpha r)$; hence $j_T = (\alpha/4\pi)B_0 J_0(\alpha r)$. Thus j_T will be alternately positive and negative, permitting multiple tearing on either side of the local current peaks and wells. This type of current distribution is particularly susceptible to overlapping resonances because of the neighboring resonant surfaces where $\mathbf{k} \cdot \mathbf{B} = 0$. Such a situation would easily occur in arches with return currents, since the currents will change sign at various minor radii.

8.5 Site Of Initial Current Buildup

We have so far argued that a sequence of resistive instabilities will occur in the hot sheath of current-carrying arches. We would also like to consider where along the arch the growth of these instabilities will be most rapid and thereby locate the probable site of the initial current buildup. To do this, we make the reasonable assumption that the arch has a transition zone within each leg much like the ambient atmosphere in which the arch is embedded. Where the temperature minima occur within each leg of the arch need not be the same as the altitude of the temperature minimum in the ambient atmosphere (due to more concentrated wave heating within each leg). However we will further assume that these minima occur within the arch at altitudes similar to the altitude of the temperature minimum in the ambient atmosphere. These assumptions necessarily imply that a steep temperature gradient exists within each leg of the arch around each minimum. Such a gradient alters one of the assumptions that was made in deriving the dispersion relation for the superheating instability: the temperature was not a function of height. When this assumption is relaxed, three new terms appear in the dispersion relation given by Eq. (4.128), which now has the form

$$\omega(z) = -i\chi_1^0 k_1^2 - i\chi_1^0 k_1^2 - \frac{\partial \chi_1^0 k_1}{\partial z} + i \frac{\partial \chi_1^0}{\partial T_0} \frac{\partial^2 T_0}{\partial z^2} - \frac{\partial \chi_1^0 k_1}{\partial T_0} \frac{\partial T_0}{\partial z} - i\nu_r + i\nu_q \frac{(k_1^2 - k_1^2)}{k^2} \quad (8.20)$$

In the limit $k_1 \rightarrow 0$ a term remains in (8.20) which is proportional to $\partial^2 T_0 / \partial z^2$ and acts as a driving term for the instability if $\partial^2 T_0 / \partial z^2 > 0$. Physically this is to be expected. As an electron that is driven by an electric field moves through a region where both the temperature and temperature gradient are increasing, the electron's mean free path is likewise increased, and the electric field can act on the electron for longer intervals

of time between collisions. The greater $\partial^2 T_0 / \partial z^2$, the greater the effective runaway. Hence, because $\partial^2 T_0 / \partial z^2$ is positive for a current with a drift velocity moving in the same direction as T_0 is increasing, and because $\partial^2 T_0 / \partial z^2$ is greatest in the transition zone, the superheating instability should be expected to have its greatest rate of growth there. Although we have not treated the density decrease with height in the arch, this decrease in n will have an effect similar to an increase in T_0 . From this we conclude that the origin of the initial preflare heating, by the mechanisms discussed, is in the region along the arch where the transition zone occurs. This may be along the leg of the arch or at its top, depending on the height of the arch and the heating mechanism causing the temperature gradient. Again it appears within the context of this model that the coronal heating mechanism may be related to the origin of the flare.

Other mechanisms that can lead to this form of current runaway are a gradual twisting of the field, a gradual shearing of the field by lateral foot motion, or a transient EMF along \mathbf{B} of unknown origin. The first two occur because the current is steadily increasing and at some stage will start to run away by the combination of resistive instabilities and the external current driver. We expect shearing to be important as a precursor effect, because as discussed in Sections 4 and 5, large shear will actually increase the likelihood of the tearing instability. The effect of a transient EMF on \mathbf{j}_\parallel is obvious.

A modification of the basic superheating instability could occur, if there were an electron beam stably trapped in the arch, since this beam could lead to an increase in bulk resistivity in the presence of an electrostatically stable current by the mechanism of Papadopoulos and Coffey (1974a, 1974b). Hence, since this resistivity is a bulk resistivity, the joule heating would increase in its presence. This increase in joule heating would then lead to more electron runaway, which then feeds the beam that generates the anomalous resistivity. If this proposed mechanism were to occur, a self-sustaining nonlinear feedback mechanism between current and beam could lead to the current buildup desired. Earlier we found that this mechanism increased the resistivity for the adopted parameters by 10^2 . In addition it was noted in Section 6 that this mechanism was most effective in increasing the resistivity in regions of lower density, which in an arch would correspond to the arch apex and within the hot sheath. Thus the mechanism fits into the sequence of instabilities discussed earlier, where the resistivity was assumed classical. The increase in η by 10^2 will lower the required j_T by 10 for the onset of the superheating instability.

Since this mechanism requires a beam of electrons, we must find a source for such a beam. The most obvious and most reasonable source of such a beam would be the runaway high-energy tail of the electron current distribution function. The number density in the tail of a Maxwellian is obtained by integrating the ambient Maxwellian from v_0 to infinity, obtaining

$$\frac{n_T}{n} = \frac{2}{\sqrt{2\pi}} \frac{\exp\left(-\frac{v_0^2}{2v_{Te}^2}\right)}{\left(\frac{v_0}{v_{Te}}\right)}. \quad (8.21)$$

Taking $v_0 \approx 3v_T$, we obtain $n_T/n \approx 2.95 \times 10^{-3}$. Since $n \approx 10^{12} \text{ cm}^{-3}$, we find $n_T \approx 2.95 \times 10^9 \text{ cm}^{-3}$, which is 10^3 times larger than the number of electrons required to form the beam as calculated earlier from Eq. (6.19). Hence, only 10^3 of the tail electrons need to run away to form the beam.

8.6 Location Of Initial Instability In The Arch

Although we have examined where the most probable initial current buildup should occur, it does not necessarily follow that the flare instability should start there. Indeed as shown in Appendix A, the safety factor will be a minimum at the apex of the arch, assuming the toroidal component of \mathbf{B} is the same in both legs. In general however B_T in one leg will not necessarily be the same as in the other. Thus, it follows that q will have its minimum, as a function of the toroidal coordinate, at different locations for different arches. However, since j_T will have its greatest growth in the transition zone of the arch, one should expect the instability to start somewhere between this region and the apex of the arch, assuming that the transition zone does not coincide with the top of the arch and that B_T is the same in both legs of the arch. For any other set of circumstances the picture becomes more complicated, and an accurate prediction can be made only when the physical details of arches become known.

9. PHENOMENOLOGICAL ASPECTS OF THE FLARE MODEL

9.1 Introduction

This section will be devoted primarily to explaining various flare phenomena and to generalizing the model. During the subsequent discussion we will at times devote our attention to answering questions raised by Svestka (1975) as they pertain to the flare model developed here. It is hoped that in this way the model and its expected effects will become clearer.

9.2 Some Speculations On The Role Of Instabilities In Other Solar Phenomena

We start by emphasizing that *any* magnetic topology which contains a current and has magnetic shear should be susceptible to just about every instability we have discussed. This should include x-ray bright points, filaments, GRF events, and loops in general. This will help in understanding the relationship between flares and filaments.

It is well known that filaments exhibit a helical magnetic field structure, appearing to unwind at times and exhibiting a winking effect, in which the filament acts *as if* it were moving up and down (Tandberg-Hanssen, 1974). In the context of the instabilities discussed here the helical structure should result from a current, and the magnetic rope effect common to filaments is the result of slowly growing long-wavelength resistive-kink modes generating helical magnetic islands. The slow growth is a result of the weak magnetic field and weak driving gradients in the filaments, and the unwinding results from kink instability. The winking may be self-induced or caused by a disturbance emanating from a flare, e.g., in the form of a shock striking the filaments. As noted

earlier, a shock striking an arch can result in perturbations which vary slowly along the arch and thus excite MHD and resistive kinks. A similar situation should occur in a *current-carrying* filament. The frequency of the kinking can explain the winking frequency ($\approx 10^{-3}$ s; Tandberg-Hansson, 1975). The excitation of the kink mode, in the filament, can cause an internal global kink to rotate at the electron diamagnetic drift frequency, which arises due to a $V_\phi \approx cE_r/B_z$ rotation of the kink. Taking $E_r \approx kT/\delta\ell e$ and $v_\phi = \omega r_n$, where r_n is radius of the kink with respect to the magnetic axis of the filament, we find $v_{rot} \approx ckT/2\pi e\delta\ell r_n B_z$. Using the values given by Tandberg-Hansson (1974) typical of a filament, i.e., $B_z \approx 10$ gauss and $T \approx 10^5$ K, we find $\delta\ell r_n \approx 10^{10}$ cm² is necessary for the frequency of rotation to be of the order 10^{-3} s⁻¹. This effect should appear as a helix slowly rotating within the filament and thereby giving the effect of winking.

The postflare loops present another situation. These loops appear to have relatively high altitudes and appear to be excited by the flare. If currents existed in these loops, one would expect behavior similar to that which occurs in flare arches, although with much less dramatic effects. This follows because the weaker are \mathbf{B} and its gradients, the slower the growth rates. Thus to heat the loops and to keep them hot requires

$$\frac{\gamma B_p^2}{8\pi} > \frac{n_e k T_e v_{Te}}{L} \quad (9.1)$$

Because L is very large, $\geq 5 \times 10^9$ cm, and n is small, $\leq 10^8$ cm⁻³, it does not take a great deal of energy to heat these loops and to maintain their high temperatures ($\approx 5 \times 10^6$ K). This would explain the long duration of heating in these loops, the appearance of high energy particles, and their subsequent rapid cooling. Their excitation also may be shock induced.

9.3 Expected Observational Characteristics Of The Model

As seen in Section 8, our flare model is intrinsically associated with preflare effects, which dictates whether a flare will or will not occur. What then is the expected phenomenological behavior of this model? Essentially two types of arches are to be considered: the emerging arch and the preexisting arch. The emerging arch is difficult to treat. Hence, while we consider them as potential candidates for flaring, we will confine our discussion to preexisting arches.

Preexisting arches will flare if one can alter the magnetic shear sufficiently to trigger the MHD kink and resistive kink modes. In addition the magnitude of this shear will determine whether the flare will exhibit weak or strong impulsive behavior in the form of nonlinear overlapping resonances and global kinks. Further, we have found there exists basically two means by which the shear of the field can be altered, namely a steepening of the current-density profile by either transport mechanisms or transient phenomena. Alteration of the current-density profile by transport mechanisms was shown to be closely related to mechanisms that are believed to heat the corona. Hence we expect this type of mechanism to result from a preheating of the arch, i.e., the flux of waves believed to heat the corona must be increasing in the arch, thereby altering the current-density profile

by the resistive modes discussed. Logically there is no reason why one arch should be singled out from other arches in an active region during this increase in wave flux. Thus we should expect preheating in all arches. If this is the case, why should a few arches flare and not all arches in the active region? The answer is that preheating, and the subsequent current density profile steepening, is only a part of a sequence of events which ultimately leads to a flare. The preheating prepares the arch for flaring, and the transient motions provide the final push necessary to start the flare. This occurs because the current steepening will be balanced by the weak dissipation of the current, when the shear becomes steep enough to excite the tearing mode, so that the system will evolve into a state of marginal stability. During this period an increase in heating will occur, above that due to the preheating. In addition impulsive behavior may occur due to weak kink modes. The actual onset of the flare will occur when either an external transient provides the push or the arch itself nonlinearly evolves into a strong global kink. The global kink will result in the effects discussed in Section 7. Some possible transient effects that may push the arch into instability are illustrated in Fig. 24.

With what has been said, what should be observed? Obviously a general preheating of the arches in the active region should be observed. This preheating should be particularly strong in the transition zone, because most of the wave flux will dissipate there. The arch should appear to brighten substantially, particularly the plasma boundary, which should sharpen with time; this occurring over a period of hours or minutes, as shown in Section 6. If the preheating is maintained for the proper interval, an extended burst and possibly weak IEBs should appear. This period corresponds to the marginal state just discussed. Two things can now occur: the arch may remain in a marginal state until the heating source is shut off and the current profile relaxes or the arch may flare, being pushed into flaring by some transient phenomena.

What occurs during the actual flare is difficult to state precisely, since the evolution of each flare is highly nonlinear and thus unique. However we can heuristically discuss the general sequence of events. If the flare is thermal, in the extreme sense discussed in Section 7, very little dynamic behavior will occur as far as the arch is concerned. The volume of energy release will generally be small compared to the total-volume field energy of the arch and will be situated in the leg of the arch where the current flows parallel to the temperature gradient. The localized energy release will cause heat to diffuse out of the heated region, increasing the volume of apparent instability. Hence, from an observational point of view, there will be a small core or cores of hot plasma surrounded by decreasing temperature gradients; i.e., the flaring arch will have a multithermal structure. Since the rate of energy release is slower, we expect any shock waves excited to be weak, if they are excited at all. We expect these flares to occur in arches with larger volumes or densities than those in which the impulsive flares which release an equivalent amount of energy occur.

The nonthermal impulsive flare is similar to the thermal flare, except the rate of energy release is much greater and strong resonant overlap can occur as well global kink modes. We can then expect strong blast waves and strong bursts of impulsively heated and accelerated particles. Figure 28 illustrates the basic sequence of events if the flare is excited by external heating mechanisms.

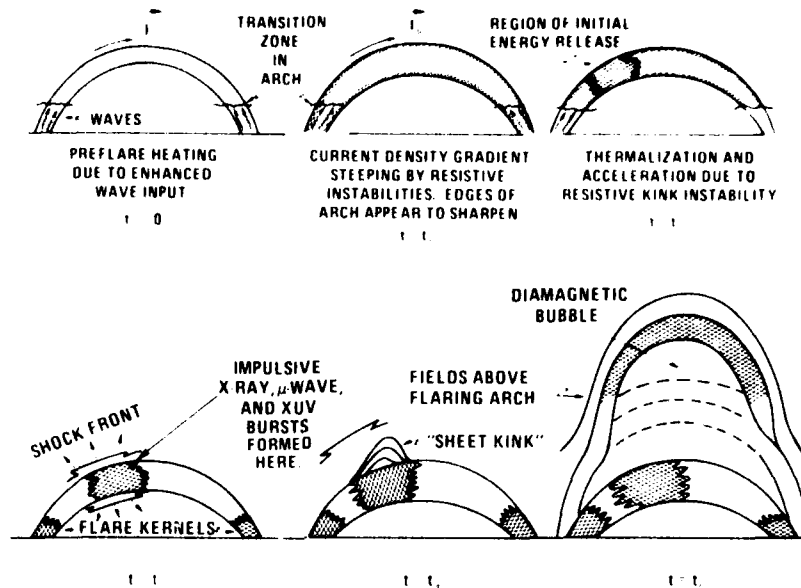


Fig. 28 — Example of events that can lead to a flare

9.4 Blast Waves and Their Effects

Since the impulsive flare in this model releases energy so rapidly from a small volume, we expect strong blast waves to occur. Under these circumstances we expect the blast waves to seriously disrupt the solar atmosphere, leading to many secondary effects which can confuse an observer's interpretation of the observed chain of events. Hence we examine here a number of effects we expect to occur during a nonthermal flare.

To begin, we emphasize that the rate of energy release in this model is the key ingredient for understanding the various phenomenological aspects of flares. Thus, because the release of energy occurs in a reasonably small volume, $\lesssim 10^{23}$ cm³, and the rate of release is $\gtrsim 10^5$ ergs/cm³ s, we expect the energetics of such an energy release to behave like a strong explosion from a small source for the most impulsive of flares. Hence an examination of how such an energy release will behave in the solar atmosphere is appropriate. We will discuss basically three variations of this energy release: the release as purely isotropic (i.e., initially, we will ignore the attendant magnetic fields), the release site as surrounded by a domelike magnetic field (i.e., the field will attempt to trap the energy release); and the release site as set between two magnetic walls whose field lines may open at higher altitudes.

Consider an isotropic release: what effects are to be expected? The answer is intrinsically related to the rate of energy release and to the fact that the solar atmosphere is exponential. The greater the release rate, the more accurate will be our conclusions. We assume the rate is sufficiently fast that it completely overwhelms all energy sinks, thereby causing a strong blast wave.

DANIEL S. SPICER

As is well known, such an isotropic release will initially yield a spherical blast wave which shortly thereafter will distort, due to the exponential atmosphere. An ascending and descending shock will occur. The descending shock will quickly decay as it encounters a higher density plasma. The ascending shock will eventually lead to a blow-out; i.e., the shock front reaches infinity in a finite time (Bach et al., 1975). The ascending shock will behave as a snowplow, concentrating most of the plasma mass near the shock front (Laumbach and Probstein, 1969). The descending shock will heat the high-density plasma, which then expands into the volume depleted of mass by the ascending shock. Thus a heaving of colder and denser plasma into higher altitudes will occur. This denser plasma will convectively mix with the lighter ambient gas by the Rayleigh-Taylor instability, leading to turbulent mixing. In addition the expanding blast will lead to Kelvin-Helmholtz instabilities at the front of the expanding blast wave, resulting in velocity shear there. This will result in a turbulent mixing interface expanding with the front (Boris et al., 1975). The addition of an enveloping magnetic field alters the behavior of the ascending blast wave. The blast wave will expand until the additional stress of the magnetic field becomes dominant.

Before proceeding, let us make some semiquantitative estimates on free expansion, in order to compare the magnetic-field-inhibited expansion. As is well known (Zel'dovich and Raizer, 1966), the expansion of the blast wave is governed by the environmental density. That is, at what altitude will the total mass of the plasma that collides with the blast wave above the energy release site equal to exceed the mass carried by the snowplow blast wave? Because the density in the solar atmosphere varies exponentially with altitude, the momentum-conserving expansion of the blast wave has a velocity

$$V(\theta) = \frac{V_0 M}{\left[M + \int_0^R 4\pi\rho(\theta)r^2 dr \right]}, \quad (9.1)$$

where R is the maximum radius of expansion, M is the total mass carried by the initial pressure pulse, V_0 is the initial velocity of expansion, and θ is the angle with respect to the vertical. Here

$$\rho(\theta) = \rho_0 \exp\left(-\frac{r \cos \theta}{H}\right), \quad (9.2)$$

where H is the scale height $kT/m_i g$ and ρ_0 is the ambient density outside the arch from which the pressure pulse originates. The shape of the blast wave at some time t is

$$R(\theta) = \int_0^t V(\theta) dt. \quad (9.3)$$

If we examine the shape of the blast wave at a time $R(0) \gg h$, we can obtain the approximate altitude above which free expansion will occur. Free expansion will not occur if

$$\int_0^{\infty} 4\pi\rho_0 \exp\left(-\frac{r \cos \theta}{H}\right) r^2 dr \gg M, \quad (9.4)$$

which yields for $R(\theta, t)$

$$R(\theta, t) = \frac{V_0 t M \cos \theta}{8\pi H^3 \rho_0}, \quad (9.5)$$

for $1 - \cos \theta < H/R(0)$. Thus free expansion occurs at a density

$$n_0 \approx M/(m_i 8\pi H^3) \quad (9.6)$$

If we demand the initial mass carried away by the snowplow pressure pulse is of the order 10^{16} g, which is of the order observed ejected during impulsive flares, and choose $T \approx 10^6$ K for the average corona temperature, we find $H \approx 8 \times 10^9$ cm and thus $n_0 \approx 5 \times 10^8$ cm $^{-3}$. Since observationally $n_0 \approx 5 \times 10^8$ cm $^{-3}$ is found at an altitude less than 8×10^9 cm, our approximation is invalid, and we conclude that the observed mass ejected by the flare is either swept up by the snowplow or ejected in the form of plasma blobs caused by mechanisms other than the flare, although possibly excited by the flare. We also conclude that the expansion is never free. After the blast wave has dissipated itself, the heated bubble formed by the blast wave will expand upward through the ambient atmosphere if it has a volume of the order $4\pi H^3/3$, since otherwise the mass density above the bubble will be greater than that in the bubble, thus preventing upward expansion.

If we neglect the presence of the ambient plasma, we expect the blast wave to simply blow a diamagnetic hole in the enveloping magnetic field if $\ddot{R} > v_A/2$. Thus a magnetic bubble will form and expand until the work done against the magnetic field equals the kinetic energy associated with the pressure pulse; i.e.,

$$2\pi R^2 \left(\frac{B^2}{8\pi} \right) / 3 = \epsilon_{\text{flare}}. \quad (9.7)$$

Taking $\epsilon_{\text{flare}} \approx 10^{32}$ ergs and $B \sim 20$ gauss yields $R \approx 5 \times 10^9$ cm. Hence the bubble will appear to have a radius of $\approx 5 \times 10^9$. The ambient magnetic field will be compressed during this time by an amount such that its pressure equals the time rate of change of the momentum of the blast wave.

During the expansion against the magnetic field, a Rayleigh-Taylor instability may occur as the high density plasma carried by the snowplow is pushed against the low-density ambient plasma. The growth rate for a perturbation of wave number k is $\gamma \approx (\ddot{R}k)^{1/2}$, which will have an amplitude $A = A_0 \exp(\gamma t)$, where \ddot{R} is the acceleration associated with the snowplow. For linear deceleration taking place in a distance R , $\ddot{R} = 2R/t$ and $\gamma = (2Rk)^{1/2}/t$, which yields an amplitude $A = A_0 \exp[(2Rk)^{1/2}]$. In the

nonlinear limit, i.e., $A \gtrsim \pi/k$, the plasma and field will be irreversibly mixed (Book, 1975) and the plasma will propagate by convection across higher and higher magnetic surfaces.

For convection to occur beyond the initial magnetic surface struck by the blast wave, the wavelength that requires the fewest e-foldings of growth to reach an amplitude greater than π/k is needed. The required wavelength will correspond to the blast wave radius of curvature R at the shock-field interface; the wavelength $\lambda = R/\pi$, i.e., $k = 2\pi^2/R$, will have an amplitude of order π/k , so that one e-folding can take place within the nonlinear limit, and the plasma will penetrate the field with a mixing length $\ell \approx R/\pi$. The plasma after being convected across the field will then expand parallel to the magnetic field, since less stress is exerted in the parallel direction.

If the blast wave strikes the overlying magnetic field at its weakest point, the plasma will expand horizontally along the field lines and fall downward into the chromosphere. On the limb this will appear as a slowly expanding hemisphere, the plasma propagating across the field lines at the nonlinear free-fall rate of \dot{R} . If the blast strikes the overlying field near where it is essentially vertical, the plasma will convect inward and move upward, away from the strong vertical field, into the weaker horizontal fields. If the blast wave has a large component of velocity parallel to the vertical field, the plasma will stream to the conjugate point of the overlying field; otherwise it will fall back. The momentum impulse transferred to the field will make it oscillate. In particular, if the field is vertical and open, the field may whiplash about in a manner similar to what occurs when a wave propagates out along a string with a free end. Under these circumstances a disturbance can propagate far out into the corona.

Next we consider what occurs if the release point is sandwiched between two vertical fields or possibly two large arches. The blast can again generate diamagnetic bubbles, field line whipping, and large-amplitude hydromagnetic waves moving along the field lines. The blast however can escape into the high corona in this situation, triggering other disturbances which we will now consider.

We make the reasonable assumption that high in the corona trapped particles exist mirrored between conjugate magnetic mirrors. What will occur if denser plasma is ejected up by the blast wave into these regions along field lines? As is well known (Kennel and Petschek, 1966), there is a limit to the number of particles that can be stably trapped, due to whistler and electromagnetic ion cyclotron modes. This limit corresponds to electrons (and protons) whose energy exceeds an energy threshold which is comparable with and scales as the energy density of the magnetic field and inversely as the electron number density, i.e., $B^2/8\pi n$. If it is assumed (Brice, 1970) that the threshold energy E_T is much greater than the characteristic energy of the particles, most of the particles are not subject to the trapping limit. If plasma of higher density is injected into the stable trapping regions, the threshold energy is reduced from E_T to E'_T . Thus electrons with energies between E_T and E'_T will be subject to the trapping limit, and the electrons and ions will try to reduce the new electron flux, pushing E'_T back to E_T . This will occur by pitch-angle scattering and precipitation (Kennel and Petschek, 1966) into the lower solar atmosphere.

Since the resonant threshold energies scale as $B^2/8\pi n$, and $B^2/8\pi n$ will generally increase rapidly near the mirrors, $B^2/8\pi n$ will probably have a minimum near the apex of

the trapping region. Hence a given wave will encounter the greatest number of particles with energies appropriate for resonance at the apex. For example, if the wave is a whistler, the resonant energies for the whistler are $(m_i/m_e)B^2/8\pi n$ for ions and $(\Omega_{ce}/\omega_{pe})B^2/8\pi n$ for electrons. Taking $B \approx 5$ gauss and $n \approx 10^7 \text{ cm}^{-3}$ yields $B^2/8\pi n = 9.92 \times 10^{-1}$ and $\Omega_{ce}/\omega_{pe} \approx 4.93 \times 10^{-1}$, which implies the wave will resonate with trapped 30-keV electrons and 113-MeV protons. Thus, if particles of these energies are stably trapped in high-altitude arches, they can easily be brought down by injection of denser plasma.

An alternate means to cause particle precipitation is for a shock to strike a trapping region. The shock can excite the various crossfield microinstabilities, collected in Appendix B, which will result in a strong momentum coupling between field and particle perpendicular to \mathbf{B} , the coupling due to these cross field instabilities being weak parallel to \mathbf{B} . Thus the energy of these particles will be predominately perpendicular to \mathbf{B} , which can lead to strong bursts of cyclotron radiation. However under such circumstances T_\perp/T_\parallel will be $\gg 1$, T_\perp being the temperature perpendicular to \mathbf{B} and T_\parallel being the temperature parallel to \mathbf{B} . As is well known, the condition $T_\perp/T_\parallel \gg 1$ can result in electromagnetic ion cyclotron and electron cyclotron (whistler) waves (Kennel and Petschek, 1966) which tend to quickly isotropize the temperatures. Thus perpendicular energy is rapidly converted to energy parallel to \mathbf{B} , and one expects the following sequence of events (Clark, 1975):

1. Part of the energy, associated with the blast wave propagating perpendicular to \mathbf{B} , is converted quickly to random energy perpendicular to \mathbf{B} by the crossfield electrostatic instabilities collected in Appendix B.

2. The resulting hot electron and ion temperature is extremely anisotropic, i.e., $T_{e,\perp}/T_{e,\parallel} \gg 1$ and, as such, is unstable to electromagnetic ion cyclotron and whistler waves, which grow and reduce T_\perp/T_\parallel .

3. Since the crossfield electrostatic instabilities result in strong momentum coupling perpendicular to \mathbf{B} , $T_{i,e\perp}$ increases preferentially. However particles with large $|\mathbf{V}_\perp/\mathbf{V}_\parallel|$ will tend to stream along \mathbf{B} , escaping into the loss cone of the mirror. Under these circumstances an electron and ion loss-cone instability is established (Rosenbluth and Post, 1965; Davidson, 1972). (We have assumed an electron loss-cone instability may also be excited.) This occurs because, in a mirror field, electrons and ions with large \mathbf{V}_\perp stream into the loss cone more rapidly than they can be replaced. Thus a hole in velocity space occurs corresponding to a depletion of \mathbf{V}_\perp particles.

4. Electrostatic fields, driven by the loss cone distribution function, will preferentially pitch-angle-scatter particles with high \mathbf{V}_\perp into the loss cone in an attempt to replace the depleted \mathbf{V}_\perp particles.

5. The system will then reach a state of marginal stability, and a steady state drizzle will occur in which particles stream down the trapping arch into the conjugate mirrors, illuminating the corona and chromosphere.

The illumination due to precipitating particles will differ at conjugate mirrors of the trapping arch. We know a particle with pitch angle α is related to the mirroring field by

DANIEL S. SPICER

$$\sin^2 \alpha = \frac{B_0}{B_M}, \quad (9.8)$$

where B_0 and B_M is the magnetic field strength at the trapping arch's apex and at one of its mirror points respectively. Let B_{1M} and B_{2M} denote the field strength at each mirror of the trapping arch. Then, since $B_0/B_M \ll 1$, we have $\sin \alpha \approx \alpha$; thus

$$\alpha_1 \approx \left(\frac{B_0}{B_{1M}} \right)^{1/2} \quad (9.9)$$

and

$$\alpha_2 \approx \left(\frac{B_0}{B_{2M}} \right)^{1/2} \quad (9.10)$$

Thus the ratio of the loss cones is

$$R(\alpha) = \left(\frac{B_{1M}}{B_{2M}} \right)^{1/2}. \quad (9.11)$$

Therefore, if $B_{1M} \gg B_{2M}$, the loss rate in the second mirror is much greater than in the first. Hence the second mirror will be illuminated by the appropriate factor due to the greater precipitation.

We have endeavored to show by reasonably simple arguments that the release of energy by an impulsive flare can literally raise havoc in the ambient solar atmosphere, leading to many secondary manifestations of the flare which, disturbingly, can mask the principal energy release and thus lead to incorrect observational conclusions.

Now we compare these effects with observations. First we identify the ascending shock produced by the pressure pulse with the type II radio burst. When the shock moves through overlying magnetic fields of sufficient magnitude, it will excite electrostatic instabilities which increase the electron thermal energy perpendicular to the magnetic field. For example the shock can excite the beam cyclotron instability, which then evolves into the ion-acoustic instability; both will heat the electrons so that V_1 will become extremely high. The heating rate is of the general form

$$\dot{T}_1^e = m_e v_d (v_d - v_i) v_{eff}. \quad (9.12)$$

Since v_{eff} is large, T_1^e will increase rapidly. Thus, because cyclotron radiation losses are proportional to $(\Omega_{ce} v_1)^2$, one should expect strong cyclotron radiation as the shock wave moves through the magnetic field and forms a diamagnetic bubble. This radiation we identify with type IV bursts. A number of obvious consequences follow from this. First, because n and B are pushed along by the snowplow, one should expect this radiation to

start immediately after the impulsive phase, if a magnetic field exists above the flaring arch, and to become stronger with time as n and B increase and finally decrease as the blast wave energy is spent. Also, the excitation of loss-cone instabilities are a possibility, giving rise to trapped electrons and protons mirroring back and forth within closed field structures. Further, a type IV burst may occur with or without a type II burst, and vice versa. This follows because B may be so large that the shock might be spent before exciting the type II burst, or B may be so small that the type IV burst would be unobservable.

The ability of the blast wave to excite Rayleigh-Taylor instabilities and thus cause plasma to be convected across field lines can explain the commonly observed rising mount on the limb, which exhibits the successive filling of flux tubes that the blast-driven Rayleigh-Taylor instability would cause. We believe the rising mount to be the so-called flare loops, blown out by the blast wave. Since the plasma will move out of the field region formed by the blast, it will stream down into the chromosphere, forming the flare ribbons. The moving apart of the flare ribbons is identified with the fact that the blast wave will convect plasma into higher and higher field lines. Thus the plasma streaming down the field lines will be coming from field lines which have a greater distance between them in the chromosphere. One should expect the flare ribbons to drift fastest at blast onset and slow down to a value corresponding to the velocity of field filling by convection. Hence the rate of expansion of the rising mount on the limb should be similar to that of the ribbons (Fig. 29). The drift of flare ribbons may be evidence for expansion of flare loops (Problem 2, Svestka, 1975).

One can make predictions associating type IV bursts, the rising mount, and flare ribbons. We should expect because they are related here by the blast wave, type IV bursts will generally occur when flare ribbons and rising mounts are observed, if the blast wave has sufficient energy. However flare ribbons and rising mounts need not occur in all flares if there is no enveloping field or if the flare generates only weak blast waves.

If the blast wave were to obliquely strike a vertical magnetic field, which is open or highly divergent with altitude, we expect an ejection of plasma out along the open field lines (Fig. 30). This we identify with the so-called spray. Hence a spray should be associated with a blast wave, if this is to valid, and the velocity of the spray should be some fraction of the blast-wave velocity. The greater the component of the blast-wave velocity parallel to B , the greater the spray velocity. Also only one flare ribbon would be formed. Here we have shown that a direct relationship exists between spray and blast wave (Problem 31, Svestka, 1975).

9.5 Svestka's Problems

Using the model developed, let us answer the various questions raised by Svestka (1975) where applicable and possible:

- Problem 1. This question is related to the complexity of the active region, the type of (flare nonthermal versus thermal), and the frequency of flares. Within the context of this model the frequency of flare occurrence and its type is clearly related to the number of available current-carrying arches or other similar magnetic topologies. Hence, since there occur observationally a larger number of arches in a complex active region as

DANIEL S. SPICER

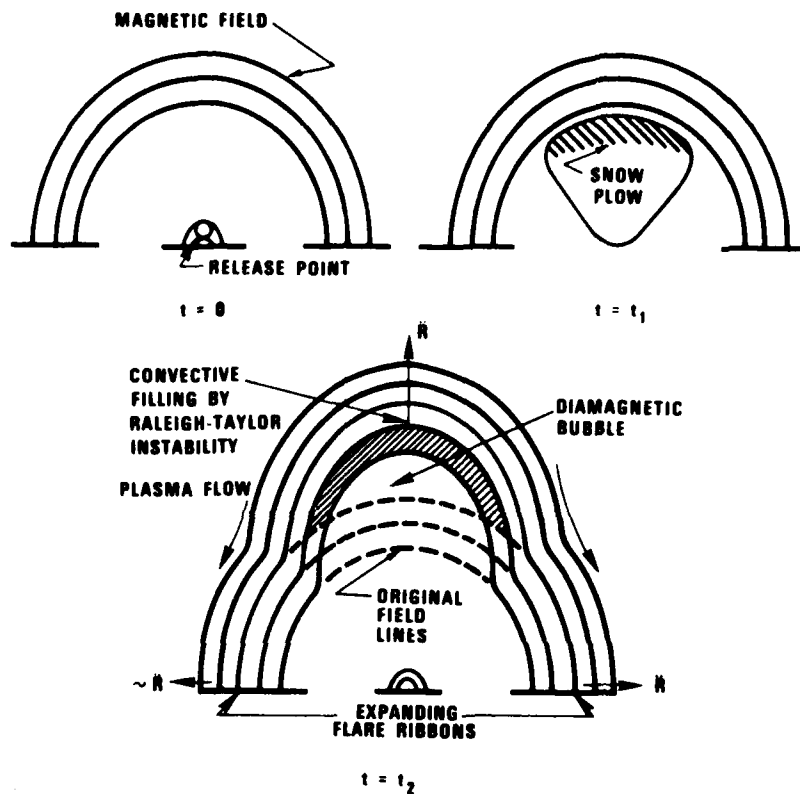


Fig. 29 — Isotropic release with an overlying magnetic field

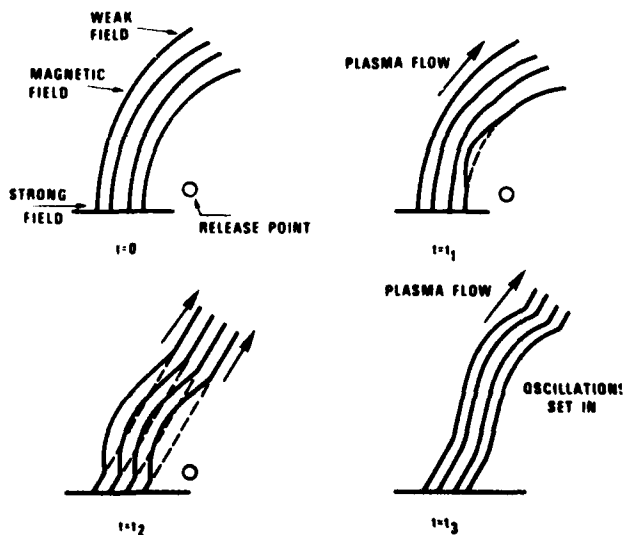


Fig. 30 — Isotropic energy release near vertical fields

opposed to simple bipolar region, statistically one should expect a greater number of flares occurring there as well as sympathetically triggered there, i.e., a domino effect. In addition, one should expect this increased sampling would make it appear that a larger number of nonthermal flares should occur in complex active regions.

Our ignorance of the origins of active regions, and thus what makes one region more complex than another, argues in favor of a greater reservoir of energy from which to drive nonthermal flares. The continued birth and death of magnetic structures within an active region also argues in favor of dynamic evolution deep beneath the photosphere, which can drive strong currents and cause various transient effects, as well as the mechanisms that heat the corona.

- Problem 3 — What is the altitude of the flare? We have answered this question. However for clarity we repeat that we expect, on the basis of stability and energy requirements, low-lying flare arches of the order 5000 km.

- Problem 4 — What role does the magnetic field play in the flare process? The magnetic field in the arch plays both a passive and active role. The toroidal component of \mathbf{B} maintains the integrity of the arch during flaring, and the poloidal component of \mathbf{B} provides the source of flare energy via $j_T \cdot B_P$ is annihilated by the reconnection process in the arch due to the processes discussed.

- Problem 4a — How is the energy stored in this theory relative to its release position? The energy is stored in the form of currents, which are probably generated beneath, or in the deeper regions of, the photosphere. Hence they may represent a huge inductive circuit, the arch being only a small portion of the total circuit. Although the bulk portion of the energy is stored elsewhere, the flare energy is released in situ, in the lower corona or transition zone.

- Problem 4b — Is the magnetic energy stored in the form of current sheets or twisted fields? In this model these alternatives are equivalent.

- Problem 6 — Are there any distinguishable time differences between flare onsets in the soft x rays and in the H_α lines, from the point of view of this model? Yes, the soft x rays should rise first, because the H_α lines are generated by manifestations of the shock, which come after the arch heating. A possible exception may be the early formation of the flare kernels in H_α .

- Problem 8 — Are there indeed two different types of flares: thermal and non-thermal? This question was answered in detail earlier; but, to repeat, there exists a hierarchy of flare types in this model.

- Problem 9 — What are the configurations giving rise to the two different types of flares? The configurations are the same, if allowance is not made for filaments, etc.

- Problem 10 — What is the altitude of the acceleration region, and does acceleration occur in expanding flare loops? In answer to the first question, the acceleration region is within the arch, which generally will be low lying if it is to generate an impulsive flare. In answer to the second question, if a loop carries a current, acceleration can

DANIEL S. SPICER

occur, or a shock striking a loop can lead to loss-cone instabilities and stochastic processes, and thus to precipitation of energetic particles.

● Problem 11 — Is the acceleration process impulsive or continuous? Both, the impulsive behavior occurs either from global kinks or when the short wavelength tearing modes are growing and overlapping resonances occurs. As longer wavelength tearing occurs, the system will saturate and evolve to a marginal stability state, thermalizing the field continuously, although at a rate decreasing with time.

● Problem 12 — Are the electrons accelerated during the thermal flare? Yes, regardless of whether the flare is thermal or nonthermal, in this model we expect some acceleration to occur.

● Problem 14 — Most type III bursts do not occur during flares; how does the model explain this? As noted in Section 7, electrons will not always escape from the arch and we do not expect sheet kinks to form on the surface of every arch; hence not every flaring arch should generate type III bursts. However we expect that most type III bursts are related to phenomenon similar to the flare mechanism discussed here.

● Problem 16a — Are the high-energy particles in flares accelerated in a one-step or a two-step acceleration process? We feel there is a two-step process. However we have examined only the first step and not the second, and we do not intend to do so here.

● Problem 16b — Since the second step is related to the shock wave, what are the conditions that give rise to the shock? As we have discussed in some detail in Section 7, either the shock will be generated when the gradients are steep enough and the B_p is large enough to cause the rate of energy release to appear explosive or global kinks will drive the shocks.

● Problem 17 — Is the visible Moreton wave a part of the same wave front that produces type II bursts? In this model the initial shock wave generated by the pressure pulse should expand in the form of a droplet, if the release is not impeded by magnetic-field barriers. Hence there is no reason to expect the Moreton wave not to be part of the same shock wave that forms the type II bursts. However, if the blast wave were to excite other flares, such as other neighboring arches or filaments, these may generate their own shocks and confuse the issue.

● Problem 19 — "Disparition brusques" are sometimes caused by shocks, but this is not always the case; how does the model explain this? As argued earlier, filaments will be subject to the same set of instabilities as the arches if they carry a current. Hence they may be excited in the same way as arches, e.g., shocks and preflare heating.

Other questions raised by Svestka are related to the second acceleration phase of the flare, which appears to be related to stochastic processes; hence they are outside the context of the model presented.

10. DISCUSSION AND CONCLUSIONS

In the development of this model we have used the observational fact that the magnetic topology of a flare is an arch. In addition we have *assumed* that a toroidal current exists in the arch. With this, we have examined the physical consequences of the assumption and how it relates to the solar flare. We have found that the consequences are many and that the model can explain many of the observations obtained from Skylab, as well as previous observations. The assumption of the existence of such a current has led, quite naturally, to a flare model that has explanations for many varied phenomena, which include:

- The role of preflare heating,
- The small volume of energy release within the arch in comparison to the total arch volume,
- The integrity generally maintained by the arch,
- Sympathetic flares,
- The difference between thermal and nonthermal flares,
- Kinking arches,
- A close relationship that may exist between flare instabilities and filament instabilities if the filaments contain currents,
- The source of the flare shock wave and the requirements for its existence,
- Sprays,
- "Disparitions brusques," and
- Flare ribbons and flare loops, and a connection between them and type IV bursts.

We predict that:

- The nonthermal flare, large or small energy release, will generally come from low altitude arches;
- Impulsive bursts are a result of nonthermal heating and strong disruptions of the plasma;
- The thermal flare will come from larger arches, unless the plasma density is very large and invalidates Eq. (7.1), even in the presence of large fields and field gradients;
- The rate of energy release decreases with increasing volume;
- Type III bursts either escape from arches by drift mechanisms and/or are caused by sheet kinks;

DANIEL S. SPICER

- Shock waves may excite multiple arches to flaring by a domino effect;
- Energy is stored mainly in the form of currents generated beneath the visible photosphere, and the total stored energy is probably much greater than the actual energy released during a flare;
- The faster the flare rise time the more nonthermal the flare; and
- High-altitude arches with weak field gradients will have large-diameter magnetic islands, and low-altitude arches with strong field gradients will have small-diameter magnetic islands, with both high and low arches having the appearance of being stranded like a rope.

Some of these explanations are heuristic, but this is by necessity and not by choice. For the theorist to develop a more quantitative model will require higher instrumental resolution, which will not become available in the foreseeable future. However the theorist must complement the observer regardless of the observer's instrumental weaknesses. Hence the theorist must, within his ability, help guide the observer in his observations, and for him to do so requires a model which is reasonably complete and which can be tested. If tests prove positive, this model or a more successful model can then be quantitatively improved, such as by a numerical modeling. However at present only particular features of this model need to be studied in more detail, e.g., overlapping resonances and the degree of enhanced reconnection, or the phenomenological release of the equivalent of a flare energy into a model solar atmosphere, using realistic numerical techniques. In this way progress can be made theoretically, and simultaneously other problem areas can be defined.

It is hoped that this model, whether correct or incorrect, will act as a catalyst for others and make the development of more realistic theoretical models of flares a reality. In addition it is hoped that the observer will give it a chance and compare theory with observations carefully, being cautious not to confuse flare manifestations with the actual event.

Appendix A
LOCATION OF LEAST HYDROMAGNETIC STABILITY

Here, we examine the hydromagnetic stability of an ideal current-carrying arch, in an attempt to determine the location where $q(r, \theta, \phi)$ is most likely to be ≤ 1 . Figure A1 illustrates the magnetic topology assumed. Here

$$R' = [R_0 + \Delta(r)]f(\phi) \quad (\text{A1})$$

and

$$R'' = [R_0 + \Delta(r)]f(\phi) - r \cos(\theta + \delta), \quad (\text{A2})$$

where $f(\phi)$ is a function describing the angular dependence of R'' and R' with altitude. If the arch fields are symmetrical, $f(\phi) = 1$ at $\phi = 0$ or π and $f(\phi)$ is a maximum at $\pi/2$, implying $f(\phi)$ is an even function. The quantity $\Delta(r)$ is a small quantity which takes into account the distortion of magnetic surfaces due to curvature. We assume for simplicity $\Delta(r) = \Delta(r)$. $\Delta(r)$ is determined by the equilibrium conditions, and δ is a quantity which can be used to make the magnetic field lines straight in the coordinates θ and ϕ , i.e., $d\theta/d\phi = \text{constant}$. However this need not be done for what is to follow.

Using Eqs. (A1) and (A2), we have

$$\begin{aligned} \mathbf{r} = & \{ [R_0 + \Delta(r)]f(\phi) - r \cos(\theta + \delta) \} \cos \phi \mathbf{e}_1 + \{ [R_0 + \Delta(r)]f(\phi) - r \cos(\theta + \delta) \} \sin \phi \mathbf{e}_2 \\ & + r \sin(\theta + \delta) \mathbf{e}_3. \end{aligned} \quad (\text{A3})$$

Assuming $\Delta/r \approx \epsilon$ and $\delta \approx \epsilon$, where $\epsilon = r/R \ll 1$, we find the metric coefficients

$$\begin{aligned} g_{11} &= 1 - 2 \cos \theta \Delta'(r)f(\phi), \\ g_{22} &= r^2 (1 + 2\partial\delta/\partial\theta), \\ g_{33} &= (R_0 + \Delta)^2 f^2(\phi)' + [(R_0 + \Delta)f(\phi) - r \cos \theta]^2, \\ g_{12} &= g_{21} = r [\Delta' f(\phi) \sin \theta + r \partial\delta/\partial r], \\ g_{32} &= g_{23} = r \sin \theta (1 + \partial\delta/\partial\theta) (R_0 + \Delta) f'(\phi), \end{aligned}$$

and

$$g_{31} = g_{13} = (R_0 + \Delta) f'(\phi) [\Delta' f(\phi) - \cos \theta + r(\partial\delta/\partial r) \sin \theta], \quad (\text{A4})$$

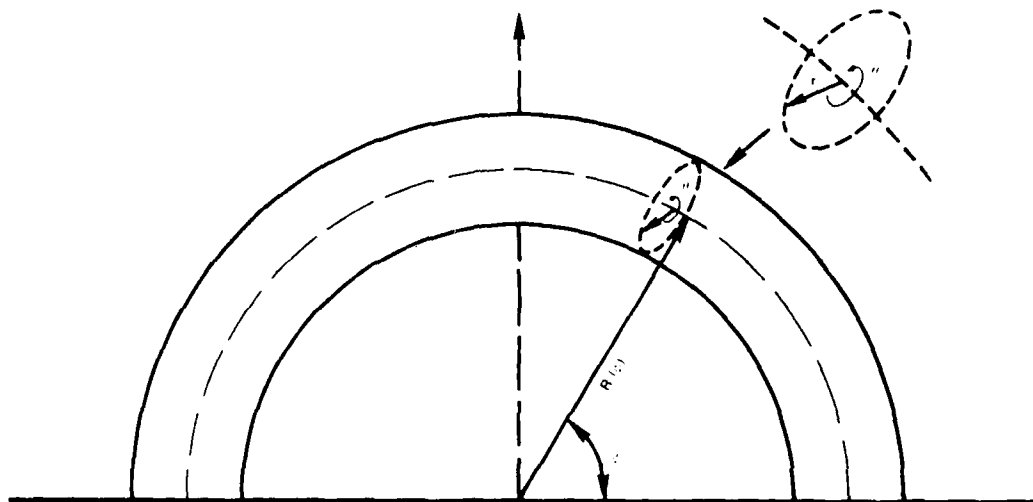


Fig. A1 - Arch geometry. $R(\phi)$ is the major radius and varies with ϕ , and r is the minor radius. The inverse aspect ration $\epsilon = r/R(\phi)$.

where $f'(\phi) = df/d\phi$ and $\Delta' = \partial\Delta/\partial r$. Now

$$\sqrt{g_{22}} d\theta/B_\theta = \sqrt{g_{33}} d\phi/B_\phi; \quad (\text{A5})$$

hence

$$d\theta/d\phi = \sqrt{g_{33}/g_{22}} B_\theta/B_\phi, \quad (\text{A6})$$

where $d\theta/d\phi$ represents the rate of twist in θ with angle (altitude) ϕ . Since the toroidal component B_ϕ decreases with altitude, we use as an example

$$B_\phi \approx B_\phi^0 (R_0/R'')^\alpha, \quad (\text{A7})$$

where B_ϕ^0 is the strength of the field at the arch feet and $\alpha \geq 1$. Now

$$(1/R'')^\alpha \approx \{1/[(R_0 + \Delta)f(\phi)]\}^\alpha [1 + (\alpha/R') \cos \theta]; \quad (\text{A8})$$

hence

$$B_\phi \approx B_\phi^0 \{R_0/[(R_0 + \Delta)f(\phi)]\}^\alpha [1 + \alpha r \cos \theta/R'].$$

We take

$$B_\theta \approx B_\theta^0 [1 + \Lambda(r, \phi) \cos \theta], \quad (\text{A9})$$

where $\Lambda(r, \phi)$ is determined by $\nabla \cdot \mathbf{B} = 0$ and B_θ^0 is obtained by assuming the total current I is approximately constant, although in reality $I = I(r)$.

Now

$$\sqrt{g_{33}/g_{22}} = A(r, \theta, \phi); \quad (\text{A10})$$

hence

$$d\theta/d\phi = A(r, \theta, \phi)B_\theta(R_0 + \Delta)^\alpha f^\alpha(\phi)/B_\phi^0 R_0^\alpha (1 + \alpha r \cos \theta/R). \quad (\text{A11})$$

Defining

$$q(r, \theta, \phi) = rB_\phi/R_0 B_\theta,$$

we have

$$d\theta/d\phi = A(r, \theta, \phi)r/R_0 q. \quad (\text{A12})$$

Evaluating $d\theta/d\phi$ at $\phi = 0$ or π and $\phi = \pi/2$ by assuming $f(\phi = \pi/2) = \gamma > 1$, we obtain

$$\left. (d\theta/d\phi) \right|_{\phi=\pi/2} / \left. (d\theta/d\phi) \right|_{\phi=0,\pi} = \gamma^{\alpha+1}; \quad (\text{A13})$$

i.e., the field lines are twisted by an amount $\gamma^{\alpha+1}$ greater at the apex than at the feet of the arch. This implies q is γ^{-1} times smaller at arch apex than at the feet; hence the arch is hydromagnetically least stable at the apex for symmetric fields. However, if $B_\phi(r, \theta, \phi)$ is not so symmetric, $d\theta/d\phi$ will have its maximum where B_ϕ is a minimum.

Appendix B TRANSPORT MECHANISMS

Here we collect the many and varied transport mechanisms that may play a role prior to and during the solar flare model proposed in Sections 6 through 10.

ANOMALOUS RESISTIVITY AND ANOMALOUS HEATING

Anomalous resistivity is a phenomenon that occurs when plasma collective effects result in the spatial correlation of ions, so that when the electrons collide with this correlation of ions, they see an effective charge-to-mass ratio much larger than e^2/m_i . This results in an increase in the effective collision frequency over and above that which occurs due to Coulomb collisions.

To model the enhanced resistivity generated by collective plasma effects, one typically introduces an effective collision frequency ν_{eff} so that the anomalous resistivity is given by

$$\eta_{AN} = (\nu_{eff}/\nu_{ei})\eta_{cl}, \quad (B1)$$

where ν_{ei} is the Coulomb collision frequency and η_{cl} is the classical resistivity. The effective collision frequency may be obtained from weak turbulence theory, and is discussed in detail by Davidson (1972). Here, we collect in Tables B1 and B2 the threshold conditions and effective collision frequencies for instabilities driven by currents parallel and perpendicular to the magnetic field, as well as the anomalous heating rates. These instabilities will be briefly elucidated later.

Anomalous heating results when the collective effects transfer the energy from the waves to the particles. The resulting increase in particle energy is not true thermal energy, strictly speaking, but rather an energy of sloshing in the wave fields. This sloshing can drive the particle distribution to Maxwellian-like distributions but never to a true Maxwellian distribution. However, as far as flare modeling is concerned, this energy can be treated as thermal, since the observable flare time scales are so much greater than the characteristic times of plasma collective effects.

Before proceeding, some general remarks are in order. As noted by Lampe et al. (1975), the principal effect of most collective plasma processes on macroscopic behavior is that the plasma system is driven to marginal stability, by which we mean the system is at the threshold from which it may be stabilized, excited, restabilized, and then reexcited temporally and spatially. Thus the threshold conditions for turn-on and turn-off various collective effects is important to us in addition to the anomalous transport resulting from collective effects. Keeping this in mind, we will proceed by noting the various means by which collective effects can be excited and then examine each in more detail.

SOURCES OF PLASMA MICROINSTABILITIES

There are in general three main sources of free energy by which plasma microinstabilities can be driven:

- *Velocity-space anisotropy*, which usually results from a skewing of the distribution function by a current or by a high-energy beam within the plasma.

- *Plasma expansion energy*, which results directly from the fact that a confined plasma, such as an arch, necessarily has a plasma distribution which is not in thermodynamic equilibrium. Such a confined plasma necessarily has gradients in temperature and/or density which are a source of free energy to drive microinstabilities. These instabilities usually take the form of drift waves which try to eliminate the driving mechanism.

- *Magnetic energy*, which is stored in distortions of the magnetic field from its vacuum state. Such distortions typically generate macroinstabilities which can drive microinstabilities; e.g., a kink thrashing about will generate shocks, which can result in a nonthermal distribution, which in turn can drive microinstabilities.

VELOCITY-SPACE ANISOTROPY

Here we collect the principal sources of velocity-space anisotropy.

A possible, although not probable, means of excitation of microinstabilities during the preflare buildup, and during the actual flare, is by currents driven parallel to the magnetic field. We note here only the Buneman instability (Buneman, 1959), the ion sound instability (Krall and Trivelpiece, 1973), and the electrostatic ion cyclotron instability (Drummond and Rosenbluth, 1962). There are instabilities associated with currents driven across magnetic fields; however they have threshold values similar to the parallel-driven-current instabilities. Thus, because the dominant current component is parallel to \mathbf{B} in an arch, we will not presently consider them. The turn-on conditions and anomalous transport coefficients are given in Table B1.

A number of comments should be made before proceeding. First, it is clear that the requirements for onset of the Buneman instability are very restrictive. In particular the gradient scale length for the poloidal component of \mathbf{B} in the arch must be of the order of a skin depth, i.e.,

$$\ell_B \lesssim B_\phi (dB_\phi/dr)^{-1} \sim (c/\omega_{pe})(1/\beta_p)^{1/2}. \quad (\text{B2})$$

Such a condition is unlikely in a quiescent solar arch, although it may be possible during the evolution of the arch, e.g., during the emergence of an arch from beneath the photosphere prior to a flare.

Table B1 — Electrostatic Instabilities Driven Perpendicular to B

Instability	Velocity Turn-On Conditions	Gradient Turn-On Conditions	Effective Collision Frequency	Effective Heating Rate	Comments
Buneman	$v_d \geq v_{Te}$	$\delta t \leq \frac{c}{\omega_{pe}} \left(\frac{1}{\beta_{pe}} \right)^{1/2}$	$\nu_{eff} \approx \left(\frac{m_e}{m_i} \right)^{1/3} \omega_{pe}$	$\dot{T}_e \approx \frac{2}{3n_e} \left(\frac{2\Omega_{ce}^2}{\omega_{pe}^2} + 1 \right) \gamma T_e \frac{1}{2\lambda_d^3}$ where $\gamma = (3)^{1/2} \omega_{pe} \exp(-v_{Te}^2/v_d^2)$ $T_i \ll T_e$	Turn-on conditions independent of T_e/T_i
Ion Sound	$v_d \geq c_s \left[\left(\frac{T_e}{T_i} \right)^{3/2} \sqrt{\frac{m_i}{m_e}} \right]$ $\exp(-2T_e/T_i)$ $T_e/T_i > 1$	$\delta t \leq \frac{c}{\omega_{pe}} \left(\frac{1}{\beta_{pe}} \right)^{1/2}$ $1 + \left(\frac{T_e}{T_i} \right)^{3/2} \left(\frac{m_i}{m_e} \right)^{1/2} e^{-T_e/2T_i}$	$\nu_{eff} \approx \frac{\sqrt{\pi}}{32} \omega_{pe} m_i \left(c_s \sqrt{3} v_{Ti} \right)^2 \frac{1}{(kT_e)^2}$ $T_e = m_e v_d^2 \nu_{eff} / k$ $\approx \left(\eta_{eff} J^2 \right) \frac{2}{3n_e k}$ $T_i = T_e \left(\frac{m_e}{m_i} \right)^{1/2} \frac{v_{Te}}{v_d}$	Depends critically on T_e/T_i	
Electrostatic Ion Cyclotron	$v_d \geq c_s$	$\delta t \leq \frac{c}{\omega_{pe}} \left(\frac{1}{\beta_{pe}} \right)^{1/2}$	$\nu_{eff} \approx \nu_{ci} (1 + v_d/v_{Te})$	$T_i = \Omega_i \frac{v_d}{v_{Te}}$	Only importance if ion sound is stable and can occur if $T_e/T_i \approx 1$

The turn-on conditions for the ion sound mode are somewhat less restrictive, since they require a gradient length

$$\ell_{LS} \leq \frac{c}{\omega_{pi}} \left(\frac{1}{\beta_p}\right)^{1/2} \frac{1}{1 + \left(\frac{T_e}{T_i} \frac{m_i}{m_e}\right)^{1/2} \exp\left(-\frac{T_e}{2T_i}\right)}, \quad (\text{B3})$$

which is $\approx 43 \ell_B$. Further for constant electric field and classical resistivity $T_e \propto v_d/c_s$; thus in principle the ion-sound instability can be triggered by a collisional heating instability, e.g., the superheating instability discussed in Section 4.

Notice that as $T_e/T_i \rightarrow 1$ the ion-sound-mode turn-on conditions evolve into the Buneman conditions. Further, notice that the conditions for the ion cyclotron mode evolve into the ion-sound mode. Physically what occurs is that when the current is very weak, or $T_e/T_i \approx 1$, we can expect the ion cyclotron mode. However, as the current density increases, the growth rate of the ion cyclotron mode will exceed the ion cyclotron frequency. When this occurs, the periodic Larmor motion of the ions is destroyed and the ions become demagnetized ($\Omega_i/\nu_{eff} < 1$). At this stage the ion cyclotron waves are destroyed by the turbulence, and the instability nonlinearly evolves into the ion sound mode. Note that a large ratio of T_e/T_i is required to excite the ion sound mode. Also note that to maintain a constant anomalous resistivity due to the ion sound instability requires $d(T_e/T_i)/dt > 1$.

As we have noted, the above instabilities arise as a result of longitudinal currents becoming electrostatically unstable. There is however a mechanism which can generate a source of enhanced plasma turbulence even when the longitudinal current is electrostatically stable. This mechanism was developed by Papadopoulos and Coffey (1974a, 1974b), and has been applied to Birkeland (field-aligned) currents that exist in the ionosphere and magnetosphere. The basic assumption made for their mechanism is that a weak beam of high-energy electrons exists in addition to the electrostatically stable Birkeland current. This fast beam interacts with the bulk current, which is electrostatically stable itself, via the beam-plasma instability in region 1 of Fig. B1. The turbulent field energy generated by this interaction cascades, by the nonlinear-oscillating-two-stream instability, into plasma waves in regions 2 and 3, and into ion-density fluctuations with phase velocities approaching zero. The cascading time must be such that it occurs on a time scale faster than the quasi-linear beam stabilization time. Thus the turbulent field energy is no longer resonant with the beam, which then cannot relax into a plateau. Hence the beam maintains its integrity. It is the excited electrostatic ion-density fluctuations created in the cascading process that yields the bulk anomalous resistivity. Papadopoulos and Coffey (1974b) give an effective collision frequency

$$\nu_{eff} \approx \omega_{pe} \left(\frac{\pi}{2}\right)^{1/2} \langle k\lambda_0 \rangle \left(\frac{W}{nkT_e}\right), \quad (\text{B5})$$

where $\langle k\lambda_0 \rangle$ represents the predominant wave number participating in the oscillating two stream instability, $W_0 (\approx n_b m_e v_b \Delta v_b)$ is the energy density of the electron plasma oscillations, nkT_e is the thermal energy density of the ambient auroral zone, n_b is the beam density, v_b is the beam velocity, and Δv_b is the thermal spread of the beam.

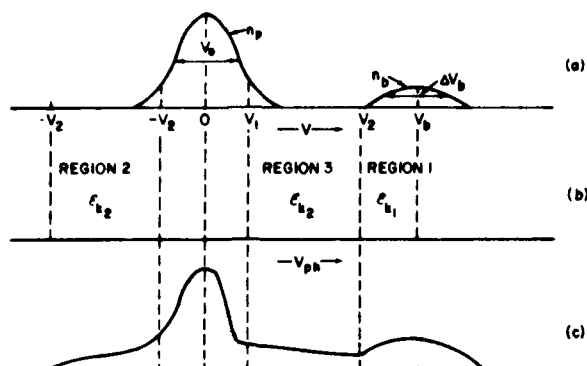


Fig. B1 — Velocity and field energy distributions: (a) Initial velocity distribution functions of the beam and the plasma electrons; (b) wave spectrum in phase velocity space, region 1 being the region of the growing waves due to the beam plasma interaction, and regions 2 and 3 being the regions of spectral energy transfer due to the oscillating two-stream instability; and (c) final marginal stability state of the beam and the plasma electron distribution functions

Papadopoulos (1975) has also considered the question of how this instability may lead to a stabilized source of anomalous resistivity. The basic arguments are simple. One first assumes a source of high-energy electrons exists which will give rise to the anomalous resistivity as discussed above. Since this new resistivity is a bulk resistivity, the joule heating will increase, altering the thermal distribution of the electrons so that more electrons can run away. These new runaway electrons then feed the beam that generates the anomalous resistivity. This behavior then leads to a self-sustaining nonlinear feedback mechanism for anomalous resistivity in the presence of an electrostatically stable current. As argued in Section 8, combination of the superheating instability and current convective instability could act as an initial injection mechanism for this source of anomalous resistivity.

PLASMA EXPANSION ENERGY

As defined earlier, plasma expansion energy is a source of plasma energy that resides primarily in temperature or density gradients or, in general, pressure gradients. Since the gradients that exist in the solar atmosphere are small, it is difficult to believe that plasma expansion energy can play a role in the triggering of a flare, although it probably plays a role during the actual flare. These instabilities are of a class usually called drift instabilities (Krall and Trivelpiece, 1973). This is because a gradient of density, temperature, or magnetic field perpendicular to \mathbf{B} results in particle drifts. In general a detailed knowledge of the particle distribution is necessary to properly describe the instability. However there are reasonable approximations one may make, since the drift velocity v_d of the particles is typically of the order

$$v_d \approx v_{Te} \rho_e / L, \quad (\text{B6})$$

where ρ_e is the electron gyroradius and L is the gradient scale size. Adopting $L \approx 1$ km, $T_e \approx 10^6$ K, and $B \approx 500$ gauss as characteristic values in one solar atmosphere yields $v_d \approx 1$ meter/s. If the wave vector of the growing wave satisfies $\mathbf{k} \cdot \mathbf{B} = 0$, the wave can extract energy from only the drifting particles and the instability may be classified as a flute instability. If $k_{\parallel} \neq 0$ but has a small component parallel to \mathbf{B} , the wave phase velocity parallel to \mathbf{B} can be comparable to the thermal velocity. Hence energy can be extracted from the parallel thermal velocity component of resonant particles. This typically results in magnetosonic or Alfvén waves.

An examination of the dispersion relation (Krall and Trivelpiece, 1973) shows that since $v_d \ll v_{T_i}$, only $|k_{\parallel}| \ll |k_{\perp}|$ is allowed. This yields a frequency $\omega^* = k_{\perp} V_d$ when $k_{\perp} \rho_i \lesssim 1$ and $\omega^* \approx 0.2v_{T_i}/L$ when $1 < k_{\perp} \rho_i$. The maximum growth rate occurring for $k_{\perp} \rho_i \approx 3$ is $\omega^* \approx 0.2v_{T_i}/L$. For the previous assumed values $\omega^* \approx 14$ Hz.

As the particles drift across the field, they tend to flatten the gradient. This takes a time of the order $t_d \approx L^2/v_{T_e} \rho_e$. Using the above values, we have $t_d \approx 10^3$ s. For steeper gradients, this time is considerably shorter, since t_d varies as L .

Some additional comments are in order concerning the applicability of these instabilities in the solar atmosphere. For example, if a density gradient exists, a drift-wave instability can occur only near Ω_i and if $v_{T_i}/L \approx \Omega_i$. This condition is highly restrictive and probably impossible to satisfy in the solar atmosphere, so it is safe to neglect density-driven drift modes. An alternate situation is when the density and the temperature have a gradient. Instability will occur if

$$[1 - (n/2T)dT/dn](n/T)dT/dn < 0. \quad (B7)$$

Since solar arches observationally have a cold core and a hot extremity, and at the same time are approximately force free, it is easy to show for this case that

$$dT/dn < 0 \quad (B8)$$

and instability can occur.

Returning to the problem at hand, we recognize that although the drift modes appear to be weak, our knowledge of preflare conditions in arches is nonexistent. Hence it is quite possible that plasma expansion energy may play a role in the flare triggering, e.g., the alteration of the current-density profile during the emergence of an arch. Because of this possibility we note various possible means by which plasma expansion energy can modify the current-density profile. We will follow, in part, McBride et al. (1975). There exist two regimes to be considered: the high-frequency regime ($\omega \gg \Omega_i$), and the low-frequency regime ($\omega \ll \Omega_i$). We have already considered (Table B1) three longitudinal current-driven instabilities which can also alter the current profile. These belong in the high-frequency regime. In Table B2 we collect, following McBride et al. (1975), the other possibilities. Before proceeding, it must be emphasized that the realization of the instabilities to be discussed has a low probability, except during the formation of the arch or if there exists a transient EMF along the arch by some as-yet unknown mechanism. In addition, if these instabilities occur, they will cause the current-density profiles to become more stable to MHD and resistive macroscopic modes, since they tend to flatten the current-density profile rather than steepen it.

Table B2 — Current Penetration Instabilities

Instability	Threshold Conditions	Comments
<p>Current shear (Horton, 1972)</p>	$\delta \ell_J = \left(\frac{1}{J_T} \frac{dJ_T}{dr} \right)^{-1}$ $< \frac{1}{4} \frac{c}{\omega_{pe}} \frac{c}{v_{Te}} \frac{1}{(1 + \omega_{pe}^2 / \Omega_{ce}^2)^{1/2}}$ $\delta \ell_J < \frac{1}{2} \frac{c}{\omega_{pe}} \frac{v_d}{c} \frac{\omega_{pe}^2}{\Omega_{ce}^2} \left(\frac{m_i}{m_e} \right) \cdot \frac{1}{(1 + \omega_{pe}^2 / \Omega_{ce}^2)^{1/2}}$	<p>$\omega > k_{ } v_{Te}$</p> <p>$\omega \gg \Omega_{ci}$</p> <p>Condition must be satisfied if $\lambda > \Omega_{ci}$ as theory assumed.</p>
<p>Current shear (Lui, 1971)</p>	$\delta \ell_J < \frac{c}{\omega_{pe}} \frac{v_d}{c} \frac{\omega_{pe}}{\Omega_{ce}} \left(\frac{m_i}{m_e} \frac{T_e}{T_i} \right)^{1/2}$ $\delta \ell_T = \left(\frac{1}{T_e} \frac{dT_e}{dr} \right)^{-1} \lesssim 2L_J$	<p>$\omega < k_{ } v_{Te}$</p> <p>$\omega \gg \Omega_{ci}$</p> <p>Temperature gradient stabilizes the mode.</p>
<p>Electron temperature gradient opposite to density gradients</p>	$1 + \left(\frac{T_i}{T_e} \right) \left(\frac{L_n}{L_s} \right)^{3/2}$ $< \left[-\frac{1}{2} \frac{L_n}{L_T} + \left(1 + \frac{T_e}{T_i} \right) \frac{k_y^2 \rho_i^2}{\sqrt{2}} \right] \cdot \left(\frac{m_e}{m_i} \right)^{1/2} \ln \left(\frac{2m_i}{m_e} \frac{L_n}{L_s} \right)^{1/2}$	<p>$\omega \ll \Omega_{ce}$</p> $L_s \approx \frac{c^2}{v_d^2} \frac{\Omega_{ce}}{\omega_{pe}^2}$ $L_n = \left(\frac{1}{n} \frac{dn}{dr} \right)^{-1}$ <p>Shear must be weak enough not to damp modes.</p>

Two possible instabilities driven by radial current gradients are those considered by Horton (1972) and Liu (1971). Horton (1972) considers a current-gradient instability which exists in the fluid limit ($\omega > k_{\parallel} v_{Te}$) and will lead to current penetration according to a diffusion equation. However McBride et al. (1975) show that one should expect the ion sound instability to be excited before the current-shear mode developed by Horton (1972), except in cases where the current gradients are very steep.

The current-shear mode considered by Liu (1971) suffers a similar fate, because it can be satisfied only if the gradient in toroidal current density is of the order $L \lesssim c/\omega_{pe}$. In addition, when the current density and temperature gradients are comparable, Liu's mode is stabilized.

An instability that exists at frequencies below the ion gyro frequency, and which may be important in low-lying steady-state arches, is the electron-temperature-gradient drift-wave instability (Kadomtsev, 1965). This instability exists when the temperature gradient is the reverse of the density gradient, as would occur if the arch were force free or if there is a current skin phase in the evolution of the arch. As shown by Liu et al. (1972), this mode requires a magnetic shear length $L \approx (c^2 \Omega_e)/(v_d \omega_{pe}^2)$. In addition Liu et al. (1972) have shown this instability leads to anomalous transport which tends to flatten the temperature gradient by convecting heat inward while convecting mass outward.

MAGNETIC ENERGY

Anomalous effects driven by magnetically stored energy, being released in the form of MHD or resistive MHD instabilities, are very likely during the flare or in the preflare period. This energy will initially be released in the form of plasma flow parallel and perpendicular to the magnetic field, driven by electric fields generated by MHD or resistive MHD instabilities, i.e.,

$$E_{\parallel} = j_{\parallel} \quad (\text{B9})$$

and

$$E_{\perp} = j_{\perp} - \mathbf{v} \times \mathbf{B}/c. \quad (\text{B10})$$

Equation (B9) can in principal generate electron streams of sufficient energy to excite instabilities driven parallel to \mathbf{B} , e.g., the Buneman instability. Alternately E_{\perp} given by Eq. (B10) will result in plasma flow across magnetic fields, so that it is possible to excite various crossfield instabilities such as the beam cyclotron instability. Such instabilities can also be excited by shock waves moving across field lines. Most of these crossfield instabilities lead to modified transport coefficients to such an extent that they should play an important role during the flare itself. In particular one should expect strong energy and momentum coupling between the flare plasma and the ambient plasma in which the flare is situated. For these reasons we will briefly discuss the various instabilities and then list their thresholds and transport coefficients.

In Table B3 we collect the various instabilities (after Lampe et al. 1975), their turn-on conditions, and the transport coefficients. The beam cyclotron instability is driven by

Table B3 — Electrostatic Instabilities Driven Perpendicular to B

Instability	Threshold Conditions	Collision Frequency and Heating Rates	Comments
Modified Two-Stream	$v_d < v_A \sqrt{1 + \beta_e} \left\{ 1 + \frac{k_{ } k_L}{1 + \sqrt{1 + \beta_e}} \left(1 + \Omega_{ce}^2 / \omega_{pe}^2 \right)^{1/2} \right\}$	$\nu_{ie} \approx \frac{.14 \omega_{pi}}{\sqrt{1 + \omega_{pe}^2 / \Omega_{ce}^2}} \left(\frac{k_{ }}{k_L} \right)^{2/3} \text{ if } \frac{k_{ }}{k_L} \leq 1$ $\nu_{ei} \approx \frac{.14 \omega_{pi}}{\sqrt{1 + \omega_{pe}^2 / \Omega_{ce}^2}} \left(\frac{k_{ }}{k_L} \right)^{1/3} \text{ if } \frac{k_{ }}{k_L} > 1$ $T_e = m_e v_d (v_d - v_{Ti}) \nu_{ei}$ $T_i = v_{Ti} T_e / (v_d - v_{Ti})$	Assuming $Z_i = 1$ $n_i/n_e = 1$ The threshold conditions for this instability are rather detailed and the reader should consult Lampe, et al. (1975). Electron heating strictly \parallel to \vec{B} and ions \perp to \vec{B} .
Beam Cyclotron	$ v_d < v_{Ti} \left\{ 1 + \left(\frac{T_e}{T_i} \right)^{3/2} \sqrt{\frac{m_i}{m_e}} e^{-T_e/2T_i} \right\}^{1/2}$ (Transition to ion-sound instability) $ v_d > v_{Ti}$ (Stabilization by Ion Landau Damping)	$\nu_{ie} \approx .75 \Omega_{ce} \left(\frac{m_e}{m_i} \right) \left(\frac{T_e}{T_i} \right)^2 \frac{v_{Te}^2}{v_d^2 c^2 \beta_e} \left[1 + \frac{v_{Ti}}{v_d} \right]$ $T_e = m_e (v_d - v_{Ti}) \nu_{ei}$ $T_i = v_{Ti} T_e / (v_d - v_{Ti})$	If $v_d > c_s$ but v_d is below threshold for ion sound instability, the magnetic field can drive beam cyclotron. Easily stabilized. Heats electrons and ions \perp to \vec{B} .
Unmagnetized Ion-Ion	$ v_d < 2.5 v_A \sqrt{\beta_e}$ (Transition to MII) $ v_d > v_{Ti}$ (Stabilization by Landau Damping)	$\nu_{ij} \approx .15 \omega_{pi} \frac{\rho_i}{\rho_T} \left\{ \xi^{2/3} + \frac{\sqrt{3}}{2^{1/3}} [\xi^{1/3} - \xi^{2/3}] \right\}$ where $\xi \equiv \min(\rho_i/\rho_j, \rho_j/\rho_i)$ $\rho_i = n_i m_i$ ion mass density (species i) $\rho_T = \sum_k^{ions} n_k m_k$ total mass density	Both MII and UII result in strong momentum coupling between ion species when operative.
Magnetized Ion-Ion	$ v_d \leq 2.5 v_A \sqrt{1 + \beta_e}$ $ v_d > 2.5 v_A \sqrt{\beta_e}$ (transition to UII) $ v_d > v_{Ti}$ Stabilization by Landau Damping	$\nu_{ij} \approx .14 \Omega_{Hi} \frac{\rho_i}{\rho_T} \left\{ \xi^{2/3} + \frac{\sqrt{3}}{2^{1/3}} [\xi^{1/3} - \xi^{2/3}] \right\}$ $\Omega_{Hi} = \sqrt{\Omega_i \Omega_e}$ Lower Hybrid frequency	

the relative drift of electrons and ions across a constant magnetic field and is due to the coupling of electron cyclotron modes with ion sound modes. This instability results in strong electron heating, and when the turbulence is strong enough, the electrons become unmagnetized ($\Omega_e / \nu_{eff} \ll 1$). When this occurs, the instability evolves into the ion sound instability.

The ion-ion two-stream instabilities fall into two classes: magnetized and unmagnetized. The unmagnetized ion-ion instability (UII) results when the relative drift velocity between counterstreaming ions becomes greater than the sound velocity. The magnetized ion-ion instability (MII) is similar to the beam cyclotron instability and occurs when the drift velocity between counterstreaming ions across a magnetic field exceeds the sound velocity. The MII evolves into the UII when the turbulence is sufficiently great that the ions become unmagnetized. However it must be recognized from the conditions in Table B3 that for certain parameter ranges both instabilities can exist, although the UII is always the faster growing and dominant instability. These ion-ion instabilities are of particular importance because they provide strong momentum coupling. However they do not cause electron heating but only ion heating.

The modified-two-stream instability (MTS) (Krall and Liewer, 1971) is caused by the relative drift of ions and electrons across a magnetic field. It is particularly important because of its role in heating electrons and ions. In addition it can be operative even in parameter regimes where no other electrostatic instabilities are present. Moreover, as discussed by Krall and Liewer (1971), the fluidlike character of the instability and its insensitivity to the electron-ion temperature make it attractive for explaining a number of experiments. Hence it may be important during solar flares.

Appendix C
RESISTIVE KINK LINEAR GROWTH RATES

Here we examine the linear growth rates of the tearing mode in cylindrical geometry. In general this requires numerical solutions to the pertinent equations, which we examine below. However one can obtain an idea of how the growth rates behave by using Eq. (4.73), i.e.,

$$\gamma = 0.5m^{2/5} \Delta'^{4/5} \frac{\eta}{4\pi}^{3/5} \left[\frac{d(B_\phi/r)dr}{(4\pi\rho)^{1/5}} \right]^{2/5} \quad (C1)$$

and assuming instability, i.e., $\Delta' > 0$.

First we note that γ depends on the gradients of B_ϕ i.e., the magnitude and distribution of the longitudinal current. Thus γ is very model dependent. This should be contrasted with the growth rates typically used for sheet flare models, where γ is simply taken as $p \sim (S/\alpha)^{2/5}$. In reality the growth rate strongly depends on the gradients of the driving fields, and even differing sheet models will have differing growth rates for the same set of mode numbers and equilibrium magnitudes. In addition

$$\Delta' = [dB_{r1}(r_s + \delta)/dr - dB_{r1}(r_s - \delta)/dr] / B_{r1}(r_s), \quad (C2)$$

strongly depends on the gradients of the perturbed radial component of \mathbf{B} , where $\epsilon \ll \delta \ll a$. It is therefore beneficial to emphasize the strong dependence of γ on the equilibrium configurations that drive the tearing mode, since this strong model dependence will also help explain the variety of flare types typically observed.

As noted earlier, the determination of growth rates generally requires numerical solutions. This can be done by numerically solving the following set of linearized equations (Killeen, 1968):

$$\frac{\partial \mathbf{B}_1}{\partial t} = \nabla \times (\mathbf{v}_1 \times \mathbf{B}_0) - \frac{c^2}{4\pi} \nabla \times (\eta_0 \nabla \times \mathbf{B}_1 + \eta_1 \nabla \times \mathbf{B}_0), \quad (C3)$$

$$\frac{\rho_0 \partial \mathbf{v}_1}{\partial t} = \frac{1}{4\pi} [(\nabla \times \mathbf{B}_0) \times \mathbf{B}_1 + (\nabla \times \mathbf{B}_1) \times \mathbf{B}_0] - \nabla p_1 + \rho_0 \nu \left[\frac{4}{3} \nabla(\nabla \cdot \mathbf{v}_1) - \nabla \times (\nabla \times \mathbf{v}_1) \right], \quad (C4)$$

$$\begin{aligned} \frac{\rho_0 \partial T_1}{\partial t} + \rho_0 \mathbf{v}_1 \cdot \nabla T_0 = & -(\gamma - 1) \rho_0 T_0 (\nabla \cdot \mathbf{v}_1) + k_1 \nabla^2 T + 2(\gamma - 1) \frac{c^2}{4\pi} \eta_0 (\nabla \times \mathbf{B}_0) \cdot (\nabla \times \mathbf{B}_1) \\ & + (\gamma - 1) \frac{c^2}{4\pi} \eta_1 (\nabla \times \mathbf{B}_0)^2 + (\gamma - 1) (S_E)_1, \end{aligned} \quad (C5)$$

$$\frac{\partial \rho_1}{\partial t} + \nabla \cdot (\rho_0 \mathbf{v}_1) = 0, \quad (C6)$$

$$p_1 = \rho_0 T_1 + \rho_1 T_0, \quad (C7)$$

and

$$\nabla \cdot \mathbf{B}_1 = 0, \quad (C8)$$

where $(S_E)_1$ corresponds to the various energy sources and sinks not explicitly included, $\gamma = C_p/C_v$, and ν is the kinematic viscosity. Here $\mathbf{B} = \phi B_\phi(r) + z B_z(r)$ and all perturbed quantities vary as $\exp i(m\phi + kz)$. To solve the resulting equations, one first introduces the dimensionless quantities introduced in Section 4 which characterize the relevant time scales of the system of equations: τ_R and τ_H . One then proceeds by using implicit differencing schemes and then solving the resulting equations via the tridiagonal algorithm (Killeen, 1969). This was accomplished by Killeen (1963) and Dibiase (1974) using two differing numerical codes: Ripple⁴ and Restab respectively. The results presented here were obtained using Restab, which has the greater versatility in that it can handle equilibrium temperature and density gradients perpendicular to \mathbf{B} as well as handling alternate energy sources and sinks and permitting compressible perturbations.

The results given are only meant to illustrate the difference between the growth rates that one would obtain for differing equilibrium models. Hence, the only case considered is the force-free model discussed in Section 4, as contrasted with the sheet model of FKR (1963). However the results are not meant to be indicative of an exhaustive parametric study of the model, since it would be both economically and physically unreasonable to generate detailed parametric studies of equilibrium models at this stage without a realistic equilibrium model of the magnetic field in a solar arch. In addition the large magnetic Reynolds numbers characteristic of the solar atmosphere require inordinate amounts of computer time to determine growth rates. Hence the results presented will be limited to Reynolds numbers pertinent to the discussions in the main text, and for modes with $m = 1$ and $\alpha = 0.2$.

Table C1 illustrates the results. Notice that generally the growth rates for the BFM are greater than the sheet model, sometimes by as much as ten or more. One should therefore expect that nonforce-free magnetic configurations will have even greater linear growth rates, since there exists additional free energy in such equilibrium configurations to drive the modes.

A consequence of these results is that the magnitudes of the poloidal component of \mathbf{B} may be reduced by a factor of 2 or 3 as compared to that adopted in Section 6 and still satisfy the requirement that $\approx 10^{28}$ ergs/s be released to explain the small flare. This also reduces the requirements on the current densities and/or the gradients found in Sections 6 and 8.

Table C1 - Comparison of Results of the Bessel-Function Model of Section 4
With the Sheet Model of FKR (1963)

n (cm^{-3})	T (K)	B_p (g)	a (cm)	S	τ_r (s)	$\gamma(\text{s}^{-1})$	
						Sheet Model	BFM ($m = 1$ mode)
10^{12}	10^5	500	10^2	2.6×10^4	0.024	4.6×10^3	1.7×10^4
10^{12}	10^5	500	10^3	2.6×10^5	2.39	1.2×10^2	9.6×10^2
10^{12}	10^5	500	10^4	2.6×10^6	2.4×10^2	2.9	5.4×10^1
10^{12}	10^5	250	10^2	1.3×10^4	0.024	3.5×10^3	1.0×10^4
10^{12}	10^5	250	10^3	1.3×10^5	2.39	8.8×10^1	5.7×10^2
10^{12}	10^5	250	10^4	1.3×10^6	2.4×10^2	2.2	3.2×10^1
10^{11}	10^5	500	10^2	7.4×10^4	0.022	7.7×10^3	4.1×10^4
10^{11}	10^5	500	10^3	7.6×10^5	2.19	1.9×10^2	2.4×10^3
10^{11}	10^5	500	10^4	7.5×10^6	2.2×10^2	4.9	1.3×10^2
10^{11}	10^5	250	10^2	3.8×10^4	0.022	5.8×10^3	2.5×10^4
10^{11}	10^5	250	10^3	3.8×10^5	2.19	1.5×10^2	1.4×10^3
10^{11}	10^5	250	10^4	3.8×10^6	2.2×10^2	3.7	7.8×10^1
10^{12}	10^6	500	10^2	6.5×10^5	0.059	6.8×10^3	7.7×10^4
10^{12}	10^6	500	10^3	6.4×10^6	59.5	1.7×10^1	4.3×10^2
10^{12}	10^6	500	10^4	6.5×10^7	5.9×10^3	0.4	2.5×10^1
10^{12}	10^6	250	10^2	3.2×10^5	0.059	5.1×10^3	4.6×10^4
10^{12}	10^6	250	10^3	3.2×10^6	59.5	7.6×10^2	2.5×10^2
10^{12}	10^6	250	10^4	3.3×10^7	5.9×10^3	0.3	1.5×10^1
10^{11}	10^6	500	10^2	2.0×10^6	0.5	1.2×10^3	1.9×10^4
10^{11}	10^6	500	10^3	2.0×10^7	5.6×10^1	2.9×10^1	1.1×10^3
10^{11}	10^6	500	10^4	1.0^8	5.5×10^3	0.7	6.1×10^1
10^{11}	10^6	250	10^2	10^6	0.55	8.7×10^2	1.2×10^4
10^{11}	10^6	250	10^3	10^7	55.6	2.2×10^1	6.4×10^2
10^{11}	10^6	250	10^4	10^8	5.5×10^3	5.5×10^{-1}	3.6×10^1

REFERENCES

- Alfven, H., and Carlquist, P.: 1967, *Solar Phys.* **1**, 220
- Bach, G.G., Kuhl, A.L., and Oppenheim, A.K.: 1975, *J. Fluid Mech.* **71**, 105
- Bernstein, I.B., Freeman, E.K., Kruskal, M.D., and Kulsrud, R.M.: 1958, *Proc. Roy. Soc. A244*, 17
- Biskamp, D., and Chodera, R.: 1971, *Phys. Rev. Letts.* **27**, 1553
- Book, D.L.: 1975a, private communication
- Book, D.L.: 1975b, private communication
- Boris, J.P., Davison, J.M., Orens, J.H., and Roberts, K.V.: 1970, *Phys. Rev. Letts.* **25**, 706
- Boris, J.P., Coffey, T.P., and Fisher, S.: 1975, NRL Memorandum Report 3125
- Brice, N.: 1970, *J. Geophys. Res.* **75**, 4890
- Brown, J.: 1974, in G. Newkirk, Jr. (editor), *Coronal Disturbances, IAU Symp.* **57**, 395
- Brueckner, G.: 1976, *Phil. Trans. Royal. Soc. (London)* **A281**, 1304
- Buneman, O.: 1959, *Phys. Rev.* **115**, 503
- Cheng, C.C., and Widing, K.: 1975, *Astrophys. J.* **201**, 735
- Chrisman, P., Clark, J., and Rome, J.: 1974, Oak Ridge Report ORNL-TM-4501
- Clark, R.: 1975, private communication
- Coppi, B., and Friedland, A.B.: 1971, *Astrophys. J.* **169**, 379
- Davidson, R.C.: 1972, *Methods in Non-linear Plasma Theory*, Academic Press, New York
- Dibiase, J.A.: 1974, UCRL-51591, Lawrence Livermore Lab., Livermore, Calif.
- Drummond, W.E., and Rosenbluth, M.N.: 1962, *Phys. Fluids* **5**, 1507
- Eastwood, J.W.: 1972, *Planet. Space Sci.* **20**, 1555
- Eastwood, J.W.: 1974, *Planet. Space Sci.* **22**, 1641
- Filonenko, N.N., Sagdeev, R.Z., and Zaslavsky, G.M.: 1967, *Nuclear Fusion* **7**, 253
- Finn, J.M.: 1975, AEC Res. Dev. Rep. Matt-1137, Princeton Univ.
- Finn, J.M., and Kaw, P.K.: 1976, AEC Res. Dev. Rep. Matt-1220, Princeton Univ.
- Foukal, P.: 1975, *Solar Phys.* **43**, 327
- Friedrichs, K.O.: 1960, *Rev. Mod. Phys.* **32**, 889
- Furth, H.P.: 1963, in W.I. Fetterman (editor), *Propagation and Instabilities in Plasmas*, Stanford University Press, Stanford, Calif.

DANIEL S. SPICER

- Furth, H.P., Rutherford, P.H., and Selberg, H.: 1973, *Phys. Fluids* 16, 1054
- Furth, H.P.: 1975, *Nucl. Fusion* 15, 487
- Furth, H.P., Killeen, J., and Rosenbluth, M.N.: 1963, *Phys. Fluids*, 6, 459
- Galeev, A.A., and Sagdeev, R.Z.: 1976, in A. Simon and W. Thompson (editors), *Advances in Plasma Physics*, Vol. 6, Wiley, New York
- Gibson, E.G.: 1976, to be published in *Solar Phys.*
- Gibson, R.D., and Whiteman, K.J.: 1968, *Plasma Phys.* 10, 1101
- Glasstone, S., and Lovberg, R.H.: 1960, *Controlled Thermonuclear Reactions*, Van Nostrand, Princeton, N.J.
- Goedbloed, J.P.: 1973, *Phys. Fluids* 16, 1927
- Guzdar, P.N., Sen, A., and Kaw, P.K.: 1975, *Nucl. Fusion* 15, 1007
- Hirose, A., and Skarsgard, H.M.: 1976, *Phys. Rev. Lett.*, 36, 252
- Hoh, F.: 1964, *Phys. Fluids* 7, 956
- Horton, W.: 1972, *Phys. Rev. Letts.* 28, 1506
- Ichimaru, S.: 1975, *Astrophys. J.* 202, 528
- Jackson, J.D.: 1962, *Classical Electrodynamics*, Wiley, New York
- Janssens, T.J., White, K.P., III, and Broussard, R.M.: 1973, *Solar Phys.* 31, 207
- Johnson, J.: 1958, *Phys. Fluids*, 1, 281
- Kadomtsev, B.B.: 1976, ERDA Translation, MATT-Trans-119
- Kadomtsev, B.B.: 1965, *Plasma Turbulence*, Academic Press, New York
- Kadomtsev, B.B., and Pogutse, O.P.: 1970 in M.A. Leontovich (editor), *Reviews of Plasma Physics*, 5, Consultants Bureau, New York
- Kadomtsev, B.B.: 1962, *Soviet Phys.-Tech. Phys.* 6, 882
- Kadomtsev, B.B., and Pogutse, O.: 1974, *J. Exp. Theor. Phys.* 38, 283
- Kadomtsev, B.B.: 1966, in M.A. Leontovich (editor), *Reviews of Plasma Physics*, 2, 153, Consultants Bureau, New York
- Kahler, S.W., Krieger, A.S., and Vaiana, G.S.: 1975, *Astrophys. J. Letts.*, 199, L57
- Kane, S.R.: 1969, *Astrophys. J. Lett.*, 157, L139
- Keller, R., Pochelon, A., and Bachman, W.: 1976, *Phys. Rev. Lett.*, 36, 465
- Kennel, C.F., and Petschek, H.E.: 1966, *J. Geophys. Res.* 71, 1
- Killeen, J.: 1968, B.J. Rye and J.C. Taylor (editors), *Physics of Hot Plasmas*, Plenum Press, New York
- Kindel, J.M., and Kennel, C.F.: 1970, *J. Geophys. Res.* 76, 3055
- Krall, N.A., and Liewer, P.C.: 1971, *Phys. Rev. A* 4, 2094

NRL REPORT 8036

- Krall, N.A., and Trivelpiece, A.W.: 1973, *Principles of Plasma Physics*, McGraw-Hill, New York
- Lampe, M., Manheimer, W.M., and Papadopoulos, K.: 1975, NRL Memorandum Report 3076
- Landau, L.D., and Lifshitz, E.M.: 1960, *Mechanics*, Addison-Wesley, Mass.
- Lauback, D.D., and Probst, R.F.: 1969, *J. Fluid Mech.* 35, 53
- Liewer, P.C., and Krall, N.A.: 1973, *Phys. Fluids* 16, 1953
- Lin, R.P.: 1974, *Space Sci. Rev.*, 16, 189
- Lin, R.P.: 1975, in S. Kane (editor), *Solar Gamma-, X-, and EUV Radiation*, IAU Symp. 68, 385
- Liu, C.S.: 1971, *Phys. Rev. Letts.* 27, 1637
- Liu, C.S., Rosenbluth, M.N., and Horton, C.W.: 1972, *Phys. Rev. Letts.* 29, 1489
- Manheimer, W.M., Lampe, M., and Boris, J.P.: 1973, *Phys. Fluids* 16, 126
- McBride, J.B., Klein, H.H., Byrne, R.N., and Krall, N.A.: 1975, *Nucl. Fusion* 15, 393
- McWhirter, P.: 1974, unpublished
- Minorvsky, N.: 1962, *Non-Linear Oscillations*, Van Nostrand, New York
- Moreton, G., and Severny, A.: 1968, *Solar Phys.* 3, 282
- Morozov, A.I., and Solov'ev, L.S.: 1966, in M.A. Leontovich (editor) *Reviews of Plasma Physics*, 2, Consultants Bureau, New York
- Morse, R.L., and Nielson, C.W.: 1971, *Phys. Rev. Letts.* 26, 3
- Mullen, D.J.: 1973, *Astrophys. J.* 185, 353
- Newcomb, W.A.: 1960, *Annals of Phys.* 10, 232
- Orens, J.H., and Dawson, J.M.: 1974, NRL Memorandum Report 2850
- Papadopoulos, K., and Coffey, T.: 1974a, *J. Geophys. Res.* 79, 674
- Papadopoulos, K., and Coffey, T.: 1974b, *J. Geophys. Res.* 79, 1558
- Papadopoulos, K.: 1975, private communication
- Parker, E.N.: 1955, *Astrophys. J.* 122, 293
- Parker, E.N.: 1973, *Astrophys. J.* 180, 247
- Patterson, N.P., Brueckner, G.E. and Scherrer, V.E.: 1976, to be published in *Solar Physics*
- Petrosso, R.D., Kahler, S.W., Kreiger, A.S., Silk, J.K., and Vaiana, G.S.: 1975, *Astrophys. J. Letts.* 199, L127
- Purcell, J.D., and Widing, K.: 1971, *Astro. Phys. Lett.* 179, 239
- Roberts, K.V., and Taylor, J.B.: 1965, *Phys. Fluids* 8, 315
- Robinson, D.C.: 1971, *Plasma Phys.* 13, 439

DANIEL S. SPICER

- Rosenbluth, M.N., Krall, N.A., and Rostoker, N.: 1962, *Nucl. Fusion*, Suppl Part 1, 143
- Rosenbluth, M.N., and Post, R.F.: 1965, *Phys. Fluids* 8, 547
- Rosenbluth, M.N., Sagdeev, R.Z., Taylor, J.B., and ZasLauski, G.M.: 1966, *Nucl. Fusion* 6, 297
- Rutherford, P.H., Furth, H.P., and Rosenbluth, M.N.: 1971, IAEA Madison Conference
- Severny, A.: 1965, *Astron. Zh.* 42, 217
- Shafranov, V.D.: 1970, *Sov. Phys. Tech. Phys.* 15, 175
- Sheeley, N.: 1975, paper presented at the Flare Buildup Study Workshop, Falmouth, Cape Cod, Mass.
- Smith, D.F., and Priest, E.R.: 1972, *Astrophys. J.* 176, 487
- Solovev, L.S.: 1971, *Soviet Atomic Energy* 30, 14
- Speiser, T.W.: 1965, *J. Geophys. Res.* 70, 4219
- Spicer, D.S., Cheng, C.C., Widing, K., and Tousey, R.: 1974, paper presented at the 2nd European Conference on Cosmic Plasma Physics, Culham, England
- Spicer, D.S.: 1975, *Bull. Am. Astron. Soc.* 7, 352
- Spitzer, L.: 1967, *Physics of Fully Ionized Gases*, Interscience, New York
- Stix, T.H.: 1973, *Phys. Rev. Letts.* 30, 833
- Stix, T.H.: 1975, ERDA preprint Matt-1187, Princeton, N.J.
- Sturrock, P.A.: 1966, *Nature* 211, 695
- Sturrock, P.A.: 1968, *I.A.U. Symp.* 35, 471
- Sturrock, P.A.: 1972, *Solar Phys.* 23, 438
- Sturrock, P.A.: 1973, p. 3 in R. Ramaty and R.G. Stone (editors), *Proc. Symposium on High Energy Phenomena on the Sun*, NASA Goddard Space Flight Center
- Suydam, B.R.: 1958, *Proc. U.N. Intern. Conf. on Peaceful Uses of Atomic Energy*, 2nd, Geneva, 31, 157, Columbia Univ. Press (I.D.S.), New York
- Svestka, Z.: 1974, *Solar Gamma-, X-, and XUV Radiation*, I.A.U. Symp. 68, 427
- Svestka, Z., and Fitsova-Suestkova, L.: 1974, *Solar Phys.* 36, 417
- Svestka, Z.: 1975, *Solar Flares*, Reidel, Dordrecht, Holland
- Tanaka, K.: 1972, Big Bear Solar Observatory preprint
- Tandberg-Hanssen, E.: 1974, *Solar Prominences*, Reidel, Dordrecht, Holland
- Tidman, D.A., and Krall, N.A.: 1971, *Shock Waves in Collisionless Plasmas*, Wiley-Interscience, New York
- Tidman, D.A., and Stamper, J.A.: 1973, *Appl. Phys. Lett.* 22, 498
- Title, A.M., and Andelin, J.P.: 1971, in R. Howard (editor), *Solar Magnetic Fields*, I.A.U. Symposium 43, Reidel, Dordrecht, Holland
- von Goeler, S., Stodiek, W., and Sauthoff, N.: 1975, Matt-1058, Princeton, N.J.

NRL REPORT 8036

- Vorpahl, J.A., Gibson, E.G., Landecker, P.B., McKenzie, D.L., and Underwood, J.H.:
1975, *Solar Phys.* 45, 199
- Voslamber, D., and Callebaut, D.K.: 1962, *Phys. Rev.* 128, 2016
- Wentzel, D.G. and Tidman, D.A., (editors): 1969, *Plasma Instabilities in Astrophysics*,
Gordon and Breach, New York
- Wentzel, D.G.: 1974, *Solar Phys.* 39, 129
- White, R., Monticello, D., Rosenbluth, M.N., Strauss, H., and Kadomtsev, B.B.: 1974,
IAEA Tokyo Conference
- Widing, K.: 1974a, *Solar Gamma-, X-, and EUV Radiation, I.A.U. Symp.* 68, 153
- Widing, K.: 1974b, *Astrophys. J. Letts.* 197, L33
- Widing, K., and Cheng, C.C.: 1975, *Astrophys. J. Letts.* 194, L155
- Yeh, T.: 1973, *Phys. Fluids*, 16, 516
- Zaslavsky, G.M., and Chirikov, B.V.: 1972, *Soviet Phys.—Uspekhi* 14, 549
- Zel'dovich, Y.B., and Raizer, Y.P.: 1966, *Physics of Shock Waves and High-Temperature
Hydrodynamic Phenomena*, Academic Press, New York

ACKNOWLEDGMENTS

The author thanks Professors D.A. Tidman and C.S. Liu and Drs. D. Book and E. Toton for many fruitful conversations during various stages of this research. The author is also grateful to Drs. K.G. Widing and G. Doschek for interesting discussions on flare observations and Dr. G. Brueckner for introducing him to the solar flare problem.

Final thanks go to Drs. H. Friedman and R. Tousey for supporting this research at NRL.

This research was supported through NASA Contracts DPR S 60404-G and DPR W 13.425.